$SU(N)$ Glueball Dark Matter

by

Bryce Cyr

A Thesis Submitted in Partial Fulfillment of the
Requirements for the Degree of

Master of Science

Advisor: James Cline

Department of Physics
McGill University

November 28th, 2017

All rights reserved. This thesis may not be reproduced in whole or in part, by photocopying or other means, without the permission of the author.

Contents

1 Introduction **1**

2 An Introduction to Particle Cosmology **4**
2.1 The Standard Model of Particle Physics 5
2.1.1 The Framework of the Standard Model 5
2.1.2 Symmetries in the Standard Model 7
2.1.3 The Electroweak Theory of $SU(2) \times U(1)$ 10
2.1.4 The Higgs Mechanism 13
2.1.5 $SU(3)$ Strong Interactions 17
2.1.6 Decay Rates and Cross Sections 21
2.2 Effective Lagrangians 23
2.2.1 The Effective Lagrangian of Weak Interactions 24
2.2.2 Effective Lagrangians Beyond the Standard Model 27
2.3 The Thermal History of the Universe 29
2.3.1 Cosmological Preliminaries 29
2.3.2 Thermodynamics and Particle Interactions 31
2.3.3 The Thermal History: A Timeline 35

3 Relic Densities and the Dark Matter Paradigm **38**
3.1 Dark Matter Candidates 40
3.1.1 Primordial Black Holes 40
3.1.2 Axion Dark Matter 41
3.1.3 Weakly Interacting Massive Particles (WIMPs) 43
3.2 The Boltzmann Equation: Determination of Relic Abundances 43
3.2.1 Out of Equilibrium Thermodynamics 44
3.2.2 Thermal Averaging 46
3.2.3 The WIMP Miracle 47
3.3 Towards a Numerical Solution of the Boltzmann Equation 49
3.3.1 Numerical Challenges and Features of the Program 50
3.3.2 Baryon-Symmetric Universe: An Example 53
3.3.3 Applicability of the Software 54

4 $SU(N)$ Glueball Dark Matter **56**
4.1 Non-Abelian Gauge Theories and their Application to Dark Matter 60
4.1.1 Properties of Non-Abelian Gauge Theories 60
4.1.2 An Introduction to Glueballs 61
4.1.3 Composite Collisions and Parton Distribution Functions 64
4.2 Coupling of Dark Glueballs to $U(1)_Y$ 67
4.2.1 Experimental Constraints and the Parameter Space 67
4.2.2 Aside: Cosmologically Long-Lived Particles 69
4.2.3 The Scattering Cross-Section 72
4.2.4 Determining $\langle \sigma v \rangle$ 77
4.2.5 Extension to Photons and Z^0 Bosons 79
4.2.6 Freeze-out Temperature/Outlook of Model 80
4.3 Dark Glueballs to Gluons: A Quirky Approach 85
4.3.1 3-Loop Line Production Diagram 85
4.3.2 1-Loop Diffuse Photon Diagram 88
4.3.3 Heavy Φ Production in Colliders 93
4.3.4 Phenomenology of Φ 95
4.4 Higgs Portal Decay 101
4.4.1 Decay Rate of the 0^{++} 101
4.4.2 $1^{+-}, 0^{-+}$ in a Sea of Metastable 0^{++} 103

5 Discussion and Outlook **106**

6 Conclusions **110**

Appendices **112**

A Overview of Units and Unit Conversions **113**

B Miscellaneous Computations **115**
B.1 Differential Element in the Computation of $\langle \sigma v \rangle$ 115
B.2 Derivative Interactions 117

C *Mathematica* Notebook **119**

List of Figures

2.1 Evolution of the Higgs potential as a function of temperature in the early universe 14
2.2 Left: Schematic illustration of how perturbation theory in QED works; the more vertices in a diagram, the more suppressed the interaction is. The second diagram is a one loop correction to e^+e^- scattering. Right: The running of couplings in the standard model, illustrating the qualitative difference between Abelian and non-Abelian gauge couplings. Figure adapted from 2004 Nobel prize website [8] 18
2.3 A schematic diagram of how confinement and flux tube generation happens in QCD. As a bound state of quarks separates, a pair of matching quarks is popped out of the vacuum when $d \sim \Lambda_{QCD}^{-1}$ 20
2.4 Feynman rule for the interaction vertex in QED 22
2.5 The schematic collapse of a Feynman diagram when using an effective Lagrangian. None of the initial or final state particles are altered, just the mathematical computation. Note the black circle is meant to emphasis that a propagator has been removed 26
2.6 The evolution of g_* as the universe cools. Different temperatures mark where certain species become non-relativistic. Figure from [15] 33
2.7 Tracking the (comoving) abundance of a weakly interacting particle species before and after decoupling from the primordial plasma 35
2.8 A schematic illustration on the relative evolution of the universe from the big bang to the present [22] 37

3.1 The rotational velocity of stars in spiral galaxies observed via $21cm$ astronomy. Figure taken from [25] 39
3.2 A code snippet specifying the input parameters to our numerical Boltzmann solver 51

3.3 Left: The time evolution of a generic dark matter candidate with parameters $(m, g, \langle \sigma v \rangle) \to (1000GeV, 100, 10^{-10}GeV^{-2})$, comparing between the stiffness switching and automatic methods. No discrepancy exists in the large x regime. Right: A comparison between the residual and stiffness switching method for parameters $(m, g, \langle v \rangle) \to (1GeV, 10, (0.139)^{-2}GeV^{-2})$, a late-time freeze out particle. The early time stability is easy to see, and is our preferred method for this solver. 52
3.4 A comparison between the baryon to photon ratios in a universe with an initial asymmetry (red), and one without (blue). Note that our program computed the blue curve, the red was added afterwards for visual comparison. 54

4.1 The glueball spectrum for a pure glue $SU(3)$ theory, from lattice QCD techniques. The masses are normalized to the mass of the lightest state (0^{++}) [45] 62
4.2 The Drell-Yan process of $pp \to \ell\bar{\ell}$ occurring via photon exchange 65
4.3 Hypergluon couplings to hypercharge gauge bosons are loop suppressed by our heavy field Φ, and so we can write an effective 4-point function. The field B refers to the hypercharge gauge boson. 75
4.4 Constraints on new particle masses from reheating, line searches [56] [58] and CMB studies [57]. Reheating constraints are computed for a variety of possible temperatures, represented by the contours, T_{reheat} and appear to be quite strong. Reheat constraints computed in $N_c = 3$. The allowed region of parameter space is above the curves set by reheating and the other constraints. Note that the contours disappear for $m_{0^{++}} > M_\Phi$, which is where we expect the EFT approach to break down. We also assume that freeze out takes place above Λ_{HC} (implicit in the calculation since we also assume $T_{reheat} > \Lambda_{HC}$). The black dashed line comes from the constraint equation for $M_{\Phi,UV}$ in section 4.2.2, where any point below that line corresponds to a model in which the dark glueballs decay on a timescale shorter than the age of the universe. The allowed region of parameter space is above all contours. 82
4.5 The lowest order loop diagrams with $SU(3)_{strong}$ couplings producing a spectral line of photons (left) and a diffuse spectrum (right) 86
4.6 Constraints on new particle masses from reheating, line searches [56] [58] and CMB studies [57] for the 3-loop QCD coupled diagram above. Parameter space constraints are almost identical to that of the electromagnetic case, due to the 1/7 suppression of α_s. Reheat constraints computed in $N_c = 3$. Reheating and cosmological lifetime constraints come from the lowest order (1-loop) gluon production diagram. Line search constraints are weaker than in the 1-loop case due to additional loop suppression factors coming from QCD loops. The allowed region of parameter space is above the curves set by reheating and the other constraints 87

4.7 Left: A comparison between the b quark and gluon final state spectra for the same energetics. Right: Evolution of the photon spectra for final state gluons as a function of $m_{0^{++}}$. x refers to the fractional energy of the photons, $x = E/m_{0^{++}}$ 90
4.8 Diffuse photon constraints from Fermi-LAT [64] and HAWC [65] experiments investigating decaying dark matter from dwarf spheroidal galaxies. As before, the allowed parameter space is that above the reheating contours, the cosmological lifetime constraint, and the diffuse photon constraints. The cosmological lifetime constraint is computed from the 1-loop gluon-hypergluon interaction. 92
4.9 Φ production can take place through quark or gluon fusion processes in colliders. All curly lines are gluons (not hypergluons). Note that hypercolor confinement will keep these final state Φ particles bound to one another. . . 94
4.10 Full production cross section of Φ particles from parton formalism. $\sqrt{s} = 13\ TeV$ for the latest LHC run. Figure adapted from [52] 97
4.11 95% confidence limits on a new fermionic Φ particle transforming as a triplet under $SU(3)_{strong}$. The hidden gauge group here has $N = 2$. Red and green shaded regions are constraints from HSCPs and monojets respectively. Projected constraints are also given for the $0T$ scenario. Unshaded lines represent projected constraints with more data. Grey dashed lines correspond to the effective length of the flux tube separating a $\Phi\bar{\Phi}$ pair. Figure credit to [73] . 100
4.12 Relic densities of the 0^{-+} and 1^{+-} states, weighted by their masses. $R = s_{HC}/s$ is the relative entropy between the two sectors, and is a conserved quantity after all confining phase transitions. The horizontal line represents the necessary value of $m \cdot Y$ to give the observed dark matter abundance in the universe today Figure adapted from [47] 105

I, BRYCE CYR, declare that this thesis titled, '$SU(N)$ Glueball Dark Matter' and the work presented in it are my own. I confirm that:

- This work was done wholly or mainly while in candidature for a research degree at this University.
- Where any part of this thesis has previously been submitted for a degree or any other qualification at this University or any other institution, this has been clearly stated.
- Where I have consulted the published work of others, this is always clearly attributed.
- Where I have quoted from the work of others, the source is always given. With the exception of such quotations, this thesis is entirely my own work.
- I have acknowledged all main sources of help.
- Where the thesis is based on work done by myself jointly with others, I have made clear exactly what was done by others and what I have contributed myself.

Signed: ____

Date: ____

Abstract

Dark matter is postulated to exist as a bound state of gauge bosons in a hidden $SU(N)$ theory, dubbed 'dark glueballs'. These dark glueballs have no direct couplings to the standard model, but are instead allowed to decay via loops of heavy mediator particles, Φ. We consider scenarios in which the Φ particles are coupled with $U(1)$ hypercharge, $SU(3)$ strong forces, and Higgs bosons respectively. Additionally, a numerical approach to solving the Boltzmann equation is considered in Mathematica. This software package can be applied and modified to a wide class of generic particle dark matter candidates.

Abrégé

Il existe une hypothèse qui stipule que la matière noire est considérée comme étant un état lié de boson de jauge suivant une théorie de $SU(N)$, surnommée boule de glu 'dark'. Ces boules de glu n'ont pas de relation directe avec le modèle standard, mais sont en effect, en mesure de se décomposer en segments égaux de particules médiatrices, Φ, ayant une grande masse. Nous considérons plusieurs scénarios dans lesquels les particules Φ sont liées avec hypercharge $U(1)$, de puissantes forces $SU(3)$, et des bosons de Higgs respectivement. De plus, nous considérons l'approche numérique afin de résoudre l'équation de Boltzmann dans Mathematica. Le progiciel proposé par Mathematica peut être manipulée afin de tester un large éventail de particules génériques de matière noire.

Acknowledgements

This work wouldn't have been possible without the love and support of many close to me. Thank you to E. Ferreira, E. McDonough, and J. Quentin for excellent office banter, S. Saha, A. Fodor, H. Pikhartova, and K. Colville for their friendship and coursework discussions. My gratitude also goes out to my parents, brother, and S. Rufh for keeping me sane in times of stress. I would also like to thank my advisor, J. Cline, for many enlightening discussions, helpful comments, and guidance throughout my time at McGill.

"*Many other people who have studied far enough to begin to understand a little of how things work, are fascinated by it, and that fascination drives them on*"
- Richard Feynman

"*The earth is a very small stage in a vast, cosmic arena*"
- Carl Sagan

Chapter 1

Introduction

For more than an age, people have gazed up and looked at the cosmos. For some, the seemingly infinite vastness is frightening, mysterious, and not reconcilable with beliefs forged here on earth. For others, the feeling of insignificance that creeps in when considering something so grand can bring comfort. It presents an exciting opportunity to probe ones past, and indeed, the past of the universe as well.

While the universe may seem so very large to us today, it wasn't always that way. The observable universe represents the causal patch of photons emanating from a so-called big bang until now, some 13 billion years ago, and was much smaller in the past. We note that from standard thermodynamics, the reduction in the size of a box, while keeping the content inside the box constant, causes an increase in temperature. Today, while the standard conditions in the universe are quite benign (aside from obvious astrophysical sources such as star forming regions, supernovae, black holes, and others), the early universe was a much more volatile and chaotic state.

Since light has a finite propagation time, remnants of the early universe remain for us to observe today, with the cosmic microwave background, the oldest photons in the universe, being our gold standard as a dataset to work with. The universe still holds many mysteries from us, and so utilizing information from early universe cosmology can be fantastic in determining exotic physics hidden to us here on earth.

The particular phenomenon we wish to study in depth is that of dark matter. Dark matter is an undiscovered form of matter postulated in order to explain various astrophysical phenomenon, such as the flat rotation curves of spiral galaxies. Many different approaches have been taken over the past few decades in describing these effects (modified gravity, primordial black holes, etc), but the most popular explanation seems to be that dark matter has some origin embedded in particle physics.

We aim to make use of the formalism granted to us by quantum field theory and particle physics to explain the abundance of dark matter as bound states of the gauge bosons of an asymptotically free $SU(N)$ theory. We refer to these states as dark glueballs, and are an attractive choice as they can be made to have naturally small indirect couplings to the standard model, and can also ease tensions with some shortcomings that standard cold dark matter experiences, such as the cusp/core problem with the inclusion of self-interaction.

In this work, we begin with a general overview of the standard model of particle physics, which will serve as our basis for understanding this new gauge theory. We then move on to discussing physics beyond the standard model in the form of low-energy effective Lagrangians, and their applications to particle cosmology. Following this, we briefly review a variety of approaches to explaining dark matter, and then talk about the Boltzmann equation in the context of setting relic densities of late-time surviving particle species. Work is then presented in chapter 3 of numerical simulations of particle evolution via the Boltzmann equation, implemented in Mathematica.

Finally, in chapter 4, we discuss how one would introduce a new $SU(N)$ force to the standard model, and discuss the possible indirect couplings our dark glueball can have to the standard model, via some heavy mediator particle, Φ. Constraints are discussed in the context of both cosmological signals, and particle collider signals before concluding. Much of this discussion is a review and commenting of work done by other authors working with non-Abelian gauge theories of dark matter. Novel ideas come from applying constraints on different couplings to the parameter space of our model, calculating the implications of reheating, and discussing the viability of different couplings on our mediator.

Chapter 2

An Introduction to Particle Cosmology

The interface between particle physics and cosmology is a complicated one, with many nuances and subtle details that should be appreciated. In this chapter, the relevant background knowledge will be presented in a pedagogical way in order to aide the reader in understanding how the two sectors are coupled.

We begin with an overview of the standard model, with a slight emphasis on strong interactions as they are the most relevant for the remainder of the thesis. After reviewing these concepts, we will introduce the technique of effective Lagrangians, which are critical when considering theories with heavy degrees of freedom. Finally, we will introduce the basic concepts of cosmology in an attempt to reconcile them with our understanding of the standard model of particle physics.

2.1 The Standard Model of Particle Physics

The standard model of particle physics is the result of a many decades effort to come up with a theoretical explanation for the fundamental observations made in particle physics. Its underlying mathematical structure appears to be group theoretic, yet ideas from complex analysis and other branches of mathematics come in handy for making accurate computations within the framework of the theory. Here we present the framework, and briefly show how it applies to electroweak interactions before discussing in more depth its application to the strong force. This review follows ideas presented in the standard undergraduate and graduate level texts [1] [2] [3] [4] [5].

The standard model describes the weak, strong, and electromagnetic forces of nature in one unified framework. Each interaction has one or more gauge bosons which carry the force, and a number of other particles (leptons, quarks, and bosons) which help build up the world we see around us. Without the inclusion of gravity, we can't consider this to be a theory of everything, but still it offers unparalleled accuracy between theory and experiment.

2.1.1 The Framework of the Standard Model

As stated above, group theory seems to be the underlying mathematical descriptor of the known particle states found in nature. Quantum field theory, however, provides physicists with a more useful toolbox in computing quantities associated with elemental particle interactions. The structure of the standard model is extraordinarily rich, with what is colloquially referred to as a zoo of particles giving rise to the macroscopic features we see in the world today.

Quantum field theory takes the viewpoint that the fundamental objects of nature are fields, and particle states arise as localized perturbations of these fields at different points in space-time. At its core, quantum field theory is just the application of quantum mechanics to relativistic particles. Taking classical field theory as a starting point, we assert that the equations of motion for particle states should be the extremized variations of an action, $\delta S = 0$, where our action is defined with a Lagrangian density, $\mathcal{L}$ as such

$$S = \int \mathcal{L}(\phi, \partial_\mu \phi) d^4x \tag{2.1}$$

Variations with respect to this give us the general Euler-Lagrange form that describes the equations of motion

$$\partial_\mu \left(\frac{\partial \mathcal{L}}{\partial(\partial_\mu \phi)} \right) - \frac{\partial \mathcal{L}}{\partial \phi} = 0 \tag{2.2}$$

This operation recovers the familiar Klein-Gordon equation for simple scalar fields, or the Dirac equation for spin 1/2 particles.

The 'quantum' in QFT refers to the fact that we interpret the dynamical variables in the action (ϕ, for example) as operators obeying commutation relations. In particular, we take these relations to be those of the harmonic oscillator, giving a physical interpretation to our fields. As an example, the Lagrangian for a Klein-Gordon field is

$$\mathcal{L} = \frac{1}{2}\partial_\mu \phi^* \partial^\mu \phi - \frac{1}{2}m^2|\phi^2| \tag{2.3}$$

Expanding the field ϕ in Fourier modes, we see using the harmonic oscillator analogy that

$$\phi(\mathbf{x}) = \int \frac{d^3p}{(2\pi)^3} \frac{1}{\sqrt{2\omega_{\mathbf{p}}}} \left(a_{\mathbf{p}} e^{i\mathbf{p}\cdot\mathbf{x}} + a_{\mathbf{p}}^\dagger e^{-i\mathbf{p}\cdot\mathbf{x}} \right) \tag{2.4}$$

where the $a_{\mathbf{p}}$ and $a_{\mathbf{p}}^{\dagger}$ are annihilation and creation operators of the Klein-Gordon field respectively. Here, $\omega_{\mathbf{p}} = \sqrt{|\mathbf{p}|^2 + m^2}$ is related to the energy of the harmonic oscillator. Noting the usual commutation relations, $[a, a^{\dagger}] = 1$ (this is for bosons, fermions carry anticommutation relations, $(\{a, a^{\dagger}\} = 1)$) we can construct the Fock state of particles by repeated use of the creation operator $a^{\dagger}$ on the ground state

$$|n\rangle = (a^{\dagger})^n |0\rangle \tag{2.5}$$

This is the general procedure used to create multiparticle states in quantum field theory. In fact, this tactic of expanding the field in terms of ladder operators is precisely what is meant when we talk about quantizing a field. From here, it is possible to construct general Lagrangians satisfying different physical and symmetry based constraints which we can then quantize in order to compute observable quantities. We will come back to the computation of these observables after a quick detour into the topic of symmetries in physics.

2.1.2 Symmetries in the Standard Model

Without the notion of symmetry, much of physics would not be tractable, and seemingly simple phenomenon would become obscured behind a mountain of mathematics. Thankfully, nature has been kind enough to us in giving symmetries to be exploited. The general aim in quantum field theory is to construct the most general Lagrangian possible, with a priori knowledge of how the field interacts, and what symmetries it possesses.

Symmetries come in both discrete and continuous forms, and are related to conservation laws via Noether's theorem. With this, important connections were formed between well established concepts. Translational invariance in time and space provided energy and momentum conservation, rotational isotropy yielded angular momentum conservation, and a newer concept, that of gauge transformations, gives us conserved charges. A Lagrangian that is invariant under a set of local continuous transformations is said to be gauge invariant under those transformations. In the simple case of an Abelian $U(1)$ field, this means that $\mathcal{L}$ is invariant under

$$\phi \to \phi' = \phi e^{i\Lambda(x)} \tag{2.6}$$

where $\Lambda(x)$ is a function of the spacetime coordinates (hence the transformation is local). Gauge theories make up the standard model, and so we consider them in more detail below. Of more importance to the idea of glueballs is the idea of some discrete symmetries, such as parity and charge conjugation.

Parity is the idea that physics should not be altered over a mirror reflection of any specific process. This symmetry may seem obvious, but in fact the weak interactions don't necessarily respect this [6]. For strong and electromagnetic interactions, however, parity is a conserved quantity. The parity operation acts as reflection in the spacial coordinates of a field, and so we can define the parity of such a field by the eigenvalues it has under this operation. In the case of a vector, the parity operation completely changes its orientation, and so we can write $P(\mathbf{v}) = -\mathbf{v}$, meaning vectors carry parity of -1. Pseudovectors are another type of field that is quantified by having a parity of $+1$, and can be formed, for example, by the cross product of two normal vectors. The story for scalars is intuitive, since there is no spacial dependence on the value of the scalar is has parity of $+1$, while pseudoscalars (formed by a scalar triple product, for example) carry parity -1. This can again be generalized to higher spin objects such as tensor fields, but will not be relevant for the remainder of the work.

The charge conjugation operation replaces all particles in a theory with their antiparticles. Like parity, the eigenstates of this operation are ± 1, however unlike parity most natural particles in nature are not eigenstates. This operation is played out by reversing the signs of all the internal quantum numbers of a particle, and so to be an eigenstate of this operator, the particle and antiparticle must be indistinguishable, otherwise known as Majorana type. Like parity it is conserved in strong and electromagnetic interactions, but not necessarily for weak decays.

The idea that the laws of physics should be unchanged when boosted or rotated from one frame to another is called Lorentz invariance. More specifically, transformations of the coordinate system

$$x^\mu \to x'^\mu = \Lambda^\mu_\nu x^\nu \tag{2.7}$$

should leave the equations of motion invariant. Having a Lagrangian that is not Lorentz invariant introduces a sort of preferred reference frame, which is in violation of the laws of relativity. This is an additional symmetry we wish to possess, and so our fields must also transform under what is called the Lorentz group.

Finally, lets turn our attention to the idea of continuous gauge symmetries. In the language of group theory, particle physics can be expressed in terms of Lie groups (groups whose elements depend on parameters that vary continuously on some closed interval), such as the general set $SU(N)$. The electroweak force is represented by the groups $SU(2) \times U(1)$, while strong interactions can be described by the $SU(3)$ group. Here, S means 'special' and refers to the group matrices having determinant $+1$, and U means we have unitarity amongst the elements. In fact, it was the identification by Gell-Mann that nature carried some $SU(3)$ symmetry that led to the weight diagram of the baryon decuplet, and subsequently the prediction and discovery of the Ω^- particle.

Generally, gauge theories represent Lagrangians that are invariant under such a continuous group of transformations. These transformations are local, and so new gauge fields need to be introduced to compensate the derivative terms of these local transformations. Consider the generalized Klein-Gordon equation used in scalar quantum electrodynamics

$$\mathcal{L}_{s-QED} = -\frac{1}{4}F^{\alpha\beta}F_{\alpha\beta} - \partial_\mu\phi^*\partial^\mu\phi - m^2\phi\phi^* \tag{2.8}$$

Where $F_{\alpha\beta} = \partial_\alpha A_\beta - \partial_\beta A_\alpha$ is the EM field strength tensor. This equation is invariant under global $\phi \to e^{-ie\Lambda}\phi$ transformations, but not local (gauge) transformations where we allow Λ to vary with the position in spacetime. This gauge is known as a $U(1)$ transformation and is representative of the underlying structure of electromagnetism. By introducing the gauge covariant derivative $D_\mu = \partial_\mu + ieA_\mu$ and noting that $A_\mu \to A_\mu - \frac{1}{e}\partial_\mu\Lambda(x)$ under a $U(1)$ transformation, we can make the scalar QED Lagrangian completely gauge invariant. This procedure is used in the $SU(2)$ and $SU(3)$ constructions of the strong and weak Lagrangians as well. The gauge invariant Lagrangian for scalar QED is thus

$$\mathcal{L} = -\frac{1}{4}F^{\alpha\beta}F_{\alpha\beta} - D_\mu\phi^*D^\mu\phi - m^2\phi\phi^* \tag{2.9}$$

With these symmetries in mind, let us turn our attention to their applications on the gauge theory structure of the standard model, starting with the electroweak interactions.

2.1.3 The Electroweak Theory of $SU(2) \times U(1)$

The most simple gauge theory was that of $U(1)$ interactions we considered above. Since the standard model is known to obey the $SU(N)$ gauge groups as well, we note the following symmetry transformation that gives us gauge invariance for these groups. For a field $\psi(x)$, the transformation

$$\psi(x) \to e^{i\alpha^a(x)t^a}\psi(x) \tag{2.10}$$

leaves the general Lagrangian invariant for an $SU(N)$ interaction, provided that the t^a (the generators of the group) satisfy the commutation relations of the group, namely $[t^a, t^b] = if^{abc}t^c$. Here, f^{abc} are the structure constants of the group and are defined for the value of N in an $SU(N)$ group. The infinitesimal transformations of the other quantities in the Lagrangian are thus

$$D_\mu = \partial_\mu - igA^a_\mu t^a \tag{2.11}$$

$$A^a_\mu \to A^a_\mu + \frac{1}{g}\partial_\mu \alpha^a + f^{abc}A^b_\mu \alpha^c \tag{2.12}$$

The kinetic term for the gauge field now has an additional term representing the structure of the group

$$F^a_{\mu\nu} = \partial_\mu A^a_\nu - \partial_\nu A^a_\mu + gf^{abc}A^b_\mu A^b_\nu \tag{2.13}$$

and obeys the infinitesimal transformation rule

$$F^a_{\mu\nu} \to F^a_{\mu\nu} - f^{abc}\alpha^b F^c_{\mu\nu} \tag{2.14}$$

These are general properties of $SU(N)$ gauge theories, and so they will be of great importance later on in this work.

In the early universe, the electromagnetic and weak forces were unified under a different set of gauge groups, namely $SU(2)_L \times U(1)_Y$ related to the weak isospin and hypercharge, respectively. As we will describe below, the cooling of the universe eventually led to a phenomenon known as spontaneous symmetry breaking in which the Higgs boson acquires a vacuum expectation value and breaks this symmetry. In the breaking of this symmetry, three of the gauge bosons acquire a mass (the $Z, W^{\pm}$), and one linear combination of the original $SU(2)_L \times U(1)_Y$ generators remains unbroken, which gives us the currently observed $U(1)_{EM}$ with the photon as the sole remaining massless gauge boson.

The number of gauge bosons in an $SU(N)$ theory are described by the number of generators in the adjoint representation, namely $N^2 - 1$. Before this symmetry breaking, the $SU(2) \times U(1)$ symmetry therefore yields three massless 'W' particles and one 'B' particle. Linear combinations of these states yield the massive $W^{\pm}, Z$ particles and the massless γ state after symmetry breaking. To keep this work modular, the full Lagrangian for electroweak theory (before symmetry breaking) is

$$\begin{aligned}\mathcal{L}_{ew} = \frac{1}{4}W_a^{\mu\nu}W_{\mu\nu}^a - \frac{1}{4}B^{\mu\nu}B_{\mu\nu} + D_\mu H^\dagger D^\mu H \\ +i(\bar{Q}_i \not{D} Q^i + \bar{u}_i \not{D} u^i + \bar{d}_i \not{D} d^i + \bar{L}_i \not{D} L^i + \bar{e}_i \not{D} e^i) \\ -\lambda\left(H^\dagger H - \frac{v^2}{2}\right)^2 \\ -y_{u,ij}\epsilon^{ab}H_b^\dagger \bar{Q}_a^i u^j - y_{d,ij}H\bar{Q}^i d^j - y_{e,ij}H\bar{L}^i e^j + h.c.\end{aligned} \tag{2.15}$$

We have split the Lagrangian up into the kinetic terms for the gauge and Higgs bosons, the kinetic terms for the fermion content of the theory, the Higgs potential which is spontaneously broken, and the Yukawa coupling terms which cause the fermions to acquire mass when the Higgs gets a vacuum expectation value (VeV). We note that the standard model is a chiral theory, and as such only the left-handed fermions transform non-trivially under $SU(2) \times U(1)$ interactions. The Q^i terms refer to left handed up and down quarks in their doublet, and L^i

the left handed leptons. u, d, e are the right handed particles which transform as singlets in this representation. We also note that the covariant derivative for $SU(2) \times U(1)$ is

$$D_\mu = \partial_\mu - igW^a_\mu \tau^a - \frac{i}{2}g' B_\mu \tag{2.16}$$

where τ^a are the generators of $SU(2)$ and related to the Pauli matrices by $\tau^a = \sigma^a/2$. The gauge bosons acquire their masses from this term after SSB. After SSB the Lagrangian becomes more cumbersome, but allows for us to compute a wide variety of observables that can be tested both in colliders and in cosmology. We will come to that later, but for now let us take a brief detour into the Higgs mechanism to better understand its couplings to the standard model.

2.1.4 The Higgs Mechanism

The Higgs mechanism ([7]) is the way in which particles in the standard model acquire their mass. It relies on an idea called spontaneous symmetry breaking (SSB). Loosely speaking, SSB occurs when the shape of the Higgs potential changes from one where the field sits in a stable minimum, to one where it sits at an unstable maximum and rolls down to a true vacuum state in an unspecified direction in field space. The changing shape of the potential is driven by finite temperature effects, and so this process occurs naturally when the universe cools below what is known as the electroweak symmetry breaking scale, about $150 GeV$. Above this scale, standard model particles did not have mass, and the $SU(2)_L \times U(1)_Y$ remains unbroken. Afterwords we are left with the broken $SU(2)_{weak}$ and the unbroken $U(1)_{em}$ forces which we observe on more accessible energy scales here on earth. For theories with massive dark matter candidates above the symmetry breaking scale, there must be another mechanism to dynamically generates its mass. If these dark matter candidates couple to the Higgs, they receive a correction to their mass as the symmetry breaking scale is reached.

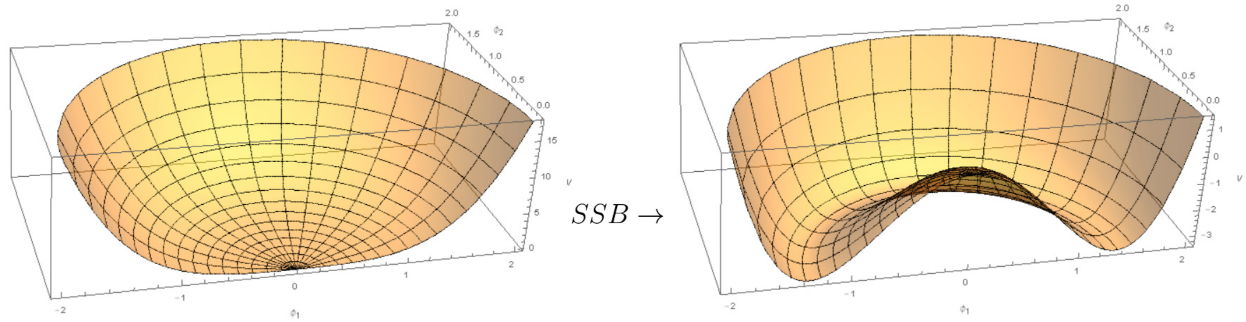

$T \gtrsim 150GeV$ $\qquad\qquad$ $T \lesssim 150GeV$

Figure 2.1: Evolution of the Higgs potential as a function of temperature in the early universe

In the spirit of electroweak symmetry breaking, lets briefly look at how symmetry breaking and the Higgs mechanism occurs in the Glashow-Weinberg-Salam (GWS) theory of weak interactions ([9], [10], [11]), in the context of gauge boson mass generation. For this explanation, we assume to be below the symmetry breaking scale. First, consider the Lagrangian for a Higgs interaction, which could be included in a theory with any $SU(N)$ gauge symmetry

$$\mathcal{L}_{Higgs} = D_\mu \phi^* D^\mu \phi - \left(-\mu^2 \phi^* \phi + \frac{\lambda}{2} (\phi^* \phi)^2 \right) \tag{2.17}$$

Where we have written the Higgs field as a complex scalar ϕ and the covariant derivative can take whichever form necessary to satisfy the gauge symmetries of the full Lagrangian. Looking now at the derivatives of this potential, we can see that there is an unstable maximum at $|\phi| = 0$, and a true (stable) minimum at $|\phi| = \phi_0 = \left(\frac{\mu^2}{\lambda}\right)^{\frac{1}{2}}$. We can make this true minimum manifest by rewriting the potential (to quadratic order) in the expansion of our complex field about this minimum

$$\begin{aligned} \phi &= \phi_0 + \frac{1}{\sqrt{2}}(\phi_1 + i\phi_2) \\ V(\phi) &= -\frac{\mu^4}{2\lambda^2} + \mu^2 \phi_1^2 + \mathcal{O}(\phi_{1,2}^3) \end{aligned} \tag{2.18}$$

Where one of our scalar fields, ϕ_1 has a mass term with $m_{\phi_1} = 2\mu^2$ and the ϕ_2 field remains massless. This massless field is known as a Goldstone boson and gives a physical interpretation to the extra degree of freedom the once massless gauge bosons of $SU(2)_L$ acquire after symmetry breaking. We see actually that the gauge freedom we have allows us to make the ϕ field real valued at all points in spacetime, thus eliminating the need for ϕ_2 at all. This is convenient to do since it negates some strange couplings of ϕ_2 to the gauge fields in the expansion of the covariant derivative. This expansion of the $|D_\mu\phi|^2$ term is precisely what gives us gauge boson masses after symmetry breaking. We note that it is also customary to label $\phi_0 = v$.

In the case of the electroweak $SU(2) \times U(1)$ theory (eq 2.15), our Lagrangian obeys the following gauge transformation

$$\phi \to e^{i\alpha^a \tau^a} e^{i\beta/2} \phi \tag{2.19}$$

where the scalar field has been given a hypercharge of $+1/2$, and we note the τ^a are related to the usual Pauli matrices. It is also useful to note that just as the global $U(1)$ invariance yielded electric charge (or hypercharge, Y before spontaneous symmetry breaking), global $SU(2)$ invariance yields another type of 'charge', this time referred to as T_3. After symmetry breaking, electric charge is determined by $Q = T_3 + \frac{1}{2}Y$. Using our gauge freedom, and specifying our field to be in the spinor representation of $SU(2)$, we can put our vacuum expectation value as

$$\langle\phi\rangle = \frac{1}{\sqrt{2}} \begin{pmatrix} 0 \\ \mathrm{v} \end{pmatrix} \tag{2.20}$$

Now, for these gauge symmetries, the covariant derivative is defined as

$$D_\mu \phi = \left(\partial_\mu - igW_\mu^a \tau^a - \frac{i}{2} g' B_\mu \right) \phi \tag{2.21}$$

Therefore, the terms quadratic (of the form $\frac{1}{2}m^2 B_\mu B^\mu$) will be generated by the kinetic term of the Higgs field. Squaring this kinetic term after the Higgs field acquires a VeV gives us the relevant mass terms

$$\begin{aligned} \mathcal{L}_{mass} = \frac{1}{2} \begin{pmatrix} 0 & \mathrm{v} \end{pmatrix} (g^2 W_\mu^a \tau^a W^{\mu,b} \tau^b + \frac{gg'}{2} W_\mu^a \tau^a B^\mu + \frac{gg'}{2} \\ + B_\mu A^{\mu,a} \tau^a + \frac{g'^2}{4} B_\mu B^\mu) \begin{pmatrix} 0 \\ \mathrm{v} \end{pmatrix} \end{aligned} \tag{2.22}$$

By inputting the generators of $SU(2)$, $\tau^a = \sigma^a/2$ this equation can be made much more provocative

$$\mathcal{L}_{mass} = \frac{1}{2} \frac{v^2}{4} \left(g^2 (W_\mu^1)^2 + g^2 (W_\mu^2)^2 + (-gW_\mu^3 + g' B_\mu)^2 \right) \tag{2.23}$$

From this we see that the original gauge fields of $SU(2)_L \times U(1)_Y$ all seem to acquire some type of mass. This is false, however, as it is possible to write these fields in a basis where only three of them acquire masses, and one remains massless. This is the symmetry breaking of $SU(2)_L \times U(1)_Y \to U(1)_{em}$. The relationship between the different bases is thus

$$\begin{aligned} W_\mu^\pm &= \frac{1}{\sqrt{2}} \left(W_\mu^1 \mp i W_\mu^2 \right) \\ Z_\mu^0 &= \frac{1}{\sqrt{g^2 + g'^2}} \left(g W_\mu^3 - g' B_\mu \right) \\ A_\mu^0 &= \frac{1}{\sqrt{g^2 + g'^2}} \left(g' W_\mu^3 + g B_\mu \right) \end{aligned} \tag{2.24}$$

Where we have made contact with the more familiar gauge bosons of the standard model. Insertion of this new (orthogonal) basis into equation (2.23) yields the mass terms

$$\begin{aligned} m_{W^{\pm}} &= \frac{gv}{2} \\ m_{Z^0} &= \frac{v\sqrt{g^2 + g'^2}}{2} \\ m_{A^0} &= 0 \end{aligned} \tag{2.25}$$

This is the Higgs mechanism and symmetry breaking pattern that happens in the early universe which causes the gauge bosons, Higgs boson, and fermions to acquire their masses. We note that the $SU(3)$ generators of the strong force remain unbroken under this effect, and so the gluons remain massless today.

2.1.5 $SU(3)$ Strong Interactions

Now, let us turn our attention to the final force in the standard model, namely the strong interactions that mediate internuclear forces. This theory is $SU(3)$ gauge invariant, and so as usual, the mediators of this force are the eight gauge bosons known as gluons. Before we write down the Lagrangian for this theory, it seems prudent to discuss another feature of gauge theory interactions, that of running coupling constants.

Standard methods in perturbative quantum field theory make note of a (usually small) coupling constant at each vertex. This coupling makes it obvious that more complex diagrams with a large number of vertices are significantly suppressed when computing observables.

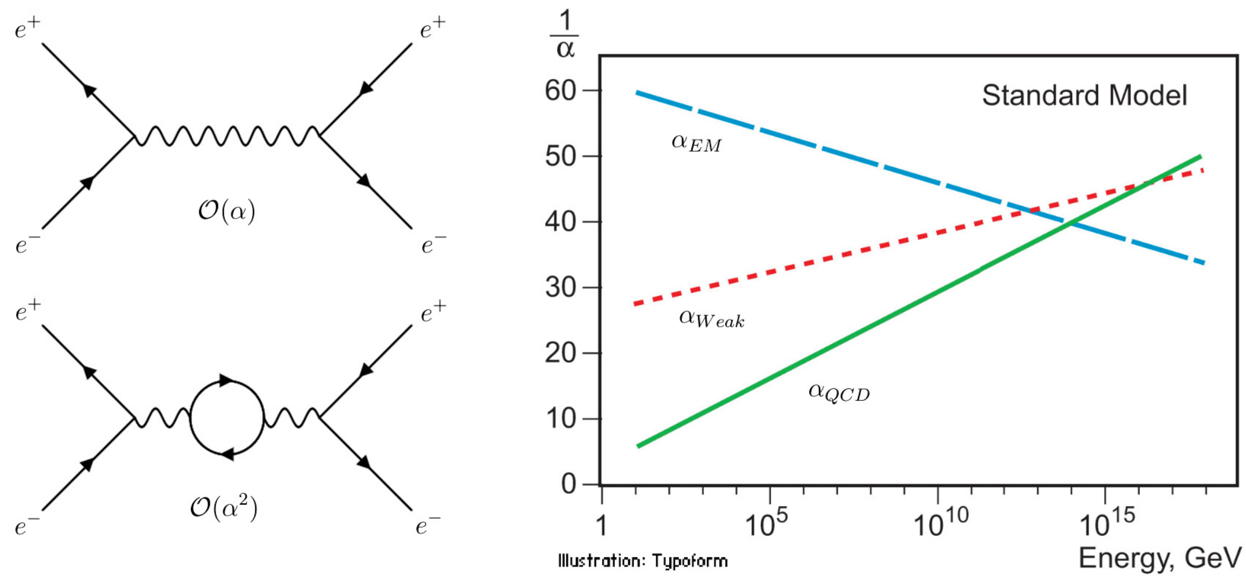

Figure 2.2: Left: Schematic illustration of how perturbation theory in QED works; the more vertices in a diagram, the more suppressed the interaction is. The second diagram is a one loop correction to e^+e^- scattering. Right: The running of couplings in the standard model, illustrating the qualitative difference between Abelian and non-Abelian gauge couplings. Figure adapted from 2004 Nobel prize website [8]

It has been found that these coupling constants are not actually constant, and appear to run with the energy scale of the interaction that they describe. This phenomenon appears as an effect of the renormalization procedure. Renormalization is a scheme that absolves the standard model of infinities that arise from higher order loop corrections to well understood processes. It is a rich and fascinating subject, but beyond the scope of this review, so we will just borrow a few results from this scheme. A particularily interesting result is the fact that in fermion-free theories, Abelian gauge theories such as $U(1)$ have a coupling that runs to infinity in the ultraviolet (high momentum scales), whereas non-Abelian theories can exhibit a property known as asymptotic freedom. Asymptotic freedom quite literally means that the coupling constant goes to zero in the UV, but is large in the infrared (low p limit). For QED, this coupling runs like

$$\bar{\alpha}_{QED} = \frac{\alpha_{QED}}{1 - (\alpha_{QED}/3\pi)\log(q^2/M^2)} \tag{2.26}$$

Here, M is scale of QED interactions (taken to be near the electron mass here), and the negative sign between the terms in the denominator is indicative of the fact that this coupling goes to a constant value in the low momentum limit ($q \to M$), and is unbounded for large q. For a non-Abelian gauge theory $SU(N)$ with n_f light fermions in the fundamental representation, the coupling instead runs as

$$\bar{\alpha} = \frac{\alpha}{1 + (\alpha/4\pi)(11N/3 - 2n_f/3)\log(q^2/M^2)} \tag{2.27}$$

The relative positive sign in this expression (that is present for a small number of n_f) is the smoking gun for an asymptotically free theory. Quantum chromodynamics (QCD) is one that follows such an evolution, and so the perturbative framework pioneered for QED is of limited use in the low energy regime. Nevertheless, perturbative calculations are useful in understanding the general features of QCD, but the non-perturbative effects cannot be neglected.

The theory of strong interactions contains six different 'flavours' of quarks, and eight different types of gluons. The quarks and gluons contain a new property exclusive to $SU(3)$ called colour charge, which must be conserved at a vertex. Quarks also contain fractional electric charge, and thus transform under the other forces as well as $SU(3)$. For completeness, lets write out the Lagrangian for QCD

$$\mathcal{L}_{QCD} = \bar{\psi}(i\not{D} - m)\psi - \frac{1}{4}G^a_{\mu\nu}G^{\mu\nu,a} - \frac{n_f g^2\theta}{32\pi^2}F_{\mu\nu}\tilde{F}^{\mu\nu} \tag{2.28}$$

Where the gluon fields implicitly defined in $\not{D}$ and $G^a_{\mu\nu}$ come are a result of the eight Gell-Man matrices used to generate infinitesimal rotations in $SU(3)$. The final term violates CP symmetry, which is an expected (but not measured) effect of QCD. This θ parameter must be very small (presenting us with a fine-tuning problem) otherwise CP violation would have been observed in QCD experimentally. This term is explored in more detail next chapter. The masses of quarks are generated along with other SM particles after spontaneous symmetry breaking in the early universe.

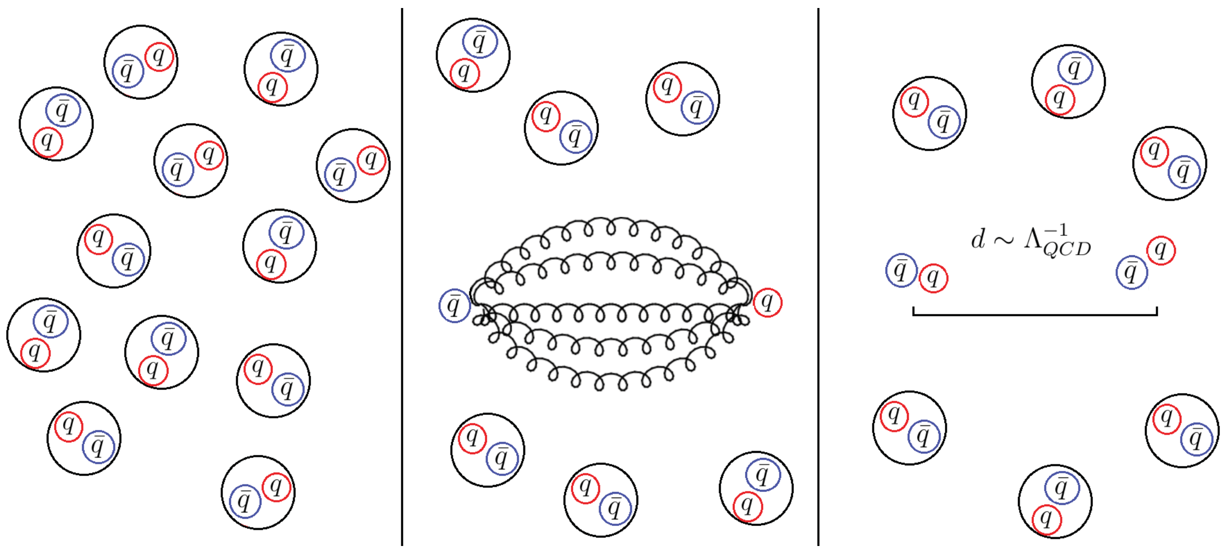

Figure 2.3: A schematic diagram of how confinement and flux tube generation happens in QCD. As a bound state of quarks separates, a pair of matching quarks is popped out of the vacuum when $d \sim \Lambda_{QCD}^{-1}$

An interesting property of the strong interactions not observed elsewhere in nature is quark confinement. Quark confinement is the statement that only colour neutral states may appear in nature. A meson is a bound state of quarks consisting of a quark-antiquark pair. One may imagine attempting to separate the two quarks in a state so that they are free from one another, but it turns out that the two remain connected by what is known as a gluon flux tube. This flux tube is merely a constant interchange of gluons between the two particles, and the energy of such a tube scales with the distance between the two quarks. As the distance between the quarks reaches Λ_{QCD}^{-1} (the inverse of the confinement scale of QCD), it becomes energetically favourable to pop a new quark-antiquark pair out of the vacuum. This process is what creates jets of particles detected in colliders.

Because of the composite states that quarks live in at collider energies, parton models of the proton and electron are commonly used to compute scatterings requiring QCD. This formalism will be reviewed later on in the context of a composite dark matter model. As primary motivation, since gluons interact with themselves, there are hypothetically a number of composite states made up purely of these gauge bosons. These composite states are referred to as glueballs, and are commonly distinguished based on their quantum numbers, J^{PC} (angular momentum, parity, and charge parity). Due to mixing with meson states, [12], glueballs are extremely challenging to detect in collider experiments, and as such have no been experimentally confirmed thus far.

2.1.6 Decay Rates and Cross Sections

Now that we have discussed the gauge structure that makes up the standard model, we turn our attention towards perhaps a more practical side, that of computing observables. Feynman diagrams are generally used to computed amplitudes, $\mathcal{M}$, which are then used to compute the observables themselves. QFT is conventionality defined in a way which gives rise to Feynman rules, or ways to bridge between the graphical interpretation of an interaction and the mathematics it encodes. These Feynman rules are usually intuitively read from the terms with field couplings. For example, the QED expanded Lagrangian is

$$\mathcal{L}_{QED} = \bar{\psi}(i\gamma^{\mu}\partial_{\mu} - m)\psi - \frac{1}{4}F^{\mu\nu}F_{\mu\nu} - e\bar{\psi}\gamma^{\mu}A_{\mu}\psi \tag{2.29}$$

The interaction vertex is easily read off from the term with two spinor fields and the one gauge field, such that

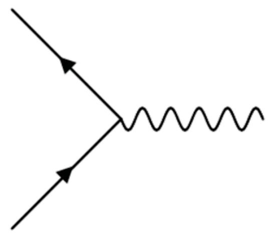

Figure 2.4: Feynman rule for the interaction vertex in QED

Now the other kinetic terms in the Lagrangian go into defining quantities such as the propagators (amplitude for a particle to go from the spacetime point μ to ν for example) of our fields. A derivation of all these Feynman rules will be left to the textbooks, even though we will quote values of propagators and vertex factors throughout this work. Suffice to say that knowledge of these rules is necessary to compute the probability amplitude, $\mathcal{M}$.

On a similar note, the derivation of differential cross sections is involved and will also be left to textbooks. First, let us present the general formula for the cross section of a $2 \rightarrow n$ particle scattering [1] [13]

$$\begin{aligned} d\sigma = \frac{1}{2E_A 2E_B |v_A - v_B|} \left(\prod_{f=1}^{n} \frac{d^3 p_f}{(2\pi)^3} \frac{1}{2E_f} \right) |\mathcal{M}(p_A, p_B \rightarrow p_1 + p_2 + \ldots p_n)|^2 \\ \times (2\pi)^4 \delta^{(4)}(p_A + p_B - p_1 - p_2 - \ldots p_n) \end{aligned} \tag{2.30}$$

For certain interactions with certain symmetries, though, simple analytic expressions exist. For example, in the centre of mass frame of a $2 \rightarrow 2$ scattering problem, the differential cross section becomes

$$\left(\frac{d\sigma}{d\Omega} \right)_{CM} = \frac{1}{2E_A 2E_B |v_A - v_B|} \frac{|\mathbf{p}_1|}{(2\pi)^2 4E_{cm}} |\mathcal{M}(p_A, p_B \rightarrow p_1, p_2)|^2 \tag{2.31}$$

Where particles A, B are the incoming state, and $1, 2$ are the outgoing. A further simplification occurs when we set all the masses of the incoming and outgoing particles identical to each other

$$\left(\frac{d\sigma}{d\Omega}\right)_{CM} = \frac{|\mathcal{M}|^2}{64\pi^2 E_{cm}^2} \tag{2.32}$$

Decay rates can almost be viewed as a simplification of the cross sectional formula, where the initial phase space only contains one particle. Without invoking any real symmetry arguments (other than being in the rest frame of the decaying particle), the decay rate of one particle into n is given by

$$d\Gamma = \frac{1}{2m_A}\left(\prod_{f=1}^{n}\frac{d^3p_f}{(2\pi)^3}\frac{1}{2E_f}\right)|\mathcal{M}(m_A \to p_1+p_2+\ldots p_n)|^2(2\pi)^4\delta^{(4)}(p_A-p_1-p_2-\ldots p_n) \tag{2.33}$$

For the simple and more common case of only two final state particles, it is straightforward to show that the differential decay rate is

$$\left(\frac{d\Gamma}{d\Omega}\right)_{1\to 2} = \frac{|\mathbf{p}|}{32\pi^2 M^2}|\mathcal{M}(M \to p_1, p_2)|^2 \tag{2.34}$$

Where M is the mass of the decaying particle, and $\mathbf{p}$ is the 3-momentum of either of the two final state particles, since they must be equal.

2.2 Effective Lagrangians

From the previous section, it is clear that the Lagrangian is a natural starting point for computing observable quantities in quantum field theory. The notation can be cumbersome, however, and good approximate methods have been developed for calculating quantities both within the standard model, and beyond it. A particularly crucial idea in Lagrangian building is that of an energy scale [2] [14].

As it stands thus far, the Lagrangian for the standard model is an accurate descriptor of the strong, weak, and electromagnetic forces that we observe phenomenologically. However, it doesn't scratch the surface on anything gravitationally related, and there is always the possibility that new effects could be discovered as we probe higher energy scales in colliders. By this, we know that $\mathcal{L}_{SM}$ cannot be what is called 'UV complete', as we don't know (but assume) that it doesn't capture the higher energy degrees of freedom that exist within nature. This is what is meant by an energy scale.

2.2.1 The Effective Lagrangian of Weak Interactions

First, to develop an intuition for effective Lagrangians, and to appreciate their power as an approximative tool, we will look at what happens in particle physics at a scale much lower than the scale of the W boson. This is often referred to as the Fermi theory. We closely follow some of the ideas presented in [2].

Consider the amplitude for the decay of a τ particle into two fermions, and a τ neutrino. This decay amplitude may be written as

$$\begin{aligned}\mathcal{M}(\tau \to \nu_\tau \bar{f}_m f_n) = e_W^2 U_{mn}^* [\bar{u}_\nu(\mathbf{l})\gamma^\mu(1+\gamma_5)u_\tau(\mathbf{k})][\bar{u}_n(\mathbf{p})\gamma^\nu(1+\gamma_5)v_m(\mathbf{q})] \\ \times \left[\frac{\eta_{\mu\nu} + (k-l)_\mu(k-l)_\nu/M_W^2}{(k-l)^2 + M_W^2}\right]\end{aligned} \tag{2.35}$$

Where e_W is the weak coupling, U is related to the quark mixing matrix, the u, v are incoming and outgoing spinors, and the last term is the W boson propagator. As usual, the bolded l, k, p, q terms represent the momenta of the particles.

In an effective theory below the W mass, we are left with all the standard fermion content, modulo the top quark. If we turn our attention to the propagator, we see that because of the low masses and momenta of the fermions compared to the W, we can introduce a simplification

$$\frac{\eta_{\mu\nu} + (k-l)_\mu (k-l)_\nu / M_W^2}{(k-l)^2 + M_W^2} \sim \frac{\eta_{\mu\nu}}{M_W^2} + \mathcal{O}(M_W^{-4}) \tag{2.36}$$

Since $M_W >> m_f$, it is appropriate to just keep the lowest order term in the expansion. Using this expression yields an amplitude

$$\mathcal{M}(\tau \to \nu_\tau \bar{f}_m f_n) = \frac{e_W^2}{M_W^2} U_{mn}^* [\bar{u}_\nu(\mathbf{l}) \gamma^\mu (1+\gamma_5) u_\tau(\mathbf{k})][\bar{u}_n(\mathbf{p}) \gamma_\mu (1+\gamma_5) v_m(\mathbf{q})] \tag{2.37}$$

The difference now, is that before in equation (2.35) we had to make use of three vertex Feynman rules for weak interactions, as well as a W propagator to determine this amplitude. Now, the expansion in M_W^2 has masked our propagator in such a way that we say the particle is 'integrated out'. Using this approximation, we are able to construct a simple, effective interaction that encodes the 4-point interaction of a $\tau \to \nu_\tau f_m \bar{f}_n$ without even recognizing the existence of the W boson, but instead having its effects encoded in the coupling term. Such an interaction term would look like

$$\mathcal{L}_{\tau \to \nu_\tau f_m \bar{f}_n} = -\frac{e_W^2}{2M_W^2} U_{mn}^* [\bar{\nu}_\tau \gamma^\mu (1+\gamma_5) \tau][\bar{f}_n \gamma_\mu (1+\gamma_5) f_m] \tag{2.38}$$

and would be included in this low energy description for the weak interactions.

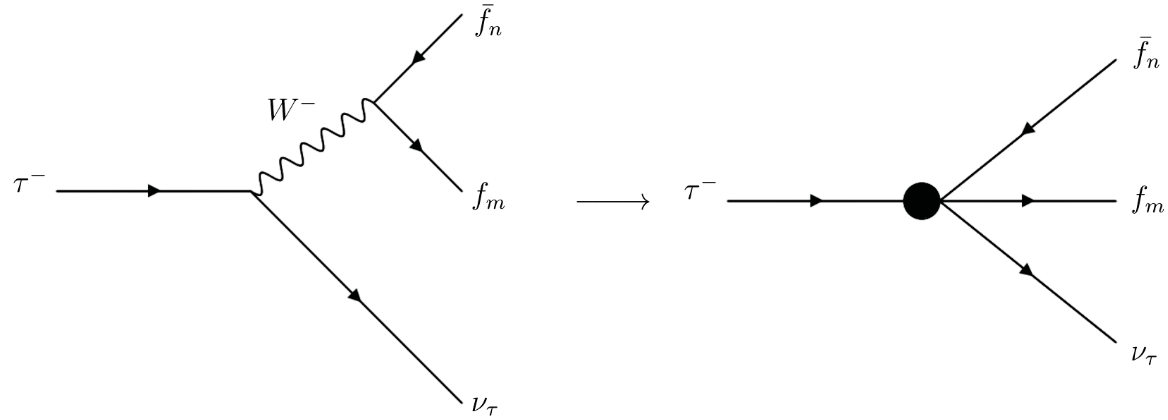

Figure 2.5: The schematic collapse of a Feynman diagram when using an effective Lagrangian. None of the initial or final state particles are altered, just the mathematical computation. Note the black circle is meant to emphasis that a propagator has been removed

Since many interactions in the standard model have light initial and final states mediated by the exchange of a W boson, it is possible to generalize this interaction Lagrangian to all such processes. Generally speaking, the W boson mediates weak processes that involve the exchange of electric charge, and couples to other light particles by way of a charged current Lagrangian,

$$\mathcal{L}_{cc} = e_W W_\mu^- C^\mu + h.c. \tag{2.39}$$

Where C^μ is a term that couples the charged interactions between fermions in the standard model (see [2] for more details). Replacing the W boson interaction yields

$$\mathcal{L}_{cc,eff} = \frac{e_W^2}{M_W^2} C^\mu C_\mu^* \tag{2.40}$$

The same can be done for the Z boson exchange in neutral current interactions, yielding

$$\mathcal{L}_{nc,eff} = \frac{e_Z^2}{2M_Z^2} N^\mu N_\mu \tag{2.41}$$

Where N_μ is the associated neutral coupling between standard model fermions. Finally, we can write a total effective Lagrangian for weak interactions below the W scale as

$$\mathcal{L}_{weak,eff} = \mathcal{L}_{cc,eff} + \mathcal{L}_{nc,eff} \tag{2.42}$$

If we were to extend our theory not just to those of weak interactions, but of the standard model in general, we would have to include effective interactions of other heavy particles such as the Higgs as well.

2.2.2 Effective Lagrangians Beyond the Standard Model

Now that we have seen how effective field theories can be implemented into the standard model, lets attempt to use these techniques as a way to probe physics that does not quite fit into the standard paradigm. This framework is particularly useful in constructions of particle dark matter, where any standard model couplings must be highly suppressed to satisfy experimental constraints.

Oftentimes, we define such a scale, Λ, as the point up to which our theory is defined. Above that, the details of the theory may be obfuscated by a lack of information on our system, so we construct an effective Lagrangian which can parametrize our ignorance in a sense, and help give predictions. Within the standard model, this can be a useful approximative tool. For example, the low energy description of QCD can be written in terms of mesons in such a way that calculations can be easily done without losing much information on the underlying composite structure of the bound state. At higher energy scales, this description must be discarded and we must once again return to the $\mathcal{L}_{QCD}$ that we discussed earlier. Another advantage is looking beyond the standard model, by introducing new (suppressed) interactions between a hidden dark sector and the standard model, we can make phenomenological predictions which may help narrow our search for an elusive dark matter candidate.

The general recipe is as follows; imagine you have some Lagrangian describing a physical process. For the sake of argument, lets say thats its scalar QED as we wrote above. As a reminder, the Lagrangian for this theory was

$$\mathcal{L}_{s-QED} = -\frac{1}{4}F^{\alpha\beta}F_{\alpha\beta} - D_\mu\phi^* D^\mu\phi - m^2\phi\phi^* \tag{2.43}$$

Now imagine that we discover in the far future that some other particle couples to our field ϕ in the theory, with an extremely small probability. This can be interpreted as having a very small coupling between the sectors. If we introduce this new field χ and couple it to the scalar in the form of a 4-point function, we would imagine equation (2.35) as the effective theory of a more complete Lagrangian, namely

$$\mathcal{L}_{s-QED} = -\frac{1}{4}F^{\alpha\beta}F_{\alpha\beta} - D_\mu\phi^* D^\mu\phi - m^2\phi\phi^* - \lambda\phi\phi^*\chi^2 \tag{2.44}$$

Now from dimensional analysis, the scalar field ϕ has mass dimension of M, since our Lagrangian must possess mass dimension 4. Indeed, all bosonic fields possess mass dimensions of M, while fermions have $M^{3/2}$. If our χ particle is a boson, no further amending is necessary. Due to the restriction on the dimension of the Lagrangian density, however, if χ is a fermion (or a vector-like fermion, as is popular in dark matter models), we can explicitly write the mass effective Lagrangian as

$$\mathcal{L}_{s-QED} = -\frac{1}{4}F^{\alpha\beta}F_{\alpha\beta} - D_\mu\phi^* D^\mu\phi - m^2\phi\phi^* - \frac{\lambda'}{M}\phi\phi^*\chi^2 \tag{2.45}$$

Where the couplings are suppressed by the scale of this interaction. If this scale is high, it gives an intuition between why these interactions take place so infrequently; the coupling is highly suppressed!

The inverse process can also be done, where you introduce some new coupling that is suppressed by a mass scale, and determine the observations that should arise from this new interaction. This can then be compared with data and then either accepted as a new interaction (almost never), or ruled out (almost always).

2.3 The Thermal History of the Universe

The setting of many of the particle interactions we wish to study is much different than what we observe here on earth. Indeed, almost all the effects mentioned above have been worked out for nice, vacuum-like conditions. In order to introduce new extensions to the standard model which may describe dark matter, we need to talk about not only their properties today, but how they evolved throughout the thermal evolution of the universe. It turns out that a great many constraints on new particles come from cosmologically based surveys, so it seems only prudent to go into a little bit of detail on the standard paradigm of the evolution of our universe. This section takes inspiration from a number of enlightening textbooks and papers [15] [16] [17] [18] [19]. In this section we aim to present a review of this material, by going roughly chronologically and speaking more specifically about different parts of the theory that can provide constraints on early time dark matter.

2.3.1 Cosmological Preliminaries

Before we begin, let us make some remarks on the mathematical framework cosmology is usually worked out in. The standard big bang picture that we will discuss below, along with observations on the large scale homogeneity and isotropy of the universe, allow us to assume a very simple metric

$$ds^2 = dt^2 - a^2(t)\left[\frac{dr^2}{1-\kappa r^2} + r^2(d\theta^2 + sin^2\theta d\phi^2)\right] \tag{2.46}$$

This is the Friedmann-Robertson-Walker metric and describes the geometry of spacetime with very few parameters. Here, $a(t)$ represents the scale factor, which grows with time, and κ represents the spatial curvature of the universe ($\kappa = -1$ for a hyperbolic universe, $\kappa = 0$ for a flat one, and $\kappa = +1$ for a spherical universe). Experimental data suggests that κ is very close to 0. The well known Hubble parameter, $H(t)$ is determined by $\dot{a}(t)/a(t)$.

With the basic structure of spacetime specified, Einstein's equations can be solved to yield the Friedmann equations. Assuming the matter in the early universe can be modelled by a perfect fluid, the energy-momentum tensor is given by

$$T_{\mu\nu} = -pg_{\mu\nu} + (p+\rho)u_\mu u_\nu \tag{2.47}$$

Where u is a velocity vector for our fluid in co-moving coordinates, p and ρ are the pressure and energy density of the fluid respectively. Einstein's equations (without a cosmoogical constant term) are

$$\mathcal{R}_{\mu\nu} - \frac{1}{2}g_{\mu\nu}\mathcal{R} = 8\pi G_N T_{\mu\nu} \tag{2.48}$$

Where $\mathcal{R}$ is the Ricci scalar, and $\mathcal{R}_{\mu\nu}$ is the Riemann tensor, both defined by the FRW metric above. From these two expressions, it is possible to construct the Friedmann equations which describe the dynamics of the universe

$$
\begin{aligned}
H^2 = \left(\frac{\dot{a}}{a}\right)^2 &= \frac{8\pi G_N \rho}{3} - \frac{\kappa}{a^2} \\
\frac{\ddot{a}}{a} &= -\frac{4\pi G_N}{3}(\rho + 3p)
\end{aligned}
\tag{2.49}
$$

Assuming a curvature parameter of 0, density parameters for each of the three major species of energy content can be determined.

$$
\Omega_m = \frac{\rho_m}{\rho_c} \qquad \Omega_{DM} = \frac{\rho_{DM}}{\rho_c} \qquad \Omega_\Lambda = \frac{\rho_\Lambda}{\rho_c} \tag{2.50}
$$

Where $\rho_c = 3H^2/8\pi G_N$ is the necessary energy density required for a flat universe. From observations, it seems that $\Omega_m + \Omega_{DM} + \Omega_\Lambda \approx 1$, or $\rho \approx \rho_c$. Note that we have excluded the energy density of relativistic species such as photons, as their contribution to the total energy density is negligible at late times. As a final note, we mention that the Friedmann equations are also useful to probe the scaling of the Hubble parameter as a function of time (temperature).

2.3.2 Thermodynamics and Particle Interactions

Before jumping into the interactions that particles undergo in the presence of an expanding, thermal background, let us review a few basic thermodynamic properties. In the early universe, the primary energy content was photons, hence this era is known as the radiation dominated epoch. First, lets note that it is straightforward to write the equilibrium energy density and pressure of a particle species

$$\begin{aligned} \rho_i &= \int E_i dn_{q_i} \\ p_i &= \frac{1}{3}\int \frac{q_i^2}{E_i} dn_{q_i} \end{aligned} \tag{2.51}$$

Where dn_{q_i} is the number density of a species, and follows the Fermi or Bose distribution depending on its spin

$$dn_{q_i} = \frac{g_i q_i^2 dq_i}{2\pi^2 \left(e^{(E_{q_i}-\mu_i)/T_i} \pm 1\right)} \tag{2.52}$$

The q_i are related to the energy of the species by $E_{q_i}^2 = m_i^2 + q_i^2$, and μ_i is the chemical potential of the species. In the radiation dominated epoch, the energy density of relativistic species is

$$\rho_{rel} = \frac{\pi^2}{30} g_*(T) T^4 \tag{2.53}$$

In this final definition, g_* refers to the number of degrees of freedom of the particles species that are still relativistic. In a thermal bath, a particle is said to be relativistic if $T > m$, so we see that as the universe cools g_* will drop as particles become nonrelativistic.

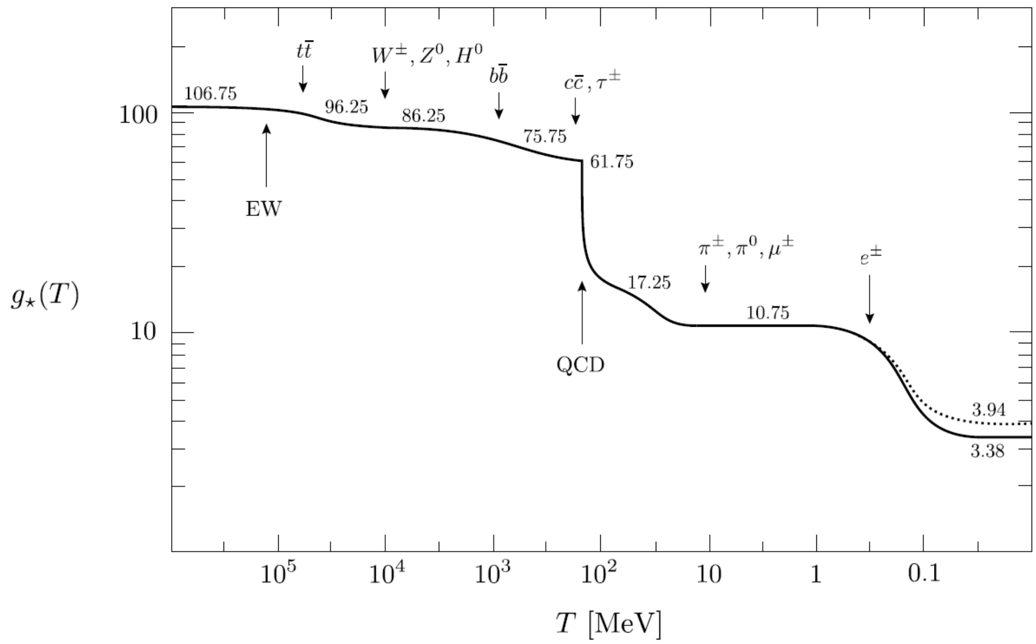

Figure 2.6: The evolution of g_* as the universe cools. Different temperatures mark where certain species become non-relativistic. Figure from [15]

We should also note that the effective degrees of freedom g_* are defined as $g_* = \sum_b g_b + \frac{7}{8}\sum_f g_f$, so fermions contribute less than bosons to this quantity. Note that the introduction of new particles above standard model masses will give a different evolution of this quantity at high temperatures.

Now, in understanding particle interactions in such a background, the idea of particle number freeze out (decoupling) from the thermal bath becomes important. In a naive realization, decoupling occurs when the rate of particle interactions falls below the Hubble expansion rate of the universe ($\Gamma < H$). The physical motivation for this is that once the universe is expanding fast enough, particles that would like to interact can no longer find each other at an efficient rate, and so the interactions effectively 'freeze out'. We will consider the more elegant method of using the Boltzmann equation to solve this problem of particle number freeze out in the next chapter.

To briefly illustrate the freeze out process, imagine you have a particle whose only interactions are $2 \to 2$ scatterings mediated by the weak force. If we assume these interactions take place at low energy scales (say, lower than the mass of the $W^{\pm}, Z$ bosons), we can use our effective Lagrangian approach to estimate the cross section. From dimensional analysis, we first note that σ has units of distance squared, and hence in our 'god-given' units this means that $\sigma \sim T^{-2}$. From equations (2.43) and (2.44), we can make the estimate for the cross section to be

$$\sigma \sim \frac{e_{W,Z}^4}{M_{W,Z}^4} T^2 \tag{2.54}$$

The rate of interactions is usually defined as $\Gamma \sim n\sigma v$ where n is the number density of the particles, and v is their average velocity. Setting $v \sim c$ and noting $n \sim T^3$. Dimensional analysis also provides us with $H \sim T^2/M_{Pl}$, and so fitting all of these together gives us a condition on the freeze out temperature of a weakly interacting particle

$$\frac{\Gamma}{H} = \frac{e_{W,Z}^4 M_{Pl}}{M_{W,Z}^4} T^3 \sim \left(\frac{T}{1MeV}\right)^3 \tag{2.55}$$

This implies weakly interacting particles decouple from the thermal bath at a temperature of around $1MeV$.

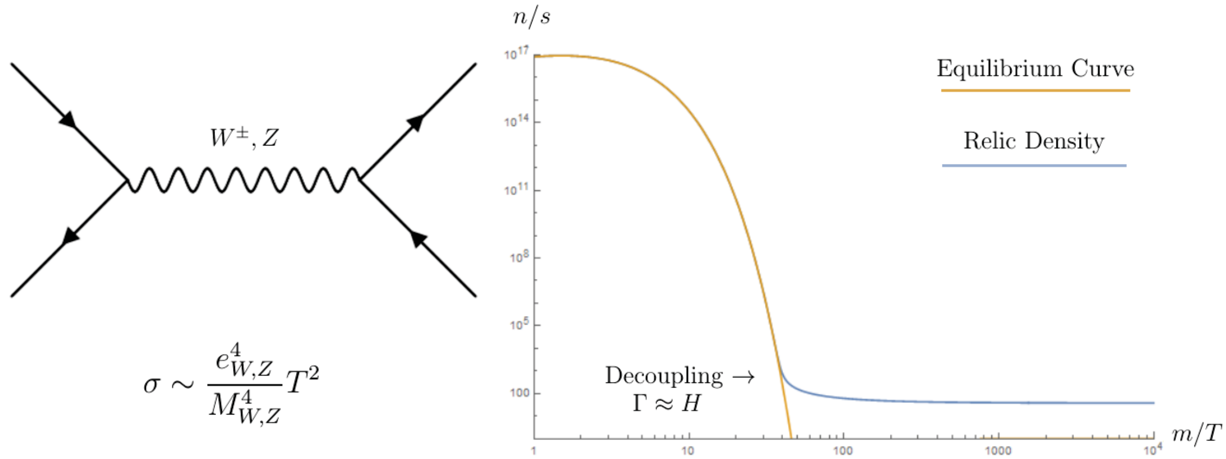

Figure 2.7: Tracking the (comoving) abundance of a weakly interacting particle species before and after decoupling from the primordial plasma

As we can see, the longer a species stays in equilibrium with the photon bath, the more exponential suppression it undergoes and therefore the lower its final number density.

2.3.3 The Thermal History: A Timeline

To finish off this section, it seems worthwhile to at least mention the different phases of the universe during its evolution from the supposed 'big bang' to now. We will label different events by the temperature of primordial photons, rather than time as is standard convention.

Though the big bang is the most popular idea of how the universe started, its introduction of a singularity causes some discomfort amongst physicists. Non-singular alternatives have been developed from string theory origins [20], as well as from a nonsingular bounce where the universe went from contracting to expanding [21]. Now we know that the universe appears to be homogenous and isotropic on large scales, but how can we get such a natural smoothness on large scales naturally? If you observe cosmic microwave background (CMB) photons, you notice that they are nearly uniform in temperature across the whole sky, but this seems very unlikely since the causal cone of CMB photons is of the degree scale. Inflation provides a solution to this problem, as well as a couple others that pop out of inconsistencies between early time and late time physics models. Inflation is a phase of the universe where the universe expands at an exponentially fast rate, allowing early time photons to be in causal contact with each other in the late universe today. This phase is generally driven by a scalar field, and it is the decay of this scalar field that is thought to source all standard model particles (and perhaps dark matter as well).

After inflation, we must find some way to introduce an imbalance between baryons and antibaryons. Such a process is called baryogenesis, and while many models have been studied to source this effect, none has so far been given preference from observations. After this, the universe cools and as it hits $T \sim 150GeV$, it undergoes the electroweak phase transition. This is where the spontaneous symmetry breaking of the Higgs takes place (as described in the section 2.1.4). Here, particles acquire their mass via the Higgs mechanism, and the electromagnetic and weak forces decouple from one another. The underlying gauge structure of the standard model breaks from

$$SU(3) \times SU(2)_L \times U(1)_Y \xrightarrow{\text{EWSB}} SU(3) \times U(1)_{em} \tag{2.56}$$

After this, the QCD phase transition takes place, at which point the strong nuclear force becomes 'strong' and quarks get bound together to form Hadrons. This transition greatly reduces g_*, as indicated in the plot above since the number of relativistic degrees of freedom in the system greatly decreases. This happens around $T \sim 150MeV$. Many different types of particle species freeze out after this point, until we reach the era of big bang nucleosynthesis. During this phase, ionized hydrogen fused with itself in order to create heavy nuclei, such as helium and deuterium. BBN takes place around $T \sim 100keV$ and limits on the observed abundances of these different elements is highly constraining to models which interact with the standard model prior to this time.

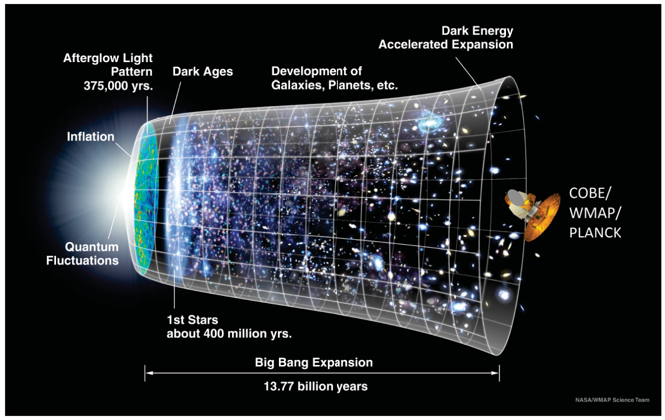

Figure 2.8: A schematic illustration on the relative evolution of the universe from the big bang to the present [22]

Arguably one of the most observable effects of the standard cosmological model is that of recombination, which takes place around $T \sim 0.25eV$. During recombination, the soup of free electrons and ionised hydrogen are finally able to recombine without photons to reionize them. This happens as the cosmological redshift of the expansion of the universe weakens the energy of each photon, to the point where they have $E_\gamma < E_{bind}$ for neutral hydrogen. With the primordial soup now electrically neutral, photons free stream from the last scattering surface, all the way to us today. These photons make up the CMB, and contain a wealth of information related to the evolution of the universe. Studying the temperature anisotropies, polarization schemes, and spectral distortions have led to many constraints on primordial physics. After this, structure eventually begins to form in the universe, and finally we evolve to the current time-slice of cosmology in front of us today.

Chapter 3

Relic Densities and the Dark Matter Paradigm

The observable universe is well described by particle cosmology thus far, but curiously, it seems that most of the content of the universe remains unobservable. In fact, a combination of galactic mass surveys, as well as the determination that the universe is roughly flat forces us to postulate the existence of exotic physical quantities. Dark energy is slated to make up about 70% of the universes mass-energy budget, and supplies a sort of negative pressure to the universe, preventing its closure. Dark energy is very strange, as it also possesses an energy density that does not dilute as the universe expands. While a fascinating subject to study, we will not consider it further, and instead step away to the other poorly described phenomenon in cosmology, dark matter.

Of the remaining mass-energy budget, ordinary baryonic matter makes up roughly 5%, and dark matter the final 25%. All of the complex scaffolding we have created to describe physics only accurately describes about 5% of the universe. Evidently we have a lot of work to do if we want to have any hope of coming up with a more complete description of physics.

Velocity rotation curves offer a compelling source of evidence for the existence of dark matter [23]. From Newton's laws it is easy to find that the rotational speed of a star that is a distance R away from the centre of the galaxy should fall off as $v_R \propto R^{-1/2}$ if the mass is localized to the centre. As the first few papers measuring this in the late 1970s found [24] [25], this was not the case. Instead, the velocities seemed to flatten out, implying a linear scaling between the enclosed mass and distance from the centre.

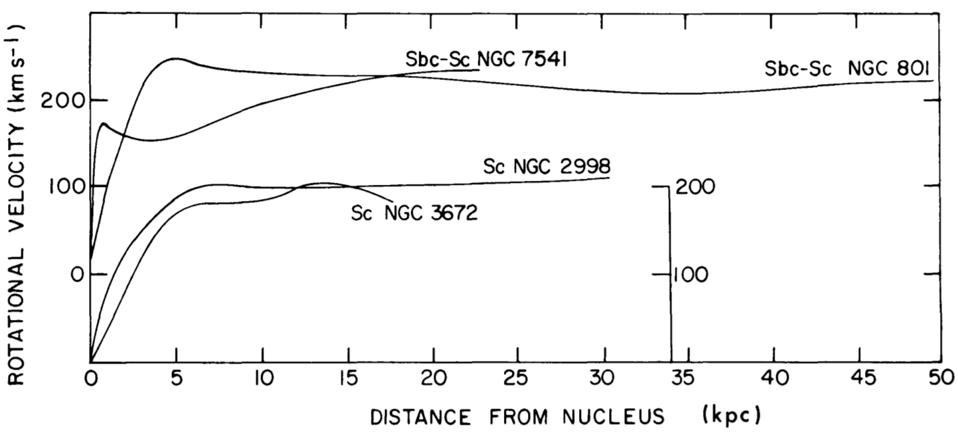

Figure 3.1: The rotational velocity of stars in spiral galaxies observed via $21cm$ astronomy. Figure taken from [25]

This observation led to the speculation that a non-visible form of matter must be lurking in clumpy, halo-like structures around galaxies. Afterwards, more observational effects of dark matter where detected via gravitational lensing, as well as in the power spectrum of the CMB. The main purpose of this work is to develop a consistent mathematical framework to describe the nature of this mysterious form of matter.

3.1 Dark Matter Candidates

In this section we will review a few of the possible explanations of dark matter, and illustrate how smoothly WIMP dark matter fits into the cosmological framework. Before we get there, however, let us first parse through a few creative solutions to the mystery of dark matter. The criteria for a (non-baryonic) dark matter candidate is that they must be stable on cosmological time scales, must have highly suppressed interactions with photons, and have to possess the observed relic density in the universe today. Baryonic dark matter is very heavily constrained by the observed abundances of light elements such as helium and deuterium [26], with constraints strengthened by recent the recent Planck satellite results [27].

3.1.1 Primordial Black Holes

Black holes forming in the early universe (called 'primordial' black holes in the literature) have been proposed as a possible source of dark matter [28]. Primordial black holes are created not due to collapsing stars as in the usual astrophysical picture, but due to large density fluctuations in the very early universe much before star formation began taking place.

Primordial black holes can hypothetically be of any mass, since they do not require core collapse to be formed [29]. The existence of Hawking radiation bounds the mass from below, however, as black holes with $m_{PBH} < 10^{15}g$ would have evaporated by this time [30]. In fact, the currently unexplained gamma ray bursts originating from the centre of galaxies can further constrain this lower bound. On the opposite side, large mass PBHs are heavily constrained due to the weak lensing signatures that they would introduce. These constraints fit us in a window of

$$10^{17} g < m_{PBH} < 10^{24} g \tag{3.1}$$

A recent paper also suggests that black holes in this mass range are ruled out due to the fact that old neutron stars still exist today in regions with high ρ_{DM}. Old neutron stars in this environment should have gravitationally captured some of these PBHs, in which case they (the neutron star) would be destroyed by the rapid accretion of matter into the black hole [31]. While the idea of PBHs is well physically motivated, their role as a dominant constituent of dark matter seems to be dwindling.

3.1.2 Axion Dark Matter

Axions are a hypothetical particle thought to give rise to the CP violation in QCD. Recall the CP violating term in the QCD Lagrangian

$$\mathcal{L}_{QCD} \subset \frac{n_f g^2 \theta}{32\pi^2} F_{\mu\nu} \tilde{F}^{\mu\nu} \tag{3.2}$$

In non-Abelian gauge theories, potentials have disjoint sectors which are accessible to one another via quantum tunnelling [32]. Because of this, the vacuum state becomes a superposition of different configurations of the minima of these potentials, which we classify by a winding number, n, labelling the minima of each disjoint sector, and θ which describes the QCD vacuum. n is the topological winding number. The vacuum configuration of QCD is labelled as

$$|\theta\rangle = \sum_n e^{-in\theta} |n\rangle \tag{3.3}$$

This θ parameter is then related to the quark mass mixing matrix $\mathcal{M}$ by $\bar{\theta} = \theta - \arg\det\mathcal{M}$, and $\bar{\theta}$ is interpreted as a dynamical field in the Peccei-Quinn solution to this strong CP problem [33] [34]. In more detail, the smallness of the θ parameter is a result of the axion field $\bar{\theta}$ relaxing to the bottom of its potential which is not quite zero due to the chiral symmetry of the standard model being broken by the masses of quarks.

Axion production in the early universe can take place by mechanisms such as vacuum realignment [35], or cosmic string decays [36]. The vacuum misalignment mechanism is one in which the axion field initially has a value not near its potential minimum. When this is the case, the field coherently oscillates around its nearest minimum, which acts as an efficient way to dissipate energy by decaying into other particles. This puts the axions in a low momentum state in the late time universe, allowing them to be considered as cold dark matter even though they are extremely light. Due to the fact that the vacuum state of QCD is not simply connected once the Peccei-Quinn symmetry is broken, we can also consider the formation of oosmic axion strings. Cosmic strings can form objects called kinks and cusps (specific solutions to the equations of motion from a Nambu-Goto action), which will radiate away parts of their field content when these objects enter the horizon. These axions can provide additional signatures to search for.

These hypothetical particles would be very light, but their abundance could be immense yielding a viable candidate for dark matter. It should be noted that standard constructions of string theory (particularly when compactification occurs) give a large number of axions that could be interpreted as dark matter as well, so there is significant theoretical motivation for the study of such particles.

3.1.3 Weakly Interacting Massive Particles (WIMPs)

Let us briefly mention one last generic type of particle dark matter that is immensely popular within the community. Observationally, we can only be sure that dark matter interacts gravitationally with the rest of the standard model. Strong constraints exist on charged dark matter, so coupling to photons is unlikely, and strong couplings would be thought to be easier to see at particle colliders. Weak interactions, however, are not so heavily constrained and thus can present us with a good channel for phenomenological discovery.

It turns out that for cross sections typical of weak processes, the number changing interactions freeze out at a time in which the remaining number of WIMPs is very nearly Ω_{DM}, the observed density of dark matter in the universe today. This is referred to as the WIMP miracle, and will be reviewed in some detail next section. This coincidental fact makes a very strong claim that dark matter could be weakly interacting.

3.2 The Boltzmann Equation: Determination of Relic Abundances

We turn now to our greatest tool in relating interactions involving dark matter (and other primordial particles), to their relic densities persisting in the universe today: the Boltzmann equation.

If we take the thermal bath of CMB photons to be our background, the evolution of thermodynamical quantities for particles in equilibrium with the photons are simple, they just track that of the photons. After decoupling, the evolution is even more simple, the number density of a species n_s dilutes with the expansion of space, as a^{-3}, and its momenta as a^{-1}.

The difficulty is describing qualities like number density right around the time of decoupling from the photon bath, or when the rate of particle interactions Γ is of the order of the Hubble parameter. The Boltzmann equation does just that, by following the microscopic evolution of the phase space distribution of a particle species, we can determine exactly when it decoupled and how much of it is left today. We follow ideas presented in [15] [16], and present the Boltzmann equation with its application to a WIMP-type dark matter candidate.

3.2.1 Out of Equilibrium Thermodynamics

Without any further ado, let us introduce the collisionless Boltzmann equation

$$\frac{dn_i}{dt} + 3\frac{\dot{a}}{a}n_i = 0 \tag{3.4}$$

This is a rather boring picture, it is simply a reflection of the fact that the number of particles in a volume a^3 is conserved. We can rewrite the left hand side as $\frac{1}{a^3}\frac{d(n_i a^3)}{dt}$. We need to add a collision term in order to determine departures from equilibrium. The most general term we can write (for an $i + a \to y + z$ 2 to 2 particle interaction with) casts the equation as

$$\frac{1}{a^3}\frac{d(n_i a^3)}{dt} = -\int d\Pi_i d\Pi_a d\Pi_y d\Pi_z (2\pi)^4 |\mathcal{M}|^2 \delta^4(p_i + p_a - p_y - p_z)[f_i f_a - f_y f_z] \tag{3.5}$$

Here, we f_i's are the phase space distributions of each type of particle involved, $\mathcal{M}$ is the amplitude of such a scattering process, and we integrate over the phase space momentum as

$$d\Pi = \frac{g}{(2\pi)^3}\frac{d^3p}{2E} \tag{3.6}$$

Where g is the internal degrees of freedom of the species in question. Its typical to redefine a couple quantities to make the calculation more tractable, so we define $Y = n_i/s$ where we recall that $s \sim a^{-3}$, and $x = m/T$ where m will be the mass of our dark matter particle. Y

will represent the evolution of our species in a fixed comoving volume, and x the timescale at which our particle freezes out. While still in thermal equilibrium, the abundance (Y) of a species goes as

$$Y \sim x^{3/2} e^{-x} \tag{3.7}$$

and so only particles that decouple shortly after they become non-relativistic ($m/T \sim 1$)will have an appreciable relic density today due to the exponential suppression. Refer to figure 2.7 for a qualitative picture of the freeze out process. With these substitutions, we can write the Boltzmann equation in the form known as the Riccati equation

$$\frac{dY}{dx} = -\frac{\lambda}{x^2}\left(Y^2 - Y_{EQ}^2\right) \tag{3.8}$$

Here we have absorbed most of the constant terms as

$$\lambda = \frac{2\pi^2}{45} g_{*s}(m) \frac{m^3 \langle \sigma v \rangle}{H(m)} \tag{3.9}$$

The information on the phase space and amplitude of the interaction are encoded in the thermally averaged cross section, $\langle \sigma v \rangle$. We will consider the challenge of evaluating this quantity in the next subsection. We have defined $H(m) = 1.67 g_*^{1/2} m^2/m_{Pl}$, and it is related to the usual Hubble parameter during the radiation dominated phase by $H = H(m)x^{-2}$. The value at which the abundance stops tracking equilibrium (when $Y \neq Y_{EQ}$) depends now on the parameter λ, which is constant over the thermal evolution of the species, with larger values freezing out slower than smaller ones.

At late times (long after decoupling), we know that $Y_{EQ} << Y$, and so we can get a good approximation on the final relic density by setting $Y_{EQ} = 0$ in the Riccati equation.

$$\frac{dY}{dx} \approx -\frac{\lambda}{x^2} Y^2 \qquad (x >> x_f) \tag{3.10}$$

Solving this differential equation and integrating from $x = x_f$ to $x = \infty$ yields the approximate solution for the late time abundance of a particle species

$$Y^{\infty} \approx \frac{x_f}{\lambda} \tag{3.11}$$

3.2.2 Thermal Averaging

Lets switch gears for a moment and consider how to go about computing the thermally averaged cross section for a scattering event, $\langle \sigma v \rangle$ [37]. This thermally averaged cross section times velocity is usually defined as

$$\langle \sigma v \rangle = \frac{\int \sigma v \, dn_1^{eq} dn_2^{eq}}{\int dn_1^{eq} dn_2^{eq}} \tag{3.12}$$

Where $n_{1,2}^{eq}$ are the equilibrium number densities of the initial state particles in a $2 \rightarrow 2$ collision. As a simplifying approximation, consider the equilibrium distributions of the particles to be Maxwell-Boltzmann (neglecting Bose-Einstein/Fermi-Dirac effects). With this simplification, the cross section becomes

$$\langle \sigma v \rangle = \frac{\int \sigma v e^{-E_1/T} e^{-E_2/T} d^3p_1 d^3p_2}{\int e^{-E_1/T} e^{-E_2/T} d^3p_1 d^3p_2} \tag{3.13}$$

Using the relativistic energy momentum equation, as well as the following change of variable

$$
\begin{aligned}
E_+ &= E_1 + E_2 \\
E_- &= E_1 - E_2 \\
s = 2m^2 + 2E_1E_2 &- 2p_1p_2cos\theta
\end{aligned}
\tag{3.14}
$$

We can rewrite the volume element for our integration in a more useful way

$$
d^3p_1d^3p_2 = 2\pi^2 E_1E_2dE_+dE_-ds \tag{3.15}
$$

Integrating the numerator and denominator of equation (3.13) yields us a simple, single integral expression for $\langle\sigma v\rangle$, as found by [37]

$$
\langle\sigma v\rangle = \frac{1}{8m^4TK_2^2(m/T)}\int_{4m^2}^{\infty}\sigma(s-4m^2)\sqrt{s}K_1(\sqrt{s}/T)ds \tag{3.16}
$$

This is the general equation we will use in the next chapter when we compute the thermally averaged cross section of a dark matter species. Note that s is the usual Mandelstam variable $s = (p_1 + p_2)^2$, and so our integration bounds run over all possible momenta of the incoming/outgoing particles. Note that K_1, K_2 refer to modified Bessel functions of the first and second kind. A few of the details of this computation have been reproduced in the appendix of this work.

3.2.3 The WIMP Miracle

Now that we understand the mechanics of the Boltzmann equation, it is time to take a look at the so called WIMP miracle. Since we know the observed dark matter density in the universe today, it is natural to ask the value of $\langle\sigma v\rangle$ necessary to reproduce this abundance.

Recall that the dark matter abundance is specified by $\Omega_{DM} = \rho_{DM,0}/\rho_{c,0}$ where the the 0 subscript refers to quantities at the present day. If we recall $\rho_c \sim 3H^2 M_{Pl}^2$ we can write this as

$$\Omega_{DM} = \frac{m_{DM} n_{DM,0}}{3M_{Pl}^2 H_0^2} = m_{DM} Y^\infty \frac{s_0}{3M_{Pl}^2 H_0^2} \tag{3.17}$$

Where we have replaced the number density of dark matter by its Boltzmann calculated abundance variable, Y, and noting that this comoving abundance is constant after freeze out. Note that the entropy of a collection of species can be written as

$$\begin{aligned} s &= \frac{2\pi^2}{45} g_{*s}(T) T^3 \\ g_{*s} &= g_{*s}^{Th} + g_{*s}^{Dec} \end{aligned} \tag{3.18}$$

Where g_{*s} counts the number of effective degrees of freedom in the entropy, split between particles that are thermally coupled to the primordial plasma, and those that are not. Using this expression for the entropy density, as well as $Y^\infty \approx x_f/\lambda$ from the previous subsection, we are left with

$$\Omega_{DM} = \frac{g_{*s}(T_0) T_0^3 H(m_{DM}) x_f}{m_{DM}^2 \langle \sigma v \rangle g_{*s}(m_{DM})} \frac{1}{3M_{Pl}^2 H_0^2} \tag{3.19}$$

Cleaning this equation up a little bit by plugging in measured values of the temperature, Hubble parameter, and effective degrees of freedom in the standard model today, we can get the suggestive form [15]

$$\Omega_{DM} h^2 \sim 0.1 \frac{x_f}{10} \left(\frac{10}{g_*(m_{DM})} \right)^{1/2} \frac{10^{-8} GeV^{-2}}{\langle \sigma v \rangle} \tag{3.20}$$

The observed dark matter abundance is $\Omega_{DM} \sim 0.1$, and we make note that numerically, freeze out happens at order $x_f \sim 10$, similarly, $g_*(m_{DM})/10 \sim 1$, so in order to reproduce this result we require our cross section to be

$$\langle \sigma v \rangle \sim 10^{-8} GeV^{-2} \sim G_f \cdot 10^{-2} \tag{3.21}$$

Where G_f is the Fermi coupling constant in front of the effective Lagrangians defined in the previous chapter for weak interactions. Since this analysis gives us a cross section typical of a weak scale interaction, it is referred to as the WIMP miracle and puts weakly interacting dark matter in a very favourable position from a model building standpoint.

Similar analysis has also been performed for all known early universe particle species, and it is precisely this that gives constraints on the abundances of light elements produced during big bang nucleosynthesis. The Boltzmann equation is arguably our best tool for constraining new types of particle species in the early universe.

3.3 Towards a Numerical Solution of the Boltzmann Equation

While the semi-analytic solutions of the Boltzmann equation offer good approximations to relic densities, it can be useful to numerically model such solutions for both accuracy, peace of mind, and ease of adjustment of model dependent parameters. While working on some models of dark matter, it became prudent to develop some Mathematica code allowing us to quickly check and scan the parameter space of generic models. In this section we will show the capabilities of this software and analyse its usefulness. A copy of the code has been attached to the appendix for the interested reader.

3.3.1 Numerical Challenges and Features of the Program

The initial idea here was to build a program to solve the Boltzmann equation for a variety of particle freeze out scenarios. While this has been done before, it was deemed a good exercise in numerical computation. Inspiration was taken from [38] in finding a computationally acceptable form of the equation, but not in the application of advanced techniques in Mathematica, nor examples.

As Mathematica has a difficult time handling some large numbers, we recall our previous form of the Boltzmann equation,

$$\begin{aligned} \frac{dY}{dx} &= -\frac{\lambda}{x^2}(Y^2 - Y_{EQ}^2) \\ \lambda = \frac{2\pi^2}{45} g_{*s} \frac{m^3 \langle \sigma v \rangle}{H(m)} &= \frac{s(m)}{H(m)} \langle \sigma v \rangle \end{aligned} \tag{3.22}$$

Where we have defined s in the previous subsection. We use the non-relativistic regime (as we are concerned with cold dark matter exclusively, relativistic forms must be used if considering warm or hot candidates) for our Y_{EQ} since this is the time in which we care to find the relic abundance of the species in question. Therefore we use the form

$$Y_{EQ} = g \left(\frac{mT}{2\pi} \right)^{3/2} e^{-m/T} \tag{3.23}$$

Now, due to Mathematica limitations, it is best to make the additional substitution $y = \frac{s(m)}{H(m)} \langle \sigma v \rangle Y$, which gives the following transformation to our equation and our equilibrium yield

$$
\begin{gathered}
\frac{dy}{dx} = -\frac{1}{x^2}(y^2 - y_{EQ}^2) \\
y_{EQ} = \frac{s(m)}{H(m)}\langle\sigma v\rangle g \left(\frac{mT}{2\pi}\right)^{3/2} e^{-m/T} \approx 0.192 M_{Pl} m \langle\sigma v\rangle x^{3/2} e^{-x}
\end{gathered} \tag{3.24}
$$

The second line here will serve as our initial condition, $y(x=1) = y_{EQ}$ in the solution to the differential equation.

The **NDSolve** method was utilized to solve the Boltzmann equation numerically, with adjustable input parameters m_{DM}, g, and $\langle\sigma v\rangle$. Use of **NDSolve** yields an interpolating function that can be plotted. The asymptotic behaviour of this function is related to the freeze out time, x_f of the dark matter candidate.

```
genericAuto =
 NDSolve[{y'[x] == -1/x^2 ((y[x])^2 - (0.192 mpl m σ x^(3/2) E^-x)^2), y[1] == 0.192 mpl m σ 1^(3/2) E^-1} /.
   {m → 1000, g → 100, σ → 10^-10, mpl → 2.44 * 10^18}, y, {x, 1, 10000}, Method → "Automatic", AccuracyGoal → ∞]
{{y → InterpolatingFunction[ Domain: {1., 1.00×10^4} Output: scalar ]}}
```

Figure 3.2: A code snippet specifying the input parameters to our numerical Boltzmann solver

Mathematica utilizes different methods for solving these equations, and for a reasonable set of parameters (such as those in the above figure), all methods seem to converge upon the same result. However, for a broader range of input parameters of interest from a model building standpoint, most methods appear to fail due to computational difficulties, for example in the limit of small mass, large cross section.

In this regime, our differential equation suffered what is known as a *stiffness* problem. Stiffness is a property of a numerical solver that takes into account the form of the equation to be solved, the method used, the initial condition, and local error tolerances. Equations deemed 'too stiff' return errors and diverge. Often stiffness occurs due to the step size in a numerical solution being too small (I suppose almost like a UV divergence in QFT). By implementing the stiffness-switching method, the solver dynamically changes the step size in order to achieve a convergent solution for our region of interest. The shortcoming is that high variance is introduced into the solution over the 'stiff' parts of the domain.

After numerical tests, the stiff regions occur in the low x regime, before freeze out. Because we are interested in the asymptotics to determine the freeze out temperature and abundance, this was deemed an acceptable solution for a short while. Eventually, a better method was found which reproduced our late-time stiffness-switching results, without the errors for low x values before decoupling of the species. We should note that while this new method, accessed by 'EquationSimplification $\rightarrow$ residual', does not impact the physically important late time results, it is a more secure method. Results of these different methods are presented in the figure below.

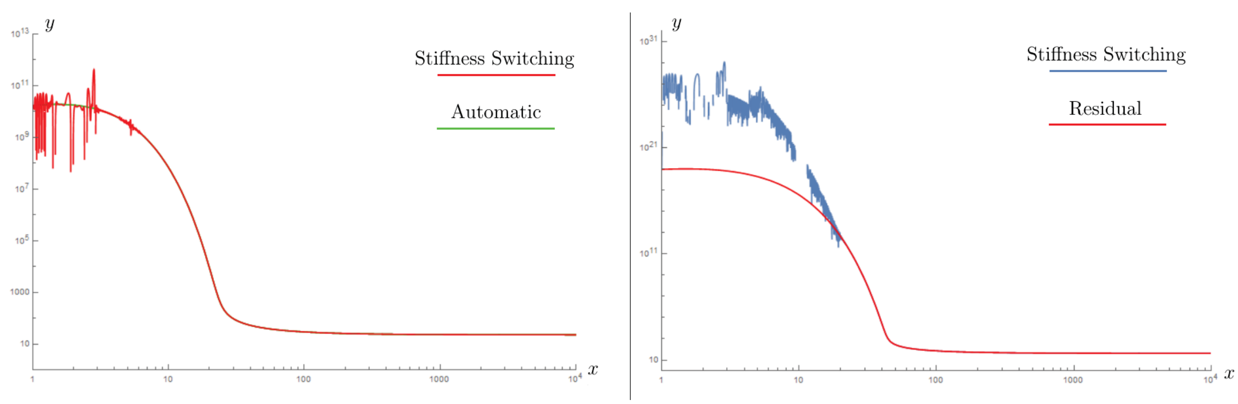

Figure 3.3: Left: The time evolution of a generic dark matter candidate with parameters $(m, g, \langle \sigma v \rangle) \rightarrow (1000GeV, 100, 10^{-10}GeV^{-2})$, comparing between the stiffness switching and automatic methods. No discrepancy exists in the large x regime. Right: A comparison between the residual and stiffness switching method for parameters $(m, g, \langle v \rangle) \rightarrow (1GeV, 10, (0.139)^{-2}GeV^{-2})$, a late-time freeze out particle. The early time stability is easy to see, and is our preferred method for this solver.

This program can be applied to a wide variety of early universe particles, whether hypothetical or not. A full section of the code is presented in the appendix for extended review. We now show the code in action as it computes the freeze out temperature and abundance of baryons in a baryon symmetric universe.

3.3.2 Baryon-Symmetric Universe: An Example

An interesting computation we can do is to determine the baryon relic abundance in a universe that did not undergo baryogenesis. This calculation will give a numerical approach to something done in Kolb and Turner [16], and indeed is the reason we expect a process that introduces asymmetry between particles and antiparticles in general.

The annihilation of a baryon-antibaryon pair takes place via pion exchange, and can be roughly estimated to have a cross section of order $\langle \sigma v \rangle \sim m_\pi^{-2}$. Without assuming any initial asymmetry (as is done when we compute relic abundances of light elements from recombination) we can plug this cross section into our program along with the baryon mass ($\sim 1GeV$), and the number of degrees of freedom in the epoch that this process freezes out ($g \sim 10$).

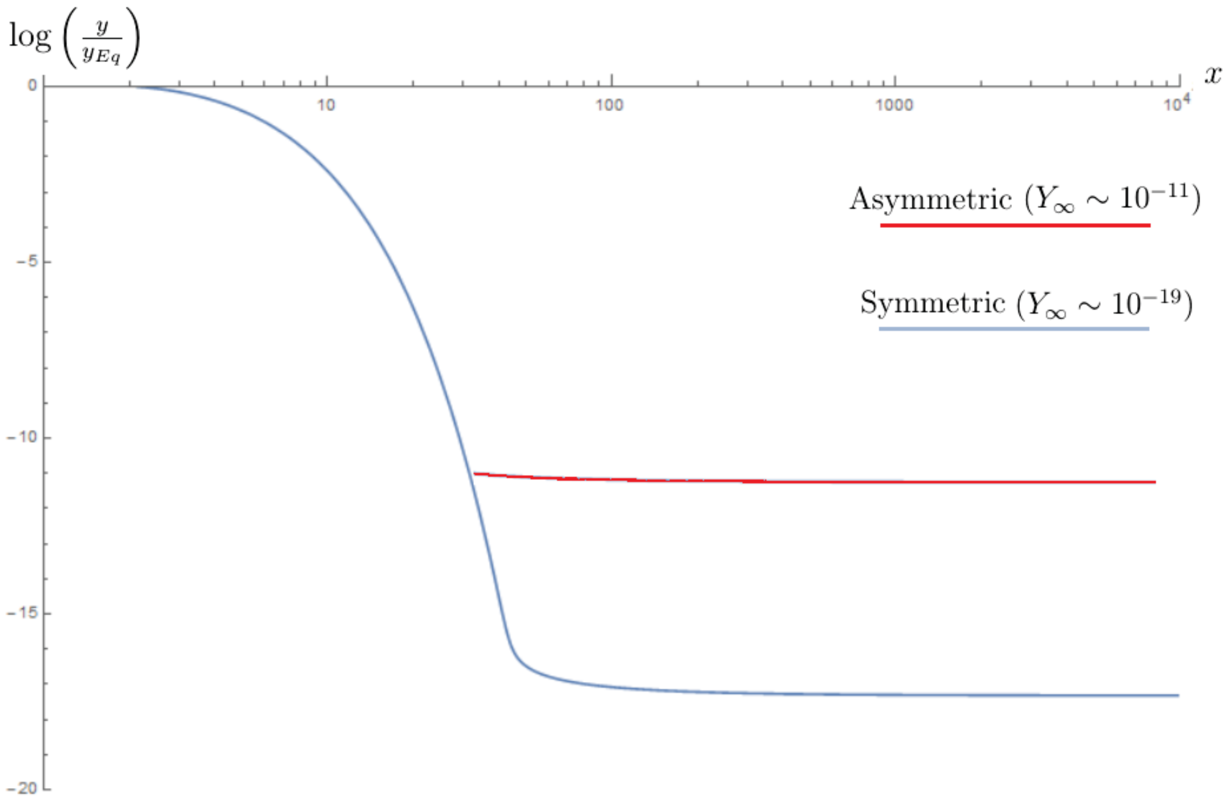

Figure 3.4: A comparison between the baryon to photon ratios in a universe with an initial asymmetry (red), and one without (blue). Note that our program computed the blue curve, the red was added afterwards for visual comparison.

Looking at the asymptotics of this result, we see that freeze out occurs at about $x_f = 42.63$, and gives a final Baryon abundance of about $Y_\infty \sim 3 \cdot 10^{-19}$. The present baryon to photon ratio is well known to be about $\sim 10^{-11}$, and so we can see that without a period of baryogenesis, we generate an abundance about 8 orders of magnitude lower than we see! Indeed, the universe would be very much more empty if this were the case.

3.3.3 Applicability of the Software

As demonstrated, this software offers a reliable and straightforward way to compute freeze out temperatures and relic densities. Results are consistent with computations presented in other textbooks and works, and so this could prove a powerful, yet simple, tool of analysis for these types of calculations.

This code is still in its early stages, and as such there are still many improvements and features that could be implemented. For example, adding the ability to introduce an initial asymmetry in particle species being considered would allow for more robust computations of particles undergoing lepto/baryogenesis. On top of this, having some software that allows for complete analysis of particles that have multiple decay channels could produce more accurate abundances. Finally, in many dark matter models, coupling constants can be allowed to run over a range of values. It should be possible to introduce a coupling variable implicitly in the $\langle \sigma v \rangle$ expression to determine a 'space' of relic densities based on the couplings.

With these improvements implemented, there should be no problem in utilizing this program to compute cosmological features of particle models in a research capacity. The raw code of a few research applications of this work have been included in the appendix for more context.

Chapter 4

$SU(N)$ Glueball Dark Matter

Dark matter model building is a rich subject with a truly staggering number of different theories emerging as plausible candidates to explain the particle cosmological mysteries left in the universe. While theorists have a hard time coming to a consensus on the precise mathematical framework of dark matter, there are a couple properties that seem universal over good candidates

- **Non-baryonic**: If dark matter were made of baryonic particles, many aspects of standard cosmology would be negatively affected. For example, baryonic dark matter would cause more helium, lithium, and other heavy elements to form during BBN, contrary to what is observed astrophysically. This points to a non-baryonic candidate.

- **'Cold'**: High velocity, relativistic dark matter is referred to as 'hot' because its free streaming length is large. Hot dark matter washes out structure on small scales, and as such is typically not thought to be manifest in the true theory of dark matter. Warm and cold dark matter moves more slowly, with free streaming scales on the order of a protogalaxy or less. This allows small-scale structure to form, and eventually clump together into clusters. This small free streaming length is preferable in candidates, and so dark matter is preferred to be cold [39].

We should also mention the interface between dark matter simulations and observations in terms of their halo distributions. Galactic rotation curves seem to predict a large amount of dark matter localized in halos around galaxies. Simulations agree with this, and can even define a density profile for the distribution of dark matter around a galaxy

$$\rho(r) = \frac{\rho_c \delta_c}{\left(\frac{r}{r_s}\right)\left(1 + \frac{r}{r_s}\right)^2} \tag{4.1}$$

This is the NFW profile [40], and here ρ_c is the typical critical density for a flat universe, δ_c is the characteristic density of the galaxy in question, and r_s is the scale radius. This leads to a problem between observations and simulations known as the cusp/core problem ([41]) which we will revisit in the next section. We should mention, however, that it need not be dark matter which causes this discrepancy, as it could be caused by baryonic feedback.

Competitive models of dark matter conform to the above criteria, but this still leaves a wide variety of different theories that could work. The most popular theory is that of WIMP dark matter, since it seems to naturally predict the relic density of dark matter 'by accident', but as we await a detection, it is important to consider other models as well.

When making comparisons to the standard model, one can naturally imagine some rich gauge structure that permeates the dark sector. Abelian extensions to the standard model have been considered and constrained using cosmological data [42]. In the $U(1)$ case, a 'dark photon' is the gauge boson responsible for the relic density of dark matter. In this work we will consider the non-Abelian case, where we have some general $SU(N)$ gauge structure to our theory that describes our candidate. This sector has at most 1 fermion (since $n_f < 11N/2$ for any $N > 1$, the theory is asymptotically free), and so the massless 'dark gluons' in our theory will undergo a confining phase transition and form bound states of glueballs, which give a contribution to the dark matter relic density.

In particle physics, the introduction of a new particle (or particles) is usually accompanied by a Lagrangian of possible couplings between the sectors. In the theory we will consider, we have a pure glue $SU(N)$ dark sector (with gauge bosons known as 'hypergluons'), as well as an auxiliary heavy fermion field (scalar field in the case of Higgs coupling, as will be discussed later), call it Φ. Pure refers the fact that the only fermion content coupling to the $SU(N)$ group is very massive, and thus integrated out at scales $E << M_\Phi$. Therefore, the running of the coupling goes exactly like a theory with α_{HC} containing $n_f = 0$, as in equation (2.27). Our hypergluon field doesn't couple directly with any of the standard model fields, but the Φ field does. We will choose more specific properties of this Φ field, such as its different quantum numbers and couplings, later on as we consider different realizations of this theory. We put the mass of this auxiliary field much higher than the scale at which these interactions will take place, allowing us to use an effective Lagrangian approach. With this mediator field integrated out, the effective Lagrangian coupling the hypergluon to the standard model is given generally by

$$\mathcal{L}_{HC} \sim \frac{\alpha_{HC}}{60M_\Phi^4} tr(H_{\mu\nu}H^{\mu\nu})[c_1\alpha_1 B_{\alpha\beta}B^{\alpha\beta} + c_2\alpha_2 tr(W_{\alpha\beta}W^{\alpha\beta}) + c_3\alpha_3 tr(G_{\alpha\beta}G^{\alpha\beta})] \tag{4.2}$$

$$+ \frac{\lambda\alpha_{HC}}{M_\Phi^2} tr(H_{\mu\nu}H^{\mu\nu})(H^\dagger H) \tag{4.3}$$

Where the HC subscript stand for 'hypercolor', in analogy with the strong $SU(3)$ interaction, and $H_{\mu\nu}$ is the non-Abelian gauge field strength for our hypergluon field. We have put the effective dimension 8 operators coupling to the standard model on the first line, and a dimension 6 operator induced by Higgs couplings on the second line. We will make contact with this effective Lagrangian throughout the chapter. We also note that in a pure-glue hidden theory, the mass of the lightest glueball is related to the confinement scale of this theory by $m_{0^{++}} \approx 7\Lambda_{HC}$ [48] for the case of an $SU(3)$ hidden gauge group. Explicit calculations in this chapter will assume our hidden gauge group is $SU(3)$, as this allows us to make use of quantities calculated from lattice QCD studies (more detail on this below). Note here that Λ_{HC} corresponds the the energy scale at which these free hypergluons become confined in their hypercolour neutral glueball states.

The idea of glueball dark matter is not novel, and has been studied previously in the literature. Authors of [47] studied the freeze-out and relic densities of dark glueballs, discussed the confining phase transition, and discuss semi-quantitatively the effects of different standard model connections. In [50], decay rates of the 0^{++} dark glueball into various standard model particles is mentioned, and the authors of [51] [52] [53] discuss these couplings to the Higgs and other standard model constituents in much greater detail. Also, authors in [54] discuss this same type of model, and also consider constraints on photon production and other mechanisms from line searches, but not on constraints from reheating, which we will study here.

The aim of this work is to both review and discuss the results presented in the aforementioned papers, as well as to consider new constraints that we can set on the model. In particular, we consider specific couplings of our mediator to $U(1)_Y$, $SU(3)_s$, and the Higgs in order to investigate the constraints and potential signals. As well as compiling line search constraints from photons, we also introduce a new, stronger constraint from reheating which severely limits the parameter space of some of these couplings for reasonable values of a reheating temperature under the assumption that the two sectors are never in thermal equilibrium with one another. In the subsection on Higgs couplings, however, we aim mostly to review the semi-quantitative arguments presented in [47][53].

4.1 Non-Abelian Gauge Theories and their Application to Dark Matter

We discussed non-Abelian gauge theories in our section on the strong interaction in chapter 2, so we will just do a quick overview of the important properties. We then describe the formation and properties of glueballs in a pure gauge theory, and finally discuss how we can calculate cross sections and other phenomenological signatures of composite particles using the parton distribution function.

4.1.1 Properties of Non-Abelian Gauge Theories

Perhaps the most surprising property of non-Abelian theories is their ability to be asymptotically free. Recall the running of a non-Abelian coupling with scale presented earlier

$$\bar{\alpha} = \frac{\alpha}{1 + (\alpha/4\pi)(11N/3 - 2n_f/3)\log(q^2/M^2)} \tag{4.4}$$

For $n_f < 11N/2$, the coupling becomes weak at high energy scales, and confinement occurs as you traverse to lower energies. In $SU(3)$ strong interactions this is seen in the rich structure of mesons and baryons that form the building blocks of the natural world we see around us.

The field theory properties of a non-Abelian gauge theory are somewhat changed as well with the field strength tensor and covariant derivative taking the form

$$
\begin{aligned}
F^a_{\mu\nu} &= \partial_\mu A^a_\nu - \partial_\nu A^a_\mu + g f^{abc} A^b_\mu A^c_\nu \\
D_\mu &= \partial_\mu - i g A^a_\mu t^a
\end{aligned}
\tag{4.5}
$$

Where g is the coupling constant for this field, f^{abc} are the structure constants of the group, and t^a are the generators of such a group. The structure constants are defined by

$$
[t^a, t^b] = i f^{abc} t^c \tag{4.6}
$$

4.1.2 An Introduction to Glueballs

Glueballs are bound states consisting only of gluons, with no quark content. They occur naturally as gluons carry color charge, and as such can make color singlets with one another. Glueballs are thought to exist within the standard model, however they have been elusive in collider experiments, and so are still considered hypothetical particles [43].

Pure-glue theories, those without fermions, have had many properties worked out from a theoretical standpoint, and are the main topic of this chapter. Most of the effort in the literature is in computing features of an $SU(3)$ pure glue theory, and so we make contact with this by making a few remarks about these complicated, composite states.

Glueballs are generally considered to be made up of two or three gluons, meaning that the spectrum consists of particles with total angular momentum (J) of $0, 1, 2$ or 3. Glueballs possess no electric charge, nor baryon number since their constituents possess neither either. Glueballs are labelled by their angular momentum (J), parity (P), and charge-parity (C) as J^{PC}.

Some properties of glueball physics cannot be determined using the standard perturbative techniques developed in QFT, and so a field known as lattice QCD was developed to address these challenges [44]. Lattice QCD is a computational technique that takes quark masses and a mass scale (Λ_{QCD} for the strong force) in order to evaluate the Green's function necessary to study features of the spectrum. The mass spectrum of glueballs for a pure glue theory are presented in figure 4.1 [45].

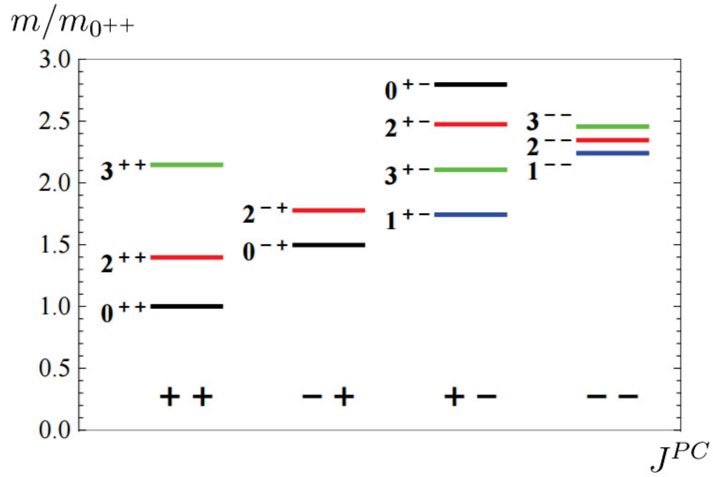

Figure 4.1: The glueball spectrum for a pure glue $SU(3)$ theory, from lattice QCD techniques. The masses are normalized to the mass of the lightest state (0^{++}) [45]

Lattice QCD has also been successful in computing glueball matrix elements for scattering cross sections, which we will come to in the subsequent sections. From pure glue lattice QCD techniques, the lightest glueball is thought to be $m_{0^{++}} = 1730 \pm 80 MeV$ ([45]). For the standard model, the presence of dynamical quarks can bring this mass down to roughly $1GeV$, though this is still an active area of research [46]. In a hidden $SU(N)$ pure glue theory, different decay channels can cause the decay of these glueballs into standard model particles and give us phenomenological signatures to hunt for in detectors and in cosmology.

In some models, the dominant number changing interaction of the particle species generally take the form of $2 \to 2$ ($\chi\chi \to \xi\xi$ where χ is dark matter and ξ is a standard model particle), or $3 \to 2$ self interactions. The benefit of these interactions in the standard model is limited, but self interactions in general in the dark sector can help ease a tension between simulation and observation known as the cusp/core problem.

The cusp/core problem ([41]) is the statement that observed dark matter density profiles do not match the form of the ones determined from N body simulations. Specifically, N body simulations give a density profile that peaks sharply near the centre of the halo (a 'cusp'), while observed densities seem to follow a much smoother curve. Self-interacting dark matter, specifically those whose relic densities are set by self interactions have been mentioned as a possible way to get rid of this problem, and so the self interactions of glueballs has been considered in the literature [54] [55].

Finally, let us consider the nature by which we perform the calculations presented below. There are two distinct objects in our theory, the dark gauge bosons of the hidden sector (hypergluons, or dark gluons), as well as the bound states they form after confinement called dark glueballs. Computations of standard scattering rates between hypergluons and standard model particles takes place in the usual way, by evaluating the four point function of the effective Lagrangian in equation (4.2), but how do we deduce the late time decay rates of glueballs?

0^{++} glueballs can be created via the scalar operator, $S = H^a_{\mu\nu}H^{\mu\nu,a}$ [52], and so the amplitude for the decay of these dark glueballs into a pair of standard model particles is

$$\langle\zeta\zeta|\ldots|0^{++}\rangle = \langle\zeta\zeta|\, SM\, |0\rangle \langle 0|\, S\, |0^{++}\rangle \tag{4.7}$$

Where 0 represents the vacuum, ζ is a standard model particle, SM represents the standard model fields generated in the coupling, and S the scalar glueball operator. The scalar operator acting on a glueball state is an analytically challenging object to work with, and is usually written $\langle 0| S |0^{++}\rangle = f^S_{0^{++}}$, the glueball decay constant. For the specific case of an $SU(3)$ dark sector, the following relationship is known from lattice computations [59] [60]

$$g^2_{HC} f^S_{0^{++}} \approx 3m^3_{0^{++}} \tag{4.8}$$

Finally, we wish to stress that in this work we consider interactions involving both the dark glueballs and dark gluons. For dark gluons, we compute the scattering cross section with different standard model particles using an effective Lagrangian approach and the usual Feynman rule analysis. This will allow us to put constraints on the model from a variety of reheating temperatures of inflation.

For dark glueballs, we are interested in computing their late time decay rates as they can be constrained by line search surveys, CMB measurements, and dwarf spheroidal galaxies (depending on the standard model connection). In these cases, the procedure outlined above in equation (4.6) and (4.7) is followed. In regards to relic densities, we note that the relic densities between dark gluons and glueballs are related, since glueballs consist only of dark gluons.

For additional information on the form of the computations of glueball decay rates, please see [52].

4.1.3 Composite Collisions and Parton Distribution Functions

We wish to introduce a bit of the theory of composite collisions, as they are necessary for studying the collider phenomenology of dark matter interactions. This discussion will follow notes from [1] [2]. We will study briefly the Drell-Yan process (figure 4.2) in preparation for determining the cross section of a fermion-like particle that could be produced in colliders in the presence of a hidden $SU(N)$ theory.

Imagine the collision of two protons in a collider producing a pair of leptons, $pp \to \ell\bar{\ell}$. Since protons are composite particles, standard Feynman rules for QED cannot be naively used. Instead, we must consider the interaction as taking place by the interaction of a quark-antiquark pair (the 'active' participants in the collision) while the other members of each proton remain as spectators.

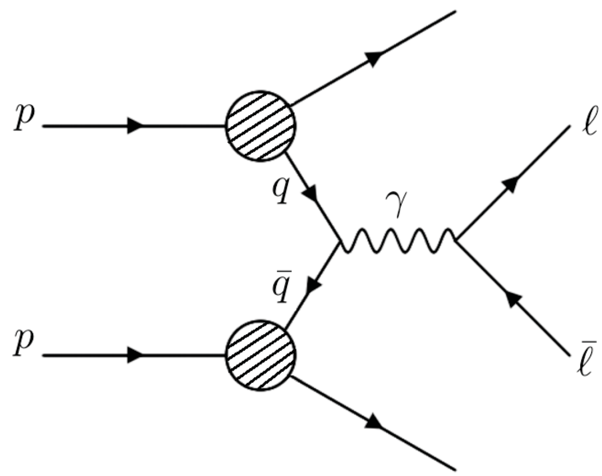

Figure 4.2: The Drell-Yan process of $pp \to \ell\bar{\ell}$ occurring via photon exchange

Before we get involved with the actual cross section, lets discuss how we determine which quarks take place in the interaction. This is done by modelling the distribution of partons (constituent quarks) inside the proton to match collider data. The exact numerics of the distribution are not necessary for this theoretical introduction, but there are constraints it must realize. For example, within a proton we expect that

$$\int_0^1 dx[f_u(x) - f_{\bar{u}}(x)] = 2 \qquad \int_0^1 dx[f_d(x) - f_{\bar{d}}(x)] = 1 \tag{4.9}$$

Where f_i is the parton distribution function for a species, i that can be any generation of quark, antiquark, or gluon. The x is defined as $x = q^2/2P{\cdot}q$ where q is the virtual momentum in the active quark participating in the interaction, and P is the momentum of the incoming proton. This effectively counts the number of up and down quarks in a proton. The quantity x can be regarded as the fraction of proton momentum that the parton undergoing scattering possesses, and so we get one more constraint for these PDFs from the total momentum

$$\int_0^1 dxx[f_u(x) + f_d(x) + f_{\bar{u}}(x) + f_{\bar{d}}(x) + f_g(x)] = 1 \tag{4.10}$$

Now we recall the cross section for the internal process, $q\bar{q} \to \ell\bar{\ell}$ is just $\sigma = \frac{4\pi\alpha_{EM}^2}{9s}Q_q^2$. Here, Q_q is the electric charge of the quarks, q involved, and $s = (q_1 + q_2)^2 \sim 2q_1 \cdot q_2$, is the usual Mandelstam variable relating the in-state momenta. Now if we have a pair of protons as our in-state particles like in Drell-Yan scattering, we would like to relate s once again to their momenta. Noting that now, the internal state quarks have a fraction of the nucleons momentum, we write $\hat{s} = (x_1q_1 + x_2q_2)^2 \sim 2x_1x_2q_1 \cdot q_2$ in the light quark limit. Relating this to the usual cross-section, we can make the substitution $\hat{s} = x_1x_2s$.

The rapidity of a system, Y, is used to compensate the fact that the centre of mass frame for the proton-proton collision is not necessarily the same as the rest frame for the final state leptons. It is defined as $Y = \frac{1}{2}\ln(x_1/x_2)$. Integrating over the momentum distributions on the partons, the differential cross section for this process becomes

$$\begin{aligned}\frac{d\sigma}{dq^2dY} = \int dx_1dx_2 \sum_f (f_f(x_1)f_{\bar{f}}(x_2) + f_f(x_2)f_{\bar{f}}(x_1)) \\ \cdot\frac{4\pi\alpha^2Q_q^2}{9q^2} \cdot \delta(q^2 - x_1x_2s) \cdot \delta\left(y - \frac{1}{2}\ln\frac{x_1}{x_2}\right)\end{aligned} \tag{4.11}$$

Where f runs over all the fermion PDFs, and we recall that q is the momentum transfer of the system, defined by $q = k - k'$, the change in momentum of one of the protons involved in the collision. This form is very useful, and will be studied in slightly more detail in the next sections when we consider collider signatures from a dark matter particle with highly suppressed strong couplings.

4.2 Coupling of Dark Glueballs to $U(1)_Y$

With the preliminaries taken care of, we now need to choose which standard model particle(s) our mediator Φ will couple to. This choice will determine the phenomenology we study and the constraints we must apply. As a first choice, let us consider a scenario where our mediator carries only hypercharge, and thus couples to the $U(1)_Y$ gauge field, B_μ before electroweak symmetry breaking, and the photon and Z^0 boson afterwards. The effective Lagrangian we will consider for this process is a subset of the one in equation (4.2)

$$\mathcal{L} \sim \frac{\alpha_{HC}\alpha_1}{60M_\Phi^4} tr(H_{\mu\nu}H^{\mu\nu})F_{\alpha\beta}F^{\alpha\beta} \tag{4.12}$$

As before, we choose to represent our $SU(N)$ field strength as $H_{\mu\nu}$. We note that $\alpha_1 = g'^2/4\pi$, where g' is coupling constant for hypercharge interactions. Couplings to photons are highly constrained as we will see shortly, and so we will consider how these hypercharge couplings translate into photon constraints further below.

4.2.1 Experimental Constraints and the Parameter Space

Dark matter can be constrained in a number of creative ways, but perhaps the most obvious signal to look for is that of decaying or annihilating dark matter in regions with high density. Annihilation or decay of these particles can produce nearly monochromatic γ rays, and so there has been considerable experimental effort in searching for such signals in the centre of galaxies, and from other astrophysical sources. The *Fermi* Large Area Telescope (LAT) is one such collaboration searching for spectral lines in the range of $5-300GeV$ [56].

Other constraints on the lifetimes of dark matter candidates can come from power spectrum measurements of the CMB [57] and other line-search techniques [58]. More details on these constraints will follow, when we plot them in order to determine the allowed regions in the parameter space between the mediator and glueball mass.

So how do we relate the glueball mass to that of the mediator? First, note that to determine the decay rate of such a process, we need to determine the amplitude of the interaction. The amplitude of transitioning from glueballs to photons can be schematically written as $\mathcal{M} \sim \langle\gamma\gamma|\frac{\alpha_{HC}\alpha_{EM}}{60M_\Phi^4}F_{\alpha\beta}F^{\alpha\beta}|0\rangle\langle 0|S|0^{++}\rangle$, where $S = H^a_{\mu\nu}H^{\mu\nu,a}$ and is the scalar glueball operator, while $\langle 0|S|0^{++}\rangle \sim f_0^S$ is the scalar glueball matrix element. Squaring and combining with the phase space factors, it is possible to write the decay as [50],

$$\Gamma(0^{++} \to \gamma\gamma) \sim \frac{\alpha_{EM}^2}{32\pi^3}\frac{m_0^3}{M_\Phi^2}\left(\frac{1}{60}\frac{g_{HC}^2 f_0^S}{M_\Phi^3}\right)^2 \tag{4.13}$$

Where $\alpha_{HC} = g_{HC}/4\pi$. The matrix element, f_0^S, cannot be solved analytically, but does have a numerical solution from lattice computations in $SU(3)$ [59] [60], $g_{HC}^2 f_0^S \approx 3m_0^3$. Using this, and noting that the decay rate is related to the lifetime by $\Gamma = 1/\tau$ we find that

$$m_0\tau = \frac{m_0}{\Gamma} \sim 7.4 \times 10^9 \left(\frac{M_\Phi}{m_0}\right)^8 > Constraints \tag{4.14}$$

The constraints come from line search surveys, and the power spectrum CMB measurements which will be explained in a bit more detail later. These constraints come in the form of τ or $m_0\tau$ vs mass plots, hence why we have written equation (4.13) in that suggestive form. We require that the computed lifetime of our dark glueballs, $m_0\tau$ be greater than constraints set by these experiments. We will revisit this result shortly.

4.2.2 Aside: Cosmologically Long-Lived Particles

In the following sections, we will make use of a few different constraints coming from experiment on the lifetime of our dark glueball states. The lowest order Feynman diagram for each scenario will set the lifetime of the dark glueballs, and so we should check which regions of parameter space yield lifetimes on the order of the age of the universe. Since the decay of glueballs to final state photons and gluons is so similar (merely replace $\alpha_{EM} \to \alpha_s$ in equation (4.13), since it is the same one loop process, as we will see in later sections), we will discuss these two cases together here. Since the age of the universe is $4.3 \cdot 10^{17}\ s$, we can cast a general constraint on the lifetime of our glueballs such that they are cosmologically long lived. This constraint is

$$\begin{aligned}\frac{1}{\Gamma} = \tau = \frac{400 \cdot 32\pi^3}{\alpha^2}\frac{M_\Phi^8}{m_0^9} \cdot 6.582 \cdot 10^{-25}\ GeV \cdot s > 4.3 \cdot 10^{17} s \\ \sim \frac{1}{\alpha^2}\frac{M_\Phi^8}{m_0^9} > 1.65 \cdot 10^{36} GeV^{-1}\end{aligned}$$

Where we have included the units to be explicit, and α can be either α_{EM} or α_s. It is easy to see that the constraint depends on the the masses of the particles, as well as the coupling between the two sectors. Since we would like to see which mass ranges of Φ and the glueball are allowed, we need only to choose a value of α to see where our theory can live. Lets first consider electromagnetism (or hypercharge) couplings.

From QFT and the renormalization group, we know that couplings run with energy scale, thus are not static entities. Glueballs form at the confining transition in the dark theory (Λ_{HC}), and so we should consider their lifetimes at any point from this confinement onwards. We will define two points to evaluate couplings at, $\alpha_{EM,UV}(\Lambda_{HC})$ and $\alpha_{EM,IR}(T_0)$ where $\alpha_{EM,UV}$ is the coupling at high energies at the dark confinement scale, and $\alpha_{EM,IR}$ is the temperature scale of the universe today. From looking at our constraint inequality, we see that the larger the coupling, more difficult it is to satisfy the constraint, thus we use the highest value of α as our cosmological bound.

For electromagnetism, we know from both theory and experiment that $\alpha_{EM,IR} \sim 1/137$. Since this theory isn't asymptotically free, the coupling gets larger as you increase the energy scale. Indeed, at LHC level energies, it is necessary to use a value of $\alpha \sim 1/128$ to reproduce experimental results (at an energy scale of $\sim TeV$). In fact, there is a Landau pole in the theory where the coupling grows to infinity. This Landau pole gets reached at very high energies ($>>> M_{pl}$), at a point where the standard model is not expected to be the proper description of the laws of nature, and so this pole is unphysical. At energies higher than EWSB, electromagnetism is no longer a good descriptor and one needs to actually consider $\alpha_{B,UV}$, the value of the hypercharge coupling at large energies. The value of this coupling near the GUT scale is $\alpha_{B,UV} \sim 1/25$. To exhibit how little our constraint changes over this range of energy levels, we compute the inequality for both the IR and UV versions of the coupling. The results are

$$M_{\Phi,IR} > 9.8 \cdot 10^3 m_0^{9/8}\ GeV^{-1/8}$$
$$M_{\Phi,UV} > 2.3 \cdot 10^4 m_0^{9/8}\ GeV^{-1/8}$$

We include the stronger of the two constraints amongst upcoming parameter space plots, and will make further comments there.

Now we should consider QCD, which is qualitatively much different than electromagnetism/hypercharge. This theory remains unbroken through EWSB, and its coupling is tiny at high energies. Thus, we know that $\alpha_{s,UV} << \alpha_{s,IR}$, and since we are looking for the higher value of α_s we just need to consider what happens at low energies to determine a maximum decay rate for the glueballs. Once again, there is a Landau pole in the theory, but it occurs at energies lower than Λ_{QCD}, the confinement energy for QCD, where we cannot trust the perturbation theory that predicts the pole in the first place. Late time decays of glueballs to gluons occur in the nonperturbative regime, so we would like to understand how α_s behaves at these low energies.

Unfortunately, the community appears to be split on the issue (see [61] for a review). The different camps argue that

- The coupling diverges as $1/Q^2$ in the $Q \longrightarrow 0$ limit
- The coupling freezes at some ($\mathcal{O}(1)$) value
- The coupling vanishes in the deep IR

Many subtleties lead to these different conclusions, including gauge choices, renormalization schemes, and others ([61] for a comprehensive list). It is prudent to make some comment about the viability of our model in the event that one of these scenarios is correct.

If the coupling diverges, $\alpha_{s,IR} \to \infty$, and our theory breaks down. In this case, the lifetimes of our dark glueballs would become infinitesimal, and no dark matter would exist at late times. If this is the correct scenario, our model fails due to lifetime constraints.

If the coupling in the IR is of order 1, we can write our constraint equation as

$$M_\Phi > 3.3 \cdot 10^4 m_0^{9/8} \ GeV^{-1/8}$$

Which we will plot and comment on in the relevant QCD coupled section.

Finally, if the coupling vanishes in the deep IR, our bound is completely satisfied for any range of m_0 and M_Φ, and so we cannot restrict the parameter space by lifetime constraints, as the glueballs would be stable at late times.

4.2.3 The Scattering Cross-Section

Before progressing any further, let us discuss entropy considerations between the two sectors. Recall the entropy density of a collection of particle species

$$s = \frac{2\pi^2}{45} g_{*s}(T) T^3 \tag{4.15}$$

Where g_{*s} is the (temperature dependent) effective number of degrees of freedom in the collection, and T is the temperature of the thermal bath the particles reside in. Two sectors that are thermally decoupled no longer exchange entropy, and so it is possible to define a conserved quantity, R, which relates the entropy densities in the dark and visible sectors (after all first order phase transitions have taken place in both sectors). This is done in [47], and reads

$$R = \frac{s_{HC}}{s} \sim \frac{g_{*s_{HC}}(T_{HC}) T_{HC}^3}{g_{*s}(T) T^3} \tag{4.16}$$

where s_{HC} is the entropy density of the dark sector. This quantity, R, is set by the assumption that inflation reheats asymmetrically to the dark and visible sectors. It is an input to the theory, and so to tie to other work on dark glueballs in the literature, we consider the range $10^{-12} < R < 10^{-3}$, for which results have been calculated by Forestell *et al* [47]. Particle species in thermal equilibrium with one another share the same temperature, T. For a scenario where the two sectors were in thermal equilibrium, and decoupled at some temperature scale, the subsequent evolution of the temperatures won't deviate by much (for example, compare the temperature difference of the CMB ($\sim 2.7K$) and the decoupled cosmic neutrino background ($\sim 1.9K$)). In order to match this range of R values, it would be necessary to have $g_{*s_{HC}}/g_{*s}$ between 10^3 and 10^{12}, or at minimum 10^3 degrees of freedom in the standard model for every 1 in the dark sector. Since this is not possible, we (and they) consider a more plausible scenario where the two sectors were simply never in thermal equilibrium at any point over the thermal history of the universe. This allows the T_{HC}/T parameter to become free, in order to explore a range of R values already investigated in the literature, from $10^{-12} < R < 10^{-3}$.

It should also be noted that R controls the relic yield of dark matter particles. This can be seen by noting that for a non-relativistic particle, the dark sector entropy density can be recast as $s_{HC} \sim \left(\frac{m_{0^{++}}}{T_{HC}}\right) n_{0^{++}}$ where T_{HC} is the temperature of the dark sector. The freeze out abundance of dark matter is then written $Y_{HC} = n_{0^{++}}/s \sim R/x_{HC}^{fo}$ where s is the entropy density of the standard model. Here, $x_{HC}^{fo} = m_{0^{++}}/T_{HC}^{fo}$, where T_{HC}^{fo} is the freeze out temperature of the dark sector. From these relations we can see that R affects the abundance of freeze-out abundance of glueballs in the late time universe.

Since we have chosen to couple our dark sector to a $U(1)$ gauge field through our mediator, we have to consider when this interaction goes out of equilibrium to determine if the sectors were ever thermally coupled. To keep a consistent picture of thermally decoupled sectors, we require that any interactions between them possess a freeze out temperature higher than the standard reheating temperature from inflation. Of course, this reheat temperature itself isn't known, so we will consider a range of them later on. This freeze out temperature between the dark gluons and standard model particles is expected to be higher than the hypercolor phase transition.

To gain more information about the freeze-out properties of dark glueballs, it is prudent to make a more detailed computation of the cross section from two hypergluons to the final state gauge bosons. Once this cross section is calculated, we can determine the freeze-out temperature of the interaction. We will start by considering the coupling to the B_μ field, and extend our results to photons and Z^0 bosons afterwards. In this, we assume that the hypercolor confining scale, Λ_{HC} is lower than the freeze out temperature of these interactions, thus the proper effective interaction to consider that couples the two sectors is the $2 \to 2$ scattering of dark gluons and photons. Recall the effective Lagrangian for this coupling (as illustrated in figure 4.3)

$$\mathcal{L} \sim \frac{\alpha_{HC}\alpha_1}{60 M_\Phi^4} F_{\alpha\beta} F^{\alpha\beta} H^a_{\alpha\beta} H^{a,\alpha\beta} \tag{4.17}$$

To fourth order in the fields (neglecting the $g f^{abc} W^b_\mu W^c_\nu$ term in the expansion of the hypergluon field, $H^a_{\mu\nu}$), this effective interaction Lagrangian will look like

$$\mathcal{L}_{4-pt} = \frac{\alpha_{HC}\alpha_1}{60 M_\Phi^4} (\partial^\mu B^\nu - \partial^\nu B^\mu)(\partial_\mu B_\nu - \partial_\nu B_\mu)(\partial^\alpha W^{a,\beta} - \partial^\beta W^{a,\alpha})(\partial_\alpha W^a_\beta - \partial_\beta W^a_\alpha) \tag{4.18}$$

For simplicity, we will work in momentum space where these derivatives are simply transformed $\partial_\mu \to k_\mu$. Our gauge fields are all vectors as well, and so they will pick polarizations when we attempt to compute the matrix element for this process. Explicitly, the process we are considering is that of two hypergluons going to two hypercharge gauge bosons via a loop of our heavy mediator particle, Φ.

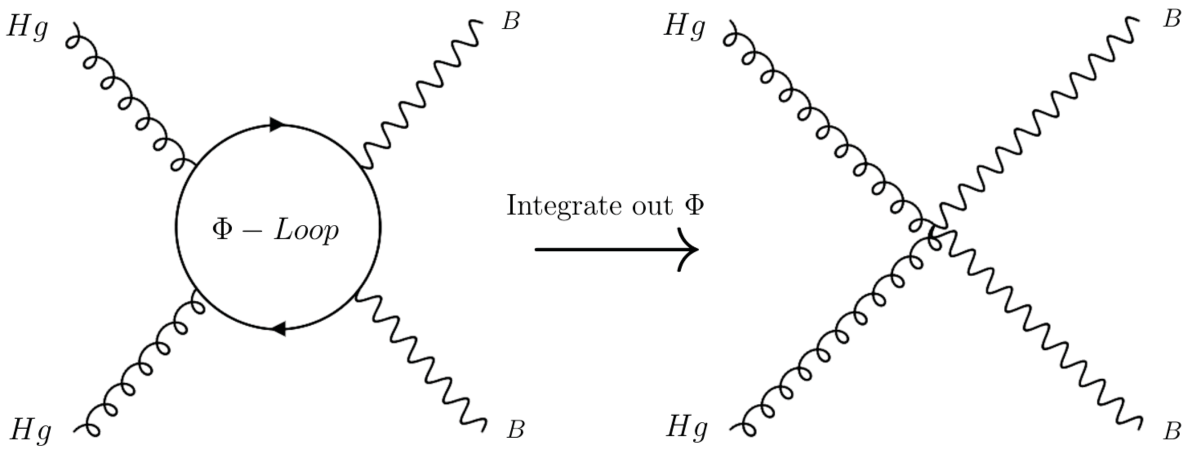

Figure 4.3: Hypergluon couplings to hypercharge gauge bosons are loop suppressed by our heavy field Φ, and so we can write an effective 4-point function. The field B refers to the hypercharge gauge boson.

Now, derivative interactions introduce momentum contractions in our calculation. Specifically, we can see that derivative interactions contracted amongst identical initial and final state particles give

$$\partial_\mu \phi^* \partial^\mu \phi^* \partial_\nu \phi \partial^\nu \phi \to 4[(k_1 \cdot k_2)(k_3 \cdot k_4)] \tag{4.19}$$

See the appendix for a more detailed description of the form of this derivative interaction. Here $k_{1,2}$ are the momenta of the two identical in-state particles, and $k_{3,4}$ the momenta of the two out-state ones. Since expansions of the 4-point Lagrangian will only have contributing terms of this form, we can pull out a factor of 4 from such interactions and write our matrix element

$$\mathcal{M} = \frac{4\alpha_{HC}\alpha_1}{60M_\Phi^4}(k_3^\mu \epsilon_3^{*,v} - k_3^\nu \epsilon_3^{*,\mu})(k_{4,\mu}\epsilon_{4,\nu}^* - k_{4,\nu}\epsilon_{4,\mu}^*)(k_1^\alpha \epsilon_1^\beta - k_1^\beta \epsilon_1^\alpha)(k_{2,\alpha}\epsilon_{2,\beta} - k_{2,\beta}\epsilon_{2,\alpha}) \tag{4.20}$$

Where we have explicitly written the polarizations of each particle, ϵ. We can now exploit the general antisymmetry of the $F_{\mu\nu}F^{\mu\nu}$ and $H^a_{\alpha\beta}H^{a,\alpha,\beta}$ terms to pull out another factor of 2^2

$$\mathcal{M} = \frac{4 \cdot 2^2 \alpha_{HC}\alpha_1}{60M_\Phi^4}(k_3^\mu \epsilon_3^{*,v})(k_{4,\mu}\epsilon^*_{4,\nu} - k_{4,\nu}\epsilon^*_{4,\mu})(k_1^\alpha \epsilon_1^\beta)(k_{2,\alpha}\epsilon_{2,\beta} - k_{2,\beta}\epsilon_{2,\alpha}) \tag{4.21}$$

Since we will be spin-averaging this cross section, we can make use of the well known relation [1]

$$\sum_{polarizations} \epsilon^*_\mu \epsilon_\nu \to -g_{\mu\nu} \tag{4.22}$$

We work in flat space, so the metric $g_{\mu\nu}$ is Minkowski. Explicitly doing the polarization sums and averaging over initial spin states, and squaring our matrix element (noting that $\mathcal{M}^*$ is just the same as $\mathcal{M}$ but with different indices), we get the complicated expression

$$\begin{gathered}\frac{1}{2\cdot 2}\sum_{\epsilon^*,\epsilon}|\mathcal{M}|^2 = \frac{1}{4}\left(\frac{16\alpha_{HC}\alpha_1}{60M_\Phi^4}\right)^2 \\ \times g^{\mu\sigma}k_1^\nu k_1^\rho (g^{\mu\sigma}k_2^\rho k_2^\nu + g^{\nu\rho}k_2^\mu k_2^\sigma - g^{\sigma\nu}k_2^\rho k_2^\mu - g^{\mu\rho}k_2^\nu k_2^\sigma) \\ \times g^{\alpha\tau}k_3^\beta k_3^\delta (g^{\alpha\tau}k_4^\delta k_4^\beta + g^{\beta\delta}k_4^\alpha k_4^\tau - g^{\tau\beta}k_4^\delta k_4^\alpha - g^{\alpha\delta}k_4^\beta k_4^\tau)\end{gathered} \tag{4.23}$$

Thankfully, this equation simplifies nicely once we contract indices using the metric, so our spin-averaged matrix element is

$$\langle \sum |\mathcal{M}|^2 \rangle = \frac{16^2}{4\cdot 60^2}(4+0-1-1)^2 \frac{\alpha_{HC}^2\alpha_1^2}{M_\Phi^8}(k_1 \cdot k_2)^4 (N_c^2 - 1) \tag{4.24}$$

Where we have introduced the group theoretic color factor stemming from contractions of the a indices in our initial effective Lagrangian. Finally, lets put this in terms of the total energy Mandelstam variable, s (which relates directly with the centre of mass energy of in-state particles in colliders). Since we have identical, massless initial and final state particles we note $k_1 \cdot k_2 = k_3 \cdot k_4 = s/2$, so

$$\langle \sum |\mathcal{M}|^2 \rangle = \frac{16s^4}{60^2} \frac{\alpha_{HC}^2 \alpha_1^2}{M_\Phi^8} (N_c^2 - 1) \tag{4.25}$$

Another way to write the differential cross section presented in chapter 2, yields the following result

$$\frac{d\sigma}{dt} = \frac{\langle |\mathcal{M}^2| \rangle}{64\pi s k_{cm}^2} = \frac{s^3}{4 \cdot 60^2 \pi k_{cm}^2} \frac{\alpha_{HC}^2 \alpha_1^2}{M_\Phi^8} (N_c^2 - 1) \tag{4.26}$$

Where t is another Mandelstam variable, $t = (k_1 - k_3)^2$. The full cross section can be obtained by integrating over t, which is trivial as our expression does not contain it at all.

$$\sigma = \int_{-4k_{cm}^2}^{0} dt \frac{d\sigma}{dt} \frac{1}{2} = \frac{s^3}{2 \cdot 60^2 \pi} \frac{\alpha_{HC}^2 \alpha_1^2}{M_\Phi^8} (N_c^2 - 1) \tag{4.27}$$

Where the factor of 1/2 in the first expression comes from the fact we have identical final state particles.

4.2.4 Determining $\langle \sigma v \rangle$

We wish to determine when such an interaction would freeze-out, and as such we must determine $\langle \sigma v \rangle$, the thermally averaged velocity weighted cross section. Thankfully, we have already formulated an expression for determining this with a little help from [37]. Recall the simple, single integral expression

$$\langle \sigma v \rangle = \frac{1}{8 m_{Hg} T K_2^2(m/T)} \int_{4m_{Hg}^2}^{\infty} \sigma(s - 4m_{Hg}^2)\sqrt{s} K_1(\sqrt{s}/T) ds \tag{4.28}$$

Now, since our hypergluons are massless, we need to find out what happens in the $m \to 0$

limit. There are no problems with the integral expression, but the prefactor gives something to worry about. Recall the expression for the modified Bessel function of the second kind, K_2

$$K_2(x) = \lim_{\alpha\to 2} \frac{\pi}{2} \frac{I_{-\alpha}(x) - I_\alpha(x)}{sin(\alpha\pi)} \qquad I_2(x) = \lim_{\alpha\to 2} \sum_{m=0}^{\infty} \frac{1}{m!\Gamma(m+\alpha+1)} \left(\frac{x}{2}\right)^{2m+\alpha} \tag{4.29}$$

We note that from this it is possible to perform a series expansion in x such that

$$\frac{1}{x^2 K_2(x)} = \frac{1}{2} + \frac{x^2}{8} + \mathcal{O}(x^3) \tag{4.30}$$

and so in the massless limit, $x = m/T \to 0$ our thermally averaged cross section becomes

$$\langle\sigma v\rangle \approx \frac{1}{32T^5} \int_0^\infty \sigma s^{3/2} K_1(\sqrt{s}/T) ds \tag{4.31}$$

This expression is only approximate as suitable corrections coming from Bose-Einstein statistics should be implemented in a more rigorous computation. Performing the integral transformation of $x = \sqrt{s}/T$ allows us to extract the proper temperature dependence, after which a straightforward integration in Mathematica is performed. Our final expression for $\langle\sigma v\rangle$ is thus

$$\langle\sigma v\rangle = \frac{4^5 \cdot 3^2 \cdot 5}{60^2\pi} \frac{T^6}{M_\Phi^8} \alpha_{HC}^2 \alpha_1^2 (N_c^2 - 1) \approx 4.07 \alpha_{HC}^2 \alpha_1^2 (N_c^2 - 1) \frac{T^6}{M_\Phi^8} \tag{4.32}$$

These gauge couplings should be evaluated at the scale T, the temperature at which the interactions take place. In particular, the pure $SU(N)$ hypercoupling was computed in Mathematica using up to the four loop beta function coefficient for our theory in the $\bar{M}S$ renormalization scheme (details outlined here [62]).

4.2.5 Extension to Photons and Z^0 Bosons

Now that we have computed $\langle \sigma v \rangle$ for hypergluons to the hypercharge gauge bosons, we can consider how this coupling will look after EWSB. The A_μ and Z^0_μ fields are related to the W^3_μ and B_μ fields by a simple rotation, characterized by the two equations

$$\begin{aligned} Z^0_\mu &= \frac{1}{\sqrt{g^2 + g'^2}}(gW^3_\mu - g'B_\mu) = \cos\theta_w W^3_\mu - \sin\theta_w B_\mu \\ A_\mu &= \frac{1}{\sqrt{g^2 + g'^2}}(g'W^3_\mu + gB_\mu) = \sin\theta_w W^3_\mu + \cos\theta_w B_\mu \end{aligned} \tag{4.33}$$

Where the coupling constants before and after the EWSB are related by the Weinberg angle, θ_w as

$$g = \frac{e}{\sin\theta_w} \qquad g' = \frac{e}{\cos\theta_w} \qquad \frac{g'}{g} = \frac{\sin\theta_w}{\cos\theta_w} \tag{4.34}$$

Now, eliminating the W^3_μ field from these equations yields an expression for our hypercharge field such that

$$B_\mu = \cos\theta_w A_\mu - \sin\theta_w Z^0_\mu \tag{4.35}$$

Since the four point function of our fields comes in the form of $\partial^\mu B^\nu \partial_\mu B_\nu$ (with different variations of the μ and ν indices), and since the couplings g, g' don't depend on spacetime coordinates, we can easily see the relation between hypercharge couplings, and the more familiar low energy photon and Z^0 couplings by inputting and expanding our equation above

$$\partial^\mu B^\nu \partial_\mu B_\nu \rightarrow \partial^\mu(\cos\theta_w A^\nu - \sin\theta_w Z^{0\,\nu})\partial_\mu(\cos\theta_w A_\nu - \sin\theta_w Z^0_\nu) \tag{4.36}$$

Which essentially means that our hypercharge coupling will give rise to decay patterns of our glueball to $\gamma\gamma$, Z^0Z^0, and γZ^0. Since our expression for $\langle \sigma v \rangle$ contains a $g'^2 = e^2/\cos^2\theta_w$ from the hypercharge couplings, we get an adjustment to the coupling constants to our photons and Z^0 bosons. With this in mind, our couplings for these three decay channels become

$$\begin{aligned} \alpha(\gamma\gamma) &\to \alpha_1 \cdot \cos^2\theta_w = \alpha_{EM} \\ \alpha(Z^0 Z^0) &\to \alpha_1 \cdot \sin^2\theta_w = \alpha_{EM} \cdot \frac{\sin^2\theta_w}{\cos^2\theta_w} \\ \alpha(\gamma Z^0) &\to \alpha_1 \cdot 2\sin\theta_w\cos\theta_w = \alpha_{EM} \cdot \frac{2\sin\theta_w}{\cos\theta_w} \end{aligned} \tag{4.37}$$

For the rest of this subsection, we will be considering explicitly the coupling to the diphoton channel (that is, replacing $\alpha_1 \to \alpha_{EM}$, though the other two channels are related to this process by the simple factors of the Weinberg angle, as derived above).

4.2.6 Freeze-out Temperature/Outlook of Model

We follow the logic discussed above, and the literature in assuming that this dark glueball sector was never in thermal equilibrium with the standard model [47] [69]. This allows us to constrain our parameter space by requiring that the freeze-out temperature of this interaction be above the reheating temperature from inflation. If we make this assumption, the dark sector temperature T evolves independently of the CMB photon temperature. To make use of this idea, consider the rate of interactions between photons and hypergluons

$$\Gamma = \langle \sigma v \rangle n \qquad n = \frac{\zeta(3) T^3 g}{\pi^2} \tag{4.38}$$

Where we have utilized the relativistic number density for the number density of photons, noting that g counts the internal number of degrees of freedom, $g = 2$. To determine when decoupling occurs, we set this equal to the Hubble rate, where $H^2 = \rho/3M_{Pl}^2$. In the early universe immediately after reheating, we enter a phase of radiation domination, where $\rho_r = \frac{\pi^2}{30} g_* T^4$. As a reminder, g_* counts the effective number of degrees of freedom in the universe. Throwing all of these together, we relate the freeze out temperature to the glueball coupling and mediator mass

$$T_f^7 = \frac{M_\Phi^8 \pi^2 \sqrt{g_*}}{12.29\alpha_{EM}^2 \zeta(3) g M_{Pl}(N_c^2 - 1)} \cdot \frac{1}{\alpha_{HC}^2(\Lambda, N_c, T)} \tag{4.39}$$

We note here that allowing the $SU(N)$ gauge coupling to run gives us another relationship between M_Φ and $m_{0^{++}}$ since $m_{0^{++}} \sim 7\Lambda$ for specified values of the reheat temperature. The $SU(N)$ gauge coupling, α_{HC} is once again related to the temperature scale T at which the interactions take place, by the 4 loop beta function coefficients defined in [62].

In order to satisfy the idea that the dark and standard sectors never be in equilibrium, we note that the temperature of reheating must be lower than the freeze out temperature of this interaction, implying the sectors are always frozen out from one another. From this, we note

$$T_{reheat} < T_f = \left(\frac{M_\Phi^8 \pi^2 \sqrt{g_*}}{12.29\alpha_{EM}^2 \zeta(3) g M_{Pl}(N_c^2 - 1)} \cdot \frac{1}{\alpha_{HC}^2(\Lambda, N_c, T)} \right)^{1/7} \tag{4.40}$$

As before, this coupling is evaluated at the T scale. We note α_{EM} should also be evaluated at this scale, but we have used $\alpha_{EM} \approx 1/128$ for simplicity, as the expression is fairly insensitive to this factor due to the 1/7 power suppression. We can make a plot with varied values of the reheating temperature, and overlay it with the constraints from line searches and other experiments. Reheating temperatures can go as low as $\sim 4MeV$ [63] without disrupting cosmological abundances, but we consider temperatures above $1GeV$ to be on the conservative side. Note that g_* is a function of T, but since we want to be out of equilibrium right at reheating, the effective number of degrees of freedom in the standard model is $g_* = 106.75$. The allowed parameter space is defined as the part of figure 4.4 above the reheating curve, as well as the constraints considered previously.

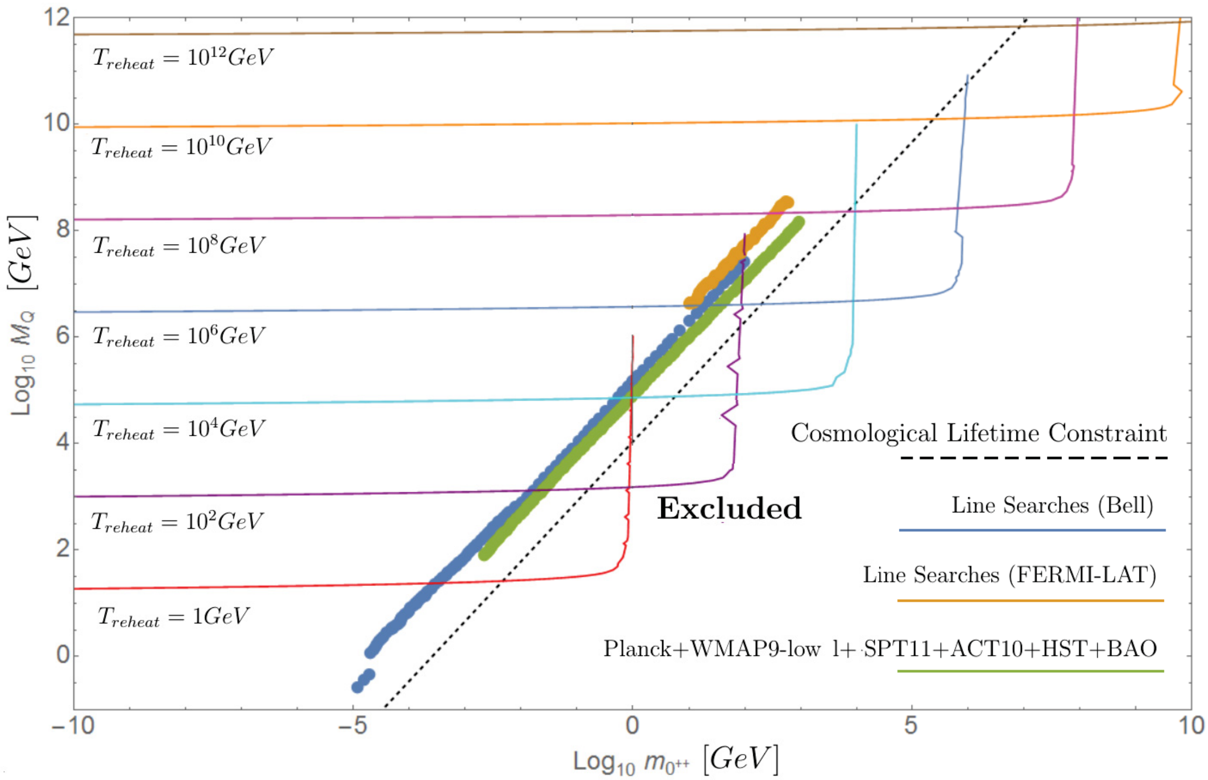

Figure 4.4: Constraints on new particle masses from reheating, line searches [56] [58] and CMB studies [57]. Reheating constraints are computed for a variety of possible temperatures, represented by the contours, T_{reheat} and appear to be quite strong. Reheat constraints computed in $N_c = 3$. The allowed region of parameter space is above the curves set by reheating and the other constraints. Note that the contours disappear for $m_{0^{++}} > M_\Phi$, which is where we expect the EFT approach to break down. We also assume that freeze out takes place above Λ_{HC} (implicit in the calculation since we also assume $T_{reheat} > \Lambda_{HC}$). The black dashed line comes from the constraint equation for $M_{\Phi,UV}$ in section 4.2.2, where any point below that line corresponds to a model in which the dark glueballs decay on a timescale shorter than the age of the universe. The allowed region of parameter space is above all contours.

Its prudent that we take a moment and discuss the constraints we have plotted in figure (4.4). Specifically, we have plotted two different constraints: line searches and constraints from CMB observations. Dark matter annihilations are capable of producing nearly monochromatic photons, and so telescope collaborations such as the Fermi large area telescope search for these spectral lines in regions of high dark matter density. It is possible to generate constraints by considering the γ ray emission from the galactic centre, as well as by looking at the diffuse, isotropic photon background. Fermi-LAT looks for these γ rays above the background signal coming from the bulge of the Milky Way galaxy. These types of constraints are considered in [56] [58].

CMB measurements also offer new approaches at restricting dark matter decays and annihilations. Annihilations or decays occurring both before recombination and after can produce spectral distortions, deviations from a perfect blackbody in the CMB photon spectrum. Dark matter decays can cause injection of photons into the intergalactic medium which can leave imprints on the polarization and temperature fluctuations of the CMB. Photons from the CMB are generally thought to be influenced by reionization of the universe from the first stars, causing them to develop temperature and polarization fluctuations from other processes as they stream through the intergalactic medium (IGM). Additional fluctuations on CMB photons (above and beyond what is predicted from IGM models) are used to constrain the lifetime of dark matter. Constraints coming from late-time dark matter decay are considered in [57].

The allowed parameter space in figure (4.4) is that which is above the lines set by the aforementioned constraints, as well as our computed reheat condition. The non-reheating based constraints are taken from plots of dark matter lifetime vs mass. We utilize equation (4.13) where we quote the decay rate of dark glueballs into photons in order to generate constraints on the above plot. Common cosmological rhetoric tends to assume a reheat temperature near the grand unified (GUT) scale $\sim 10^{15} GeV$. While there is no real consensus on when reheating occurred, values of T_{reheat} orders of magnitude below the GUT scale still highly constrain our parameter space. This puts significant pressure on a model with electromagnetic couplings, as we are are restricted to very high mediator masses.

The constraints presented from reheating seem to cover a large portion of the parameter space for this model. As such, it is interesting to also consider different types of indirect couplings between the dark sector and standard model. Couplings to the $SU(3)$ strong force are relatively easy to study (since they are unaffected by EWSB), and give a qualitatively different picture as they can produce a diffuse spectrum of photons, not just lines. We note that the above constraint from reheating appears to be a novel result.

We should also note that coupling photons to the Φ mediator creates a scenario in which Φ has electric charge. Strict constraints exist on the production and abundance of electrically charged dark matter candidates, and so this is undesirable. However, if the Φ particles carry a non-appreciable abundance in the late-time universe (as in, their existence is mainly to mediate the interactions between the dark glueballs and photons), these restrictions can be avoided. We have implicitly assumed this during the analysis above.

In the above references, constraints are given in the form of a lifetime (or mass-weighted lifetime) vs. dark matter mass plot. Lower bounds on these lifetimes are converted to parameter space plots such as figure 4.4 by relating the lifetime of glueballs to the mediator mass M_Φ and $m_{0^{++}}$ using equation 4.13. Quantitatively, this relationship (for photon decay products) became

$$m_{0^{++}}\tau = \frac{m_{0^{++}}}{\Gamma} \sim 7.4 \times 10^9 \left(\frac{M_\Phi}{m_{0^{++}}}\right)^8 > Constraints \tag{4.41}$$

Which we used to generate the non-reheating constraints on figure 4.4.

4.3 Dark Glueballs to Gluons: A Quirky Approach

Now that we have generated a parameter space plot in the $U(1)_Y$ coupled case, we can move on to consider other mediator couplings. By replacing the coupling of our mediator to the $U(1)_Y$ gauge bosons (and subsequently, to photons after EWSB), we can adapt the model in a way that hopefully relaxes the reheating constraints, but what phenomenological signatures can we look for?

A natural next choice is to allow coupling of Φ to the $SU(3)$ strong force, instead. $SU(3)$ remains an unbroken symmetry throughout the standard model at cosmologically accessible temperatures, and so we don't need to consider any mixing as we did in section 4.2.4. The phenomenology is different here as well, as it is possible to produce both a diffuse spectrum of photons, and lines that astrophysical experiments can search for. Here, we consider two different types of diagrams. First, a three loop diagram of the form of 4.5 (left) allows us to reuse the previous line search constraints, while also seeing how a replacement of $\alpha_{EM} \to \alpha_s$ effects the reheating contours. Second, we can consider a diagram like 4.5 (right) that will give us a diffuse final state of photons to hunt for. Additional constraints on diffuse photons from Fermi-LAT and the HAWC survey of dwarf spheroidal galaxies are used to further constrain this case.

4.3.1 3-Loop Line Production Diagram

The question of which phenomenological signature to look for is still open. The effective Lagrangian for our couplings between the dark sector and $SU(3)_{strong}$ is as follows

$$\mathcal{L} \sim \frac{\alpha_{HC}\alpha_s}{60M_\Phi^4}(H^a_{\mu\nu}H^{a,\mu\nu})(G^b_{\alpha\beta}G^{b,\alpha\beta}) \tag{4.42}$$

Where $G^b_{\alpha\beta}$ is the gluon field strength. The cleanest signal we can hope to detect is once again in the photon channel, so it is useful to see how we can construct such a scenario. The lowest order interaction producing a spectral line from glueball decay, is having a gluon loop attached to the hyperquark loop, and then attaching another regular quark loop on the end which can emit photons. This diagram is shown below on the left, in figure 4.5.

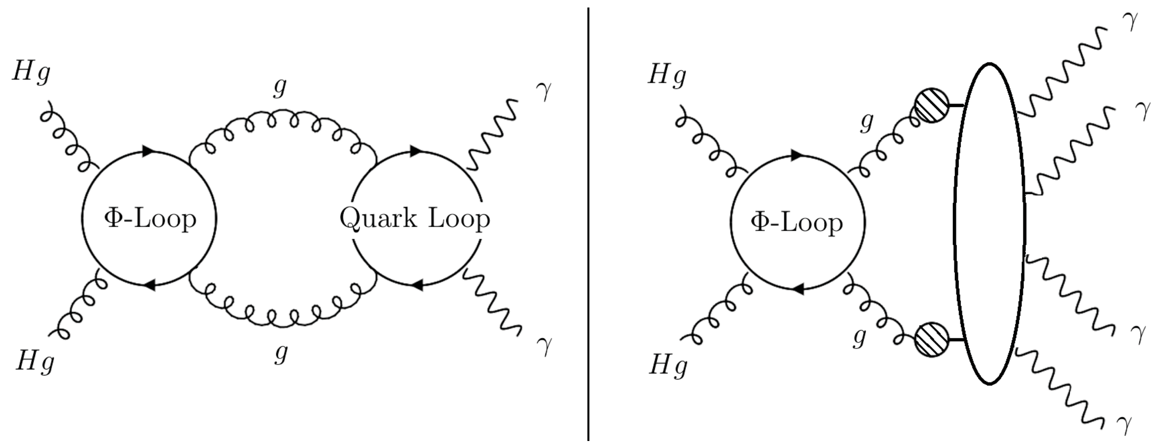

Figure 4.5: The lowest order loop diagrams with $SU(3)_{strong}$ couplings producing a spectral line of photons (left) and a diffuse spectrum (right)

Figure 4.5 (left) shows that a three loop process can yield a resonant photon signal that we could potentially hunt for. Since the reheating constraints come from the lowest order interaction coupling standard model and dark matter particles, the one loop of $Hg\ Hg \to g\ g$ will set the reheating temperature. Drawing analogues to the electromagnetic case, we see that the cross sections of the two interactions should just be related by $\alpha_{EM} \to \alpha_s$ with an additional color factor coming from the colored final state.

$$\sigma_{strong} \approx \sigma_{EM}(\alpha_{EM}(T) \to \alpha_s(T)) \cdot (N^2 - 1) \tag{4.43}$$

Here, σ_{EM} is the cross section computed in the previous subsection for photon couplings on our mediator, and $N = 3$ is the strong coupling gauge group. Throughout we have explicitly put the scale that the couplings should be evaluated at (the temperature scale of the interactions, T). We note that in our computation of $\Gamma = \langle \sigma v \rangle n$, the freeze-out temperature is related to the 1/7 power of our cross section. This means that any changes obtained by the $\alpha_{EM} \to \alpha_s$ in σ_{strong} are fairly minuscule.

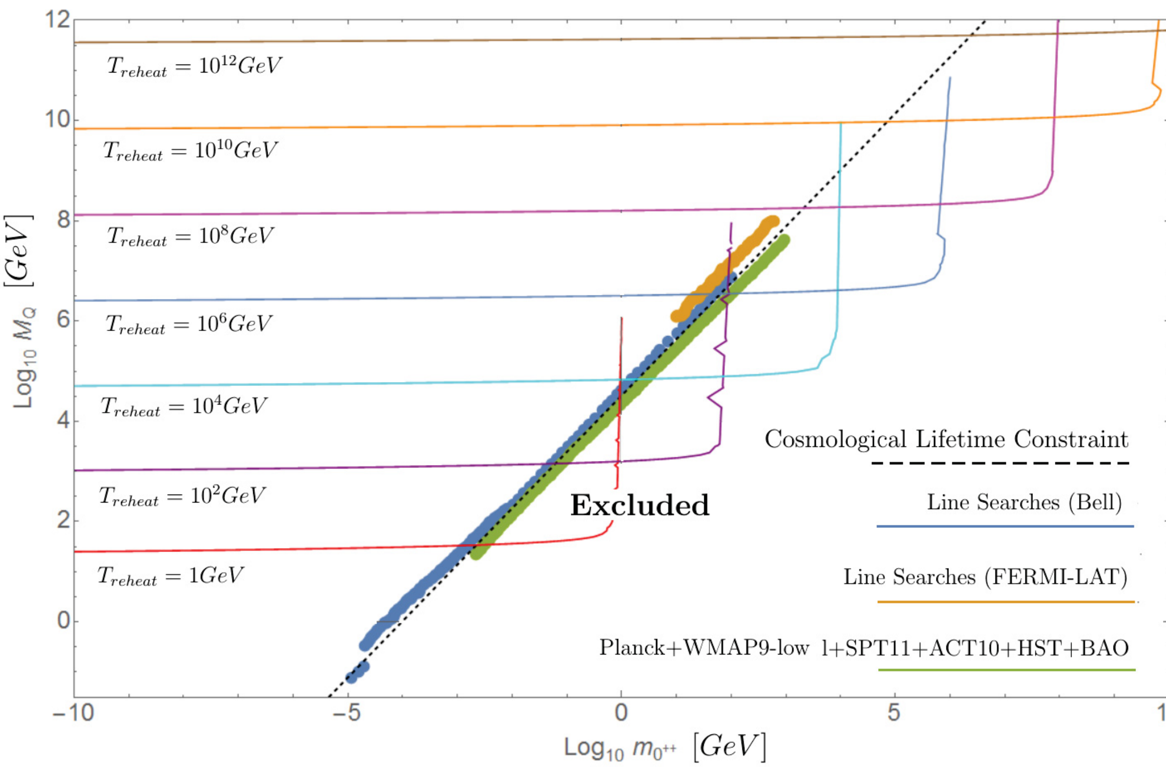

Figure 4.6: Constraints on new particle masses from reheating, line searches [56] [58] and CMB studies [57] for the 3-loop QCD coupled diagram above. Parameter space constraints are almost identical to that of the electromagnetic case, due to the 1/7 suppression of α_s. Reheat constraints computed in $N_c = 3$. Reheating and cosmological lifetime constraints come from the lowest order (1-loop) gluon production diagram. Line search constraints are weaker than in the 1-loop case due to additional loop suppression factors coming from QCD loops. The allowed region of parameter space is above the curves set by reheating and the other constraints

As can be seen in figure 4.6, the reheating constraints remain stringent for values of the reheat temperature approaching the GUT scale. The replacement of couplings does not offer much of a qualitative or quantitative change compared to the direct photon case.

We should also note that our line constraint equations have been modified in regards to the one loop photon production of the previous subsection. In particular, the amplitude to go from a glueball to two resonant photons becomes

$$\langle\gamma\gamma|\frac{\alpha_{HC}\alpha_{EM}}{60M_\Phi^4}F_{\alpha\beta}F^{\alpha\beta}|0\rangle\langle 0|S|0^{++}\rangle \longrightarrow \langle\gamma\gamma|\frac{\alpha_{HC}\alpha_{EM}}{60M_\Phi^4}F_{\alpha\beta}F^{\alpha\beta}\frac{\alpha_s^2}{16\pi^2}|0\rangle\langle 0|S|0^{++}\rangle$$

Where each QCD loop adds a suppression factor of $\alpha_s/4\pi$. The decay rate goes as the square of this, and so to constrain the lifetimes of photon production from glueballs in the QCD coupled scenario, we get a constraint inequality that goes as

$$m_0\tau_{3-loop} = \frac{m_0}{\Gamma_{3-loop}} \sim 9.9 \times 10^9 \left(\frac{M_\Phi}{m_0}\right)^8 \frac{1}{\alpha_{EM}^2\alpha_s^4} > Constraints$$

This additional suppression loosens the constraints set by line searches, bringing them down slightly compared to the one loop photon production. The changes are small due to the 1/8 power suppression on the change of the prefactor in the constraint inequality between the one loop and three loop cases.

4.3.2 1-Loop Diffuse Photon Diagram

Phenomenologically, we can also consider the case of a one loop diagram, in which the gluons hadronize and produce a diffuse spectrum of final state photons for us to detect, as illustrated in the right hand side of figure 4.5. This process is lower order in the couplings compared to the three loop photon case. Reheating constraints remain relevant as we must still check that the interaction rate between hypergluons and regular gluons is always below the Hubble rate to maintain the out of equilibrium condition. Line searches no longer constrain us, however, as the final state photons are not monoenergetic. For this, we turn to constraints from other astrophysical sources.

It is possible to constrain this diagram by way of dwarf spheroidal galaxies. Dwarf spheroidals exhibit gravitational effects that imply much more mass than is observed through luminous matter. This implies a rich region of dark matter. They also seem to have low diffuse gamma ray emission, both from galactic and astrophysical sources. The coupling of these effects makes them an attractive candidate to observe and/or constrain signatures produced from decaying or annihilating dark matter, as has been done by the Fermi-LAT and HAWC surveys [64] [65].

Dwarf spheroidals utilize the diffuse gamma ray flux from dark matter interactions to constrain cross sections and lifetimes. The differential gamma ray flux coming from an astrophysical source can be given by [65]

$$\frac{dF}{dE_{ann}} = \frac{\langle \sigma v \rangle}{8\pi M_{0^{++}}^2} \frac{dN_\gamma}{dE} J \qquad\qquad \frac{dF}{dE_{decay}} = \frac{1}{4\pi\tau M_{0^{++}}} \frac{dN_\gamma}{dE} D \tag{4.44}$$

Where the J and D factors are dark matter densities integrated along the line of sight and solid angle of a source, and dN_γ/dE is the diffuse spectrum of gamma rays produced (indirectly) by the dark matter interactions. For the purposes of our work, we are concerned with dF/dE_{decay}, the flux stemming from decaying dark glueballs.

A possible way to determine the produced photon spectrum is to use the PPPC [66] and/or Pythia [67] software packages. With these packages, it is possible to go from the decay products of our 0^{++} glueballs (regular gluons), to a final photon spectrum, dN_γ/dE. We look at a mathematica package from a recent paper by Slatyer et al [68] which does just that. Note that in this paper, the spectra are presented for a 'cascade' of multiple decays within the dark sector. Our diagram above would then be for a 'direct spectrum' in the jargon of [68].

Before going further, we need to clarify any differences and justify the usage of [68] in our work. One point to make is that in the Slatyer software package, the analysis takes place by imagining the initial process is a dark matter annihilation, generically speaking $\chi\chi \to gg$, whereas we are interested in the decay of a glueball. However, since the final state photon spectrum calculated is sourced by the hadronization and cascade of gluons, it becomes hard to distinguish between an initial decay vs. annihilation. In fact, Slatyer et al. state that the production of direct spectra can be viewed as either a direct annihilation or a decay, and are seen as analogous processes. This is because PPPC (the software utilized by Slatyer) cares only about the energetics of the produced final state particles, and not so much about the production mechanism.

Using their software, we compute the direct spectrum of photons from both final state gluons, and $b\bar{b}$ in figure 4.7.

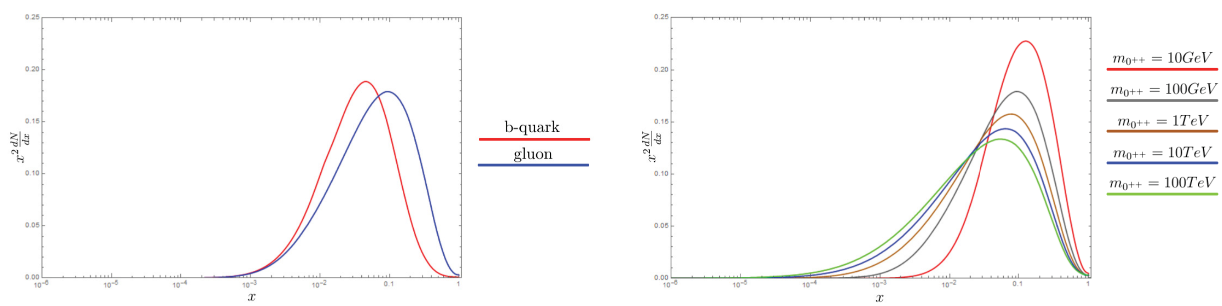

Figure 4.7: Left: A comparison between the b quark and gluon final state spectra for the same energetics. Right: Evolution of the photon spectra for final state gluons as a function of $m_{0^{++}}$. x refers to the fractional energy of the photons, $x = E/m_{0^{++}}$

Constraints from dwarf spheroidals are generally only applied in the literature to final state $b\bar{b}$ particles, and not to gluons. Thus we need to convince ourselves that it is acceptable to use these $b\bar{b}$ constraints for our gluon final state scenario.

Qualitatively, the $b\bar{b}$ spectrum is very similar in shape to the gg spectrum. In fact, if we change the production energy for both decay particles in the same way, the spectrum also changes in qualitatively the same way (they both follow an evolution like the right side of figure 4.7). In both cases, increasing the glueball mass causes the photon spectrum to broaden and shift its peak to smaller values of x. It is this behaviour that motivates us, as well as other authors such as [68] to treat the two spectra as similar enough to apply $b\bar{b}$ constraints to our scenario of final state gluons.

Now, since we have justified the use of the $b\bar{b}$ constraints for our case, we can constrain the parameter space of the gluon coupled model from the Fermi-LAT [64] and HAWC [65] experiments. To relate the lifetime constraints from these experiments to the masses $m_{0^{++}}$ and M_Φ, we estimate the lifetime of our dark glueballs in the same way as was done in section 4.2.1 (specifically equation 4.12) to find [50]

$$\Gamma(0^{++} \to gg) = \frac{1}{\tau} \sim \frac{\alpha_s^2}{32\pi^3} \frac{m_{0^{++}}}{M_\Phi^2} \left(\frac{1}{60} \frac{g_{HC}^2 f_0^S}{M_\Phi^3} \right)^2 \tag{4.45}$$

Applying these diffuse photon constraints, as well as the reheating constraints allows us to once again plot the parameter space below in figure 4.8

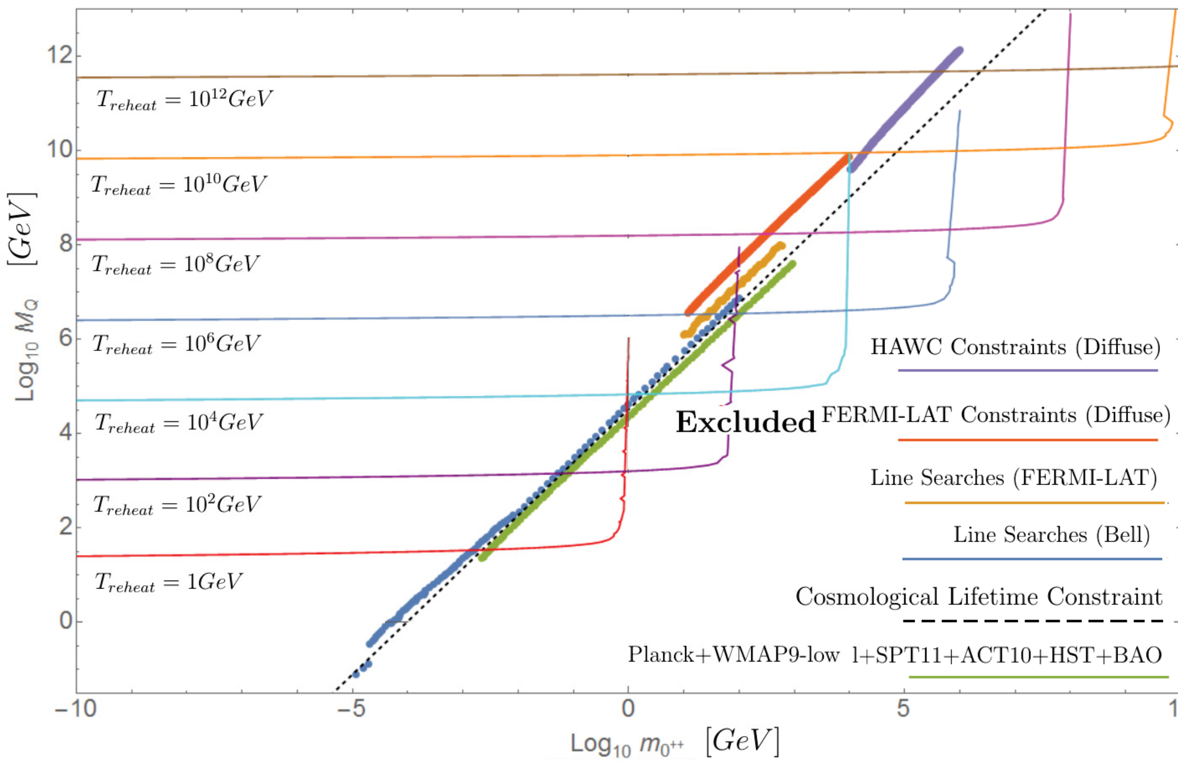

Figure 4.8: Diffuse photon constraints from Fermi-LAT [64] and HAWC [65] experiments investigating decaying dark matter from dwarf spheroidal galaxies. As before, the allowed parameter space is that above the reheating contours, the cosmological lifetime constraint, and the diffuse photon constraints. The cosmological lifetime constraint is computed from the 1-loop gluon-hypergluon interaction. We have also included the constraints from line searches presented in figure 4.6 for ease of comparison.

No excess signal has been detected by the Fermi-LAT or HAWC teams as of this point, and so these constraints come from non-detection of an additional source of diffuse photons. Fermi-LAT offers the strongest constraints for a dark matter candidate with $m_{0^{++}} < 4\ TeV$, whereas for higher glueball masses from $10\ TeV < m_{0^{++}} < 100\ TeV$ HAWC offers the best constraints.

For our analysis, we relate once again the lifetimes of the dark glueballs using the expression (4.45). We estimate $\alpha_s \sim 1$ as the strong coupling for the decays of glueballs in dwarf spheroidals.

4.3.3 Heavy Φ Production in Colliders

As we have seen so far, the heavy Φ particle allows our dark glueballs to decay because it possesses both an $SU(N)$ dark charge, as well as some standard model coupling. If this is the case, though, the direct couplings of Φ to the standard model fields should create an observable imprint on observational particle data. Cosmologically speaking, if these heavy particles are produced rarely we will see little impact on observables such as structure formation and CMB measurements. Colliders, however, could produce noticeable quantities of these new particles, and hence we can estimate the signal expected from such a Φ particle. We note that this has been considered already in the literature, and the existence of a heavy quark like particle has been called a 'quirk', but we will stick to Φ for our work as we present a brief review [52] [70].

Consider proton-proton collisions in the LHC as our method to probe the existence of this Φ particle. The process happens in a similar fashion to Drell-Yan scattering, but includes multiple diagrams (see figure 4.9). This subsection will be concerned with computing the scattering cross-section of the production mechanism, and we discuss the phenomenological effects in the following subsection.

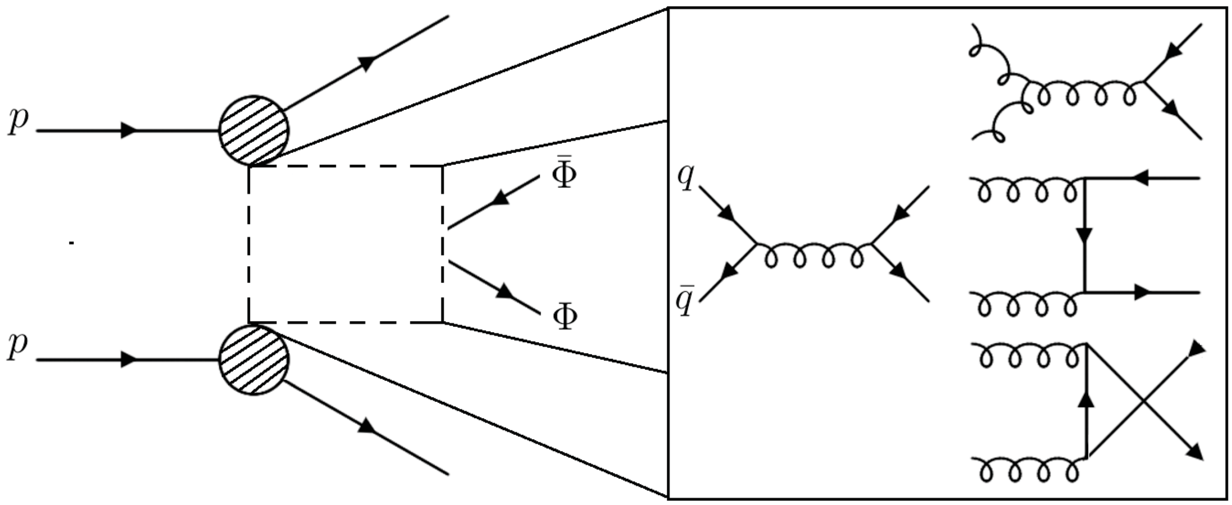

Figure 4.9: Φ production can take place through quark or gluon fusion processes in colliders. All curly lines are gluons (not hypergluons). Note that hypercolor confinement will keep these final state Φ particles bound to one another.

As this production makes use of hadron-hadron collisions, we must employ the parton formalism to compute the cross-section. To determine these cross sections, we follow [2] and [52]. The internal interaction responsible for the production of Φ particles takes place by either quark or gluon fusion, as described in the above figure. From our parton formalism, we must compute the cross section of each internal interaction in order to determine the full cross section for this production process. Quoting [2], the differential cross sections for quark and gluon fusion are

$$\begin{aligned} \frac{d\hat{\sigma}}{dt}(q\bar{q} \to \Phi\bar{\Phi}) &= \frac{4\pi\alpha_s^2 N}{9\hat{s}^4}\left[(m^2-\hat{t})^2+(m^2-\hat{u})^2+2m^2\hat{s}\right] \\ \frac{d\hat{\sigma}}{dt}(gg \to \Phi\bar{\Phi}) &= \frac{\pi\alpha_s^2 N}{8\hat{s}^2}[\frac{6(m^2-\hat{t})(m^2-\hat{u})}{\hat{s}^2} - \frac{m^2(\hat{s}-4m^2)^2}{3(m^2-\hat{t})(m^2-\hat{u})} \\ &+\frac{4(m^2-\hat{t})(m^2-\hat{u})-8m^2(m^2+\hat{t})}{3(m^2-\hat{t})^2}+\frac{4(m^2-\hat{u})(m^2-\hat{t})-8m^2(m^2+\hat{u})}{3(m^2-\hat{u})^2} \\ &-3\frac{(m^2-\hat{t})(m^2-\hat{u})+m^2(\hat{u}-\hat{t})}{\hat{s}(m^2-\hat{t})}+3\frac{(m^2-\hat{u})(m^2-\hat{t})+m^2(\hat{t}-\hat{u})}{\hat{s}(m^2-\hat{u})}] \end{aligned} \tag{4.46}$$

Here, $m = M_\Phi$ has been made for clarity, and variables with the hat denote their parton versions, for example $\hat{s} = (x_1 p_1 + x_2 p_2)^2$ where x_1 is the momentum fraction of the parton coming from one of the incoming protons p_1, and x_2 the momentum fraction of the other parton stemming from the proton with momentum p_2. N is related to our gauge group, $SU(N)$ and is representative of the degeneracy in the number of 'hidden' colors in our dark sector. Integrating these equations and defining a dimensionless quantity, $z = 4m^2/\hat{s}$ yields

$$\begin{aligned}\hat{\sigma}(q\bar{q} \to \Phi\bar{\Phi}) &= \frac{4\pi\alpha_s^2 N}{27\hat{s}}(2+z)\sqrt{1-z} \\ \hat{\sigma}(gg \to \Phi\bar{\Phi}) &= \frac{\pi\alpha_s^2 N}{48\hat{s}}\left[-(28+31z)\sqrt{1-z} + (16+16z+z^2)\ln\frac{1+\sqrt{1-z}}{1-\sqrt{1-z}}\right]\end{aligned} \tag{4.47}$$

With these, we can write the full cross section for production of these Φ particles coming from proton-proton collisions.

$$\begin{aligned}\sigma(P_1 P_2 \to \Phi\bar{\Phi}) = \int_0^1 & dx_1 dx_2 [g_{P_1}(x_1) g_{P_2}(x_2) \hat{\sigma}(gg \to \Phi\bar{\Phi}) \\ &+ (q_{P_1}(x_1)\bar{q}_{P_2}(x_2) + \bar{q}_{P_1}(x_1) q_{P_2}(x_2))\hat{\sigma}(q\bar{q} \to \Phi\bar{\Phi})]\end{aligned} \tag{4.48}$$

Where P refers to the proton parton distribution function, empirically found. This equation can be solved numerically to acquire constraints on the mediator mass M_Φ.

4.3.4 Phenomenology of Φ

The idea of the production of this Φ particle has been considered in detail in [52], and so we will review some of the results here. We stress that our aim is to present a heuristic review of results presented by other collaborations, and that future work should include a more complete and quantitative analysis of the constraints set by the LHC. It is important to first recall a little about color confinement and how it applies to the production of heavy particles interacting under the strong force.

Very schematically, recall that in the usual strong interactions, production of quarks or gluons create jets of particles due to color confinement. Since free particles cannot have color, the production of say, a quark antiquark pair is not free, and the two particles are bound by a so called flux tube. This flux tube consists of a stream of color charged particles, and increases in energy as the newly formed quarks increase their physical separation. At a separation of about $d \sim \Lambda_{QCD}^{-1}$, it becomes energetically favourable for these flux tubes (or QCD strings) to break and pop a corresponding quark-antiquark pair out of the vacuum. This is because $m_q < \Lambda_{QCD}$, and so the flux tubes have more than enough energy to create light quarks out of the vacuum. This creation allows for color neutral mesons or baryons to be formed, ensuring the final state particles do not possess color.

In a theory with a very heavy quark-like object such as our Φ particles, this is not possible. In general, flux tubes have energy per unit length of order Λ^2, and since for a heavy, integrated out degree of freedom, $M_\Phi >> \Lambda$, the tube does not have the energy required to pop a $\Phi\bar{\Phi}$ out of the vacuum. This leads to a bound state that has been dubbed 'quirkonia' in recent literature where such particles are called quirks.

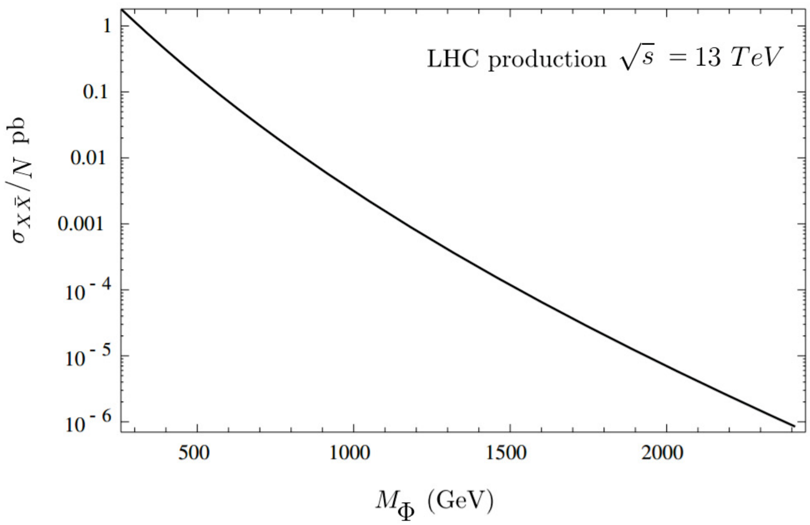

Figure 4.10: Full production cross section of Φ particles from parton formalism. $\sqrt{s} = 13\ TeV$ for the latest LHC run. Figure adapted from [52]

As shown in figure 4.10, the heavier the mediator particle, the less likely it is to be produced. The size of the gauge group N also suppresses this cross section linearly. For a sufficiently light enough Φ particle, there could be a significant 'missing energy' signal to look for in proton-proton collisions at the LHC. This missing energy would come from the production of Φ particles, which would escape without being detected, thus giving us a deficit at some resonant energy. Alternatively, a $\Phi\bar{\Phi}$ found state will oscillate, producing gluons, dark gluons, and/or dark glueballs. Since the dark glueballs are stable, they will leave the detector unperturbed yielding missing energy. The radiation of colored particles such as gluons will produce jets that can also be used to constraint the model. A similar scenario happens in the case that a bound state of Φ annihilates inside the detector, potentially producing both standard model and dark sector particles. particles The full quantitative theory on the production of the $\Phi\bar{\Phi}$ bound states is beyond the scope of this work, but we will review arguments presented in [52] on how these states can decay.

As stated beforehand, we cannot break the flux tube separating two Φ particles due to their high mass, so the produced Φ and $\bar{\Phi}$ in a collision oscillate about their classical turning points. These oscillations are damped, however, due to the non-perturbative emission of dark glueballs, and the perturbative emission of standard gluons. After sufficient damping occurs, the $\Phi\bar{\Phi}$ state can annihilate with itself to produce even more particles, giving us potential signals to hunt for in detectors. Possible annihilation products include hypergluons (which will bind into dark glueballs at long distances) as well as standard quarks or gluons.

Three different types of decays are reviewed in the literature. Hard annihilations occur when the $\Phi\bar{\Phi}$ state annihilate directly into hypergluons (and subsequently, more dark glueballs). Radiative decays are also possible, with both the standard model and the hidden sector playing a role. From the standard model side, the bound state can slowly decay by a cascade of gluons, which would hadronize into pions and kaons (mostly). It is also possible to have dark glueball radiative decays, in which a bound state emits a standard J^{PC} glueball as a way to lower its energy. We should note, however, that this is a non-perturbative effect from a hidden sector, so this mechanism is highly uncertain. For $\Lambda_{HC} << M_{\Phi}$, a potential model similar to that for heavy quarkonium can be used as an analogue for this decay. Detailed results for the decay rates of these different processes are available in chapter 4 of [52].

An additional point to consider are constraints coming from bound states of $\Phi\bar{\Phi}$ in the limit of a low hidden confinement scale. This is interesting because the lower we take Λ, the further away (in physical space) the bound state of Φ particles can travel from each other before reaching their classical turning points and snapping back together. For values of the scale, $1eV < \Lambda < 10^4 eV$, the length of the flux tube connecting the Φ particles can become macroscopic (in relation to CMS and LHC detector sizes), creating signatures that could be seen in the LHC or CMS experiments [73]. Specifically, it has been found in the literature that in the Nambu-Goto approximation, the flux tube connection between our Φ bound state has an effective length, given by

$$\ell_{eff} \approx 10m \left(\frac{m_\Phi}{1TeV}\right) \left(\frac{100eV}{\Lambda}\right)^2 \left(\frac{v}{0.7}\right)^2 \tag{4.49}$$

Where m_Φ is the mass of our Φ particle, Λ is the confining scale in our dark sector, and v is the relative velocity of a Φ particle with respect to the centre of mass of the bound state of $\Phi\bar{\Phi}$. If we are looking for phenomenology due to the macroscopic separation of the mediator particles, we are looking at $1eV < \Lambda < 10keV$. For smaller confinement scales, the flux tube is too large ($\Lambda \sim d^{-1}$) and wont impose any signatures on collider data. For larger confinement scales, the separation distance is smaller than the tracking resolution of the detectors. Φ in this regime can be constrained by observing non-standard particle tracks in detectors. Standard quarks exhibit helical shaped trajectories in the xy plane, so deviations from this can stem from a new hidden gauge group. Note that these helical trajectories are produced by a magnetic field, so these constraints can only be applied to a case with electrically charged Φ particles. The signature in this intermediate Λ regime is thus deviations from helical trajectories inside the detector. Heavy stable charged particle searches (HSCPs) have been reinterpreted by [73] using datasets from the CMS [74] and Atlas detectors [75]. Monojet search results from CMS [76] and Atlas [77] are also reinterpreted to give constraints on the Φ parameter space.

Finally, it is also possible to utilize $0T$ data from CMS [78] (no external magnetic field in the tracking) to constrain the parameter space further. The idea here is that in the absence of a magnetic field, quarks travel in straight lines, whereas these Φ particles still have their paths bent due to the flux tube connecting a pair of them. In this case, Φ does not need to be electrically charged. Combining constraints in this low Λ regime, the authors of [73] produced a plot of the Φ parameter space (figure 4.11)

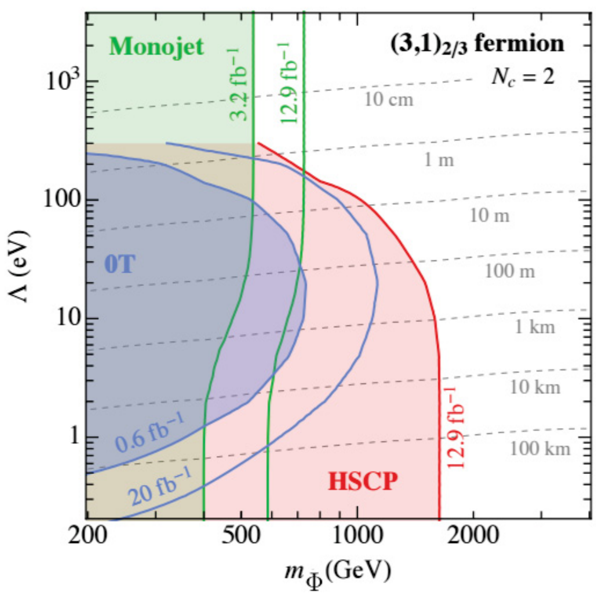

Figure 4.11: 95% confidence limits on a new fermionic Φ particle transforming as a triplet under $SU(3)_{strong}$. The hidden gauge group here has $N = 2$. Red and green shaded regions are constraints from HSCPs and monojets respectively. Projected constraints are also given for the $0T$ scenario. Unshaded lines represent projected constraints with more data. Grey dashed lines correspond to the effective length of the flux tube separating a $\Phi\bar{\Phi}$ pair. Figure credit to [73]

As with any constraints, we need to choose a few properties of the Φ particle to make a parameter space plot. Here, the authors of [73] assume the hidden gauge group is $SU(2)$, and that Φ transforms as a fermionic triplet under the standard model $SU(3)$.

Further constraints on this 'quirky' Φ scenario have been considered by [71], and so for a more quantitative analysis of this case the reader is invited to examine this paper, as well as the arguments presented by [52] [70].

4.4 Higgs Portal Decay

As our final point of discussion, let us consider the case in which our dark glueballs interact with Φ mediators like usual, but the Φ particles don't couple to any standard model gauge bosons. Instead, decays happen via Higgs portal interactions. This is possible by specifying that the mediator in this case is a scalar particle, and couples to the Higgs in the form of a H^2S^2 type interaction. These decays happen primarily via dimension six operators, as opposed to the dimension eight suppressed operators in the previous two subsections.

In the absence of any other standard model couplings, the 0^{++} glueball (normally thought to be the vastly abundant species) is allowed to decay via this dimension six Higgs operator. However, the lack of standard model couplings prevents the 1^{+-} glueball from radiatively decaying into a 0^{++} (due to conservation of charge parity), and so conversely, if we can allow the 0^{++} state to decay fast enough, our dark matter candidate could be the vector glueball state. We also note that the 0^{-+} glueball may be protected by some additional symmetries that prevents decay into the 0^{++}, but this is much more model dependent [47] [53] [72]. In this subsection, we primarily report the work of the aforementioned citations, and briefly discuss consequences of such a coupling on an $SU(N)$ dark theory of this kind.

4.4.1 Decay Rate of the 0^{++}

As in the previous subsections, we induce decays of our glueballs via higher dimensional operators with our scalar mediator particle, Φ. The Lagrangian for our Φ particle is assumed to take the form given in [47] (also see [49])

$$\mathcal{L}_\Phi \sim M_\Phi^2 \Phi^2 + \lambda \Phi^2 |H|^2 \tag{4.50}$$

At scales lower than M_Φ but higher than the dark confinement scale and EWSB, we get the following dimension 6 operator mediating the coupling between the dark gluons and the Higgs sector

$$\mathcal{L}_{eff} \sim \frac{\lambda \alpha_{HC}}{M_\Phi^2}(H^\dagger H)(H^a_{\mu\nu} H^{a,\mu\nu}) \tag{4.51}$$

Where we have used the momentarily confusing notation of H being the Higgs doublet, and $H^a_{\mu\nu}$ being our hypergluon field strength. The suppression coming from a combination of λ and $1/M_\Phi^2$ coefficients can lead to large suppressions (potentially even larger than those of the dimension 8 operators considered above), and so corrections from any standard model couplings could become important. We negate this issue by considering a pure coupling of our Φ particles to the Higgs sector.

While we have a spectrum of dark glueballs, radiative decays allow most (but not all!) of the heavier states to decay to the 0^{++} state. This state is thus thought to be the most abundant, and in some models thought to be the dominant contribution to the dark matter density, Ω_{DM}. Because of this, analysis of the decay of 0^{++} is of the paramount importance. From the effective Lagrangian, it is possible to deduce the decay rate of a 0^{++} to a pair of standard model particles via an s-channel Higgs exchange. Quoting [47] (and[53]), this decay rate is

$$\Gamma(0^{++} \to \xi\xi) \approx \left(\frac{\lambda v_H g_{HC}^2 f_0^S}{4\pi^2 M_\Phi^2 (m_H^2 - m_{0^{++}}^2)} \right)^2 \Gamma(h \to \xi\xi; m_{0^{++}}^2) \tag{4.52}$$

where m_H is the mass of the Higgs ($\approx 126GeV$), v_H is the vacuum expectation value of the Higgs ($\approx 246GeV$), $\Gamma(h \to \xi\xi; m_{0^{++}}^2)$ is the decay width of a Higgs to standard model particles if it had a mass $m_{0^{++}}$, and f_0^S is the 0^{++} decay constant. If we recall from above, lattice calculations for a pure $SU(3)$ theory that $g_{HC}^2 f_0^S \approx 3m_{0^{++}}^3$. With this substitution, the decay rate takes a more tractable form

$$\Gamma(0^{++} \to \xi\xi) \approx \left(\frac{\lambda v_H m_{0^{++}}^3}{4\pi^2 M_\Phi^2 (m_H^2 - m_{0^{++}}^2)} \right)^2 \Gamma(h \to \xi\xi; m_{0^{++}}^2) \tag{4.53}$$

This is the only decay channel for $m_{0^{++}} < 2m_H$, so it makes sense to expand in the limit $m_{0^{++}}^2 << m_H^2$, noting that the Higgs is related to its VeV by $m_H \sim v_H$. This expansion yields

$$\Gamma(0^{++} \to \xi\xi) \approx \left(\frac{\lambda m_{0^{++}}^3}{4\pi^2 M_\Phi^2 v_H} \right)^2 \Gamma(h \to \xi\xi; m_{0^{++}}^2) \qquad (m_{0^{++}}^2 << m_H^2) \tag{4.54}$$

If $m_{0^{++}} > 2m_H$, the decay channel of a glueball to a pair of Higgs particles also opens up. The width of this decay can be written as [53]

$$\Gamma(0^{++} \to hh) = \frac{1}{32\pi m_{0^{++}}} \left(\frac{\lambda m_{0^{++}}^3}{4\pi^2 M_\Phi^2} \right)^2 \left(1 + \frac{3m_H^2}{m_{0^{++}}^2 - m_H^2} \right)^2 \sqrt{1 - \frac{4m_H^2}{m_{0^{++}}^2}} \tag{4.55}$$

In the opposite mass range, for very heavy dark glueballs such that $m_{0^{++}}^2 >> m_H^2$, this decay rate becomes

$$\Gamma(0^{++} \to hh) = \frac{1}{32\pi m_{0^{++}}} \left(\frac{\lambda m_{0^{++}}^3}{4\pi^2 M_\Phi^2} \right)^2 \qquad (m_{0^{++}}^2 >> m_H^2) \tag{4.56}$$

These limiting expressions roughly match other results found in the literature [47] for the case of an $SU(3)$ hidden sector.

4.4.2 $1^{+-}, 0^{-+}$ in a Sea of Metastable 0^{++}

As stated earlier, there are two possible scenarios for Higgs coupled glueball dark matter. First off, we can carry out the usual procedure where we determine the freeze out temperature of the 0^{++} decays and push it above the reheating temperature to see how tight the constraints on our parameters have to be. Due to the vast number of glueball states that can decay down to the 0^{++} via Higgs radiative processes, these dark glueballs would be the dominant contribution to Ω_{DM}. With no additional couplings on our mediator, however, there are a couple other glueball states that persist as they are protected by other symmetries. These other glueballs would become the subdominant contribution to Ω_{DM}.

Alternatively, it is possible to paint a picture where the 0^{++} glueballs decay very quickly via the Higgs portal. This idea is first discussed in [47], and so we restate their arguments here. This is only possible if we have conservation of C and P quantities independently in the dark sector, and so we take that as an assumption in what follows. If the 0^{++} particles are cosmologically short-lived, they would not contribute to the dark matter density at all, and instead we must look for another candidate. Luckily, there are a couple that naturally occur in a Higgs-only connection between the standard model and the hidden sector, and those are the 1^{+-} and 0^{-+} glueballs. The 1^{+-} is the lightest particle in the $C = -$ sector, and so any decays it could undergo would have to change its charge conjugation number. The Higgs is unable to do so, therefore in the absence of additional standard model couplings, it is stable. In the absence of extensions to the standard model such as additional parity violation in the or a two Higgs doublet model, the 0^{-+} is stable as well. The radiative decay $0^{-+} \to 0^{++}h$ cannot occur because in order to conserve angular momentum ($L_{before} = L_{after} = 0$), you must violate parity. Both of these glueballs make for potential candidates in the scenario where the lifetime for the 0^{++} is cosmologically short. This unique characteristic of dark glueballs is still unexplored, and would be a great extension to the work presented here.

We should note a possible shortcoming of this idea, however. Since the standard model does have C violation, it is possible that higher loop orders could induce C violation allowing this 1^{+-} state to decay. This is possible as the Higgs couples to C violating processes in the standard model, but these processes would be suppressed by additional loop factors, so it is not clear that they would significantly effect the lifetimes of the 1^{+-} states. This is not considered in the arguments of Forestell *et al* [47].

Relic densities for dark glueballs have been computed in [47]. The abundance of the lightest glueball (0^{++}) was calculated assuming $3 \to 2$ number changing processes set the yield. The heavier glueballs are expected to decay to the lightest state in the absence of additional dark sector symmetries, so their $3 \to 2$ interactions are not as important as the $2 \to 2$ transfer reactions. We assume the decays of the 0^{++} have all occurred by the late-time universe, and so we wont be interested in that result. Heavier glueballs had their Boltzmann yield calculated assuming $2 \to 2$ transfer processes. These relic densities are plotted by Forestell *et al* in [47], which we have reproduced as figure 4.12.

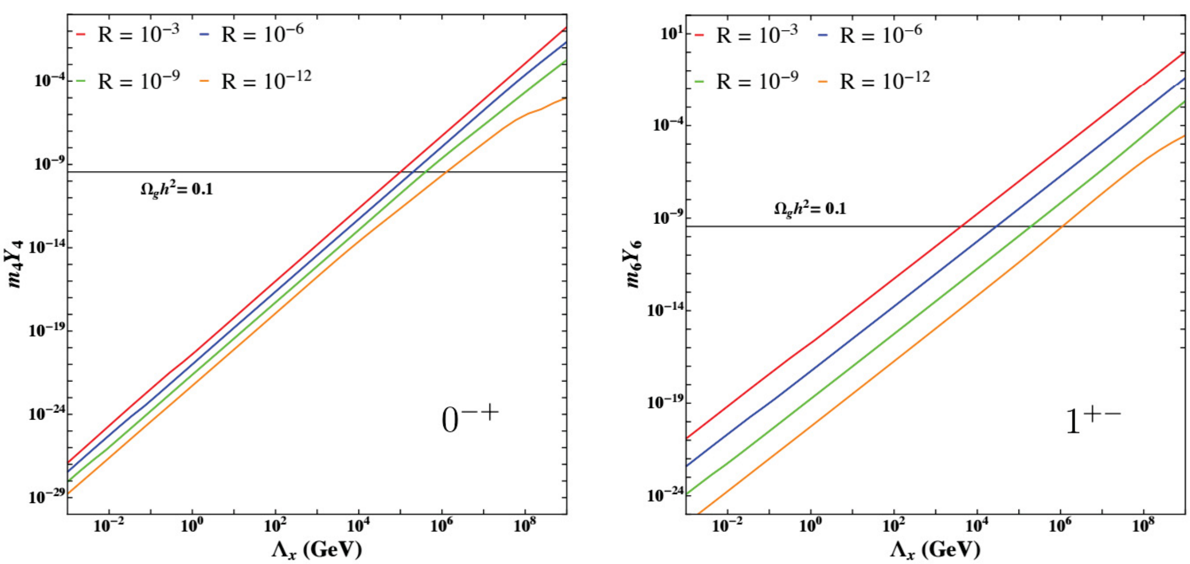

Figure 4.12: Relic densities of the 0^{-+} and 1^{+-} states, weighted by their masses. $R = s_{HC}/s$ is the relative entropy between the two sectors, and is a conserved quantity after all confining phase transitions. The horizontal line represents the necessary value of $m \cdot Y$ to give the observed dark matter abundance in the universe today Figure adapted from [47]

Chapter 5

Discussion and Outlook

The aim of this work was to present a coherent and modular attempt at explaining dark matter in terms of an $SU(N)$ hidden gauge group, in the context of particle cosmology. To that end, we found it prudent to introduce many of the main concepts in quantum field theory and cosmology, before applying them in the context of the Boltzmann equation for determining relic densities of primordial particle species. After concluding this, we finally came to the description of an $SU(N)$ glueball making up the dominant dark matter density in the universe. In this section we go over open questions, problems, and ideas concerning our work on the numerical Boltzmann equation code, as well as the dark matter model constructed in the previous chapter.

In chapter 3, we presented a work-in-progress of a mathematica notebook capable of computing Boltzmann yields and freeze out temperatures for generic classes of particle dark matter. At this stage, the code seems capable of reproducing accepted results such as the abundance of baryons in a baryon-antibaryon symmetric universe (presented analytically in Kolb and Turner [16]), and thus seems to be trustworthy. Because of this solid foundation, it is natural to ask what improvements can be made on such a piece of code.

Improvements can come on computational, user-friendly, and robustness fronts. Computationally, much of this code has been written in such a way that it performs the tasks set in front of it, but not necessarily in the most efficient ways. Time has not been invested in determining the efficiency at which the NDSolve and other functions run within Mathematica. It is possible that when considering more complicated forms of dark matter, we may run into efficiency issues, and so this aspect should be investigated. On the user-friendly side, as it stands the code can be cumbersome and confusing to work with. If made available to other working groups in their computations, it would benefit with the addition of a graphical user interface (GUI). GUIs are easily made in Mathematica using the GUIkit package, and would highlight the simple elegance of our software.

Lastly, in order to make our software more robust, additional attributes, both on a cosmological and on a particle physics side, should be included in our calculation. This could be realized with additional parameters specifying any initial asymmetry in particle species being considered, allowing for corrections to relic densities from more than one decay/number changing channel, and allowing coupling constants of interactions to run with the energy scale. Improving the software with the above suggestions could make the package an attractive choice for other research groups wishing to determine relic densities and decoupling times in a simple, yet powerful, manner.

Moving forward, we next considered our $SU(N)$ glueball dark matter candidate. We allowed for the decay of this glueball to occur via loops of a heavy mediator particle, Φ, which we considered to possess couplings to different standard model fields. We will briefly discuss each of these couplings once more, and discuss the outlook of each scenario.

First, we considered coupling the Φ particle to $U(1)$ hypercharge (and subsequently, electromagnetism and the Z below EWSB). Due to a number of line search surveys over the past decade, constraints on the decay modes of this dark matter were quite stringent. From entropy considerations, we required that the two sectors were never in thermal equilibrium with one another. Pushing the freeze-out temperature above sensible values of the reheat temperature from inflation showed that the parameter space was highly constrained. In an effort to study how this phenomenology changes, we considered different standard model couplings.

Couplings to the strong force were introduced instead. First, we considered a diagram that would produce a line of photons, as in the previous case. This happens at the three loop level, though no change of the reheat temperature constraints was observed, as the $\alpha_{EM} \to \alpha_s$ was raised to the 1/7th power. Next, we considered the production of a diffuse spectrum of photons by allowing the final state gluons to hadronize and emit particles. Constraints from the HAWC and Fermi-LAT surveys were utilized to constrain this scenario, along with our reheat constraints. This coupling does give the ability to detect Φ particles in colliders, as they should be produced abundantly in proton-proton collisions. The collider phenomenology of this is discussed above, and in depth in [52].

To conclude, we discussed the possibility of Higgs couplings on our Φ mediator. Higgs couplings are different than other gauge bosons in that these glueball decay operators come at dimension 6 rather than dimension 8. This allows us to consider two possibilities:

- The Higgs couplings could produce extra suppression that would counteract the fact that the operator is suppressed by only mass dimension 6. This is the standard approach attempted with the previous two couplings, and so we could hope this additional suppression allows us to raise the freeze out temperature substantially. This seems unlikely, however, due to the scaling between T_f and σ discussed above.

- The Higgs couplings are not very suppressed, and decay of the lightest and most abundant 0^{++} dark glueball occurs very rapidly. With only Higgs couplings, the next lightest glueballs, 1^{+-} and 0^{-+} are stable due to symmetries. These other glueballs could then form the dominant dark matter contribution.

Though both scenarios are possible, the second case with the fast decaying 0^{++} dark glueball seems of particular interest to the author. If a large proportion of these decays take place in the early universe, they could generate additional signals such as μ or y type spectral distortions in the CMB.

Spectral distortions are departures from a blackbody for the CMB frequency spectrum. Since decaying glueballs would transfer energy from the dark sector to the standard model, they can perturb the thermal frequency spectrum of the thermal bath of photons. These distortions can potentially be observed by future satellites such as PIXIE or EUCLID, who would probe these distortions to a $\Delta I/I \sim 10^{-9}$ level. Significant energy releases at a redshift of $z \leq 10^6$ that could be observed. For an interesting read, refer to [79] and references therein on potential new physics that can be constrained by spectral distortions.

The next step in this project should be to investigate these Higgs portal connections in much more detail.

Chapter 6

Conclusions

In this work we have presented a general overview of particle cosmology, analytic and numeric methods to solving the Boltzmann equation, and introduced a new $SU(N)$ gauge group in an attempt to describe the dark matter phenomenon. We have attempted to keep everything as self-contained as possible.

The numerical Boltzmann code developed has been shown to correctly predict relic densities and freeze out temperatures of analytically calculated phenomenon. Moreover, it serves as a simple tool for determining freeze outs and relic densities for generic classes of particle dark matter. With some tune-ups, both computationally and visually, this software could be a simple, yet powerful tool for easily determining Boltzmann yields.

A pure $SU(N)$ theory gives dark glueballs as the main massive species contributing to the observed dark matter density in the universe today. Phenomenological signals can be obtained by considering a heavy mediator Φ acting as a portal between the dark and standard sectors. Decays of the lightest 0^{++} into photons and gluons seem constrained by aspects of cosmological reheating, though gluon couplings do present the opportunity for interesting phenomenology at colliders. Couplings induced via the Higgs can present an interesting scenario where the lightest glueballs decay quickly, and the $1^{+-}, 0^{-+}$ become the dominant late-time species as their decay is protected by some symmetries. This scenario should be investigated in more detail.

Appendices

Appendix A

Overview of Units and Unit Conversions

The units used in this thesis are such that $c = \hbar = k_B = 1$ in order to make the formulae less cumbersome. To the unfamiliar reader, a lot of the units presented in this thesis can look utterly wrong, so let us go over a few scenarios.

We have a matter-energy equality, leading us to present quantities such as the dark matter mass in terms of an energy ($m_{DM} = 5MeV$). This comes from Einstein‘s famous relationship

$$E = mc^2$$

As $c = 1$ in this situation, we can see that expressing mass in energy units is natural. We also have a temperature-energy equality, which stems from the units of the Bolztmann constant. In SI units the Boltzmann constant, k_B, is

$$k_B = 1.38 \cdot 10^{-23} \frac{J}{K}$$

In units where $k_B = 1$, we can always multiply or divide an equation by k_B in order to switch between units of temperature and of energy. The same goes for the units of $\hbar$, but this substitution has rarely been used in our thesis.

We have chosen the mostly minus signature for our metric, conforming to that of Peskin's textbook [1].

Appendix B

Miscellaneous Computations

Here we present a couple of computations that are perhaps not the most obvious. As such, we expand upon these computations in order to provide motivation for forms used in the above work.

B.1 Differential Element in the Computation of $\langle \sigma v \rangle$

If we recall in section 3.2.2, we had the differential element $d^3p_1 d^3p_2$ in our computation. This form is relatively unusable in actually computing the thermally averaged cross section times velocity, and so we include in more detail the transformation done to give us a more practical integral.

Note in transforming from a Cartesian type differential to a spherical one, we have

$$d^3p_1 = |p_1|^2 d|p_1| d(\cos\theta) d\phi \tag{B.1}$$

We note now that the rest of our integrand is independent of θ, ϕ and thus we can perform a couple of integrations on this element. Since we want to eventually introduce the Mandelstam variable s which has an angular dependence between p_1 and p_2, its prudent to align our coordinate system with the direction of p_1 and integrate the angle of p_2 with respect to its angle with this rotation. This means we can write

$$\int |p_1|^2 d|p_1| d(\cos\theta') d\phi \int |p_2|^2 d|p_2| d(\cos\theta) d\phi = \int 4\pi |p_1|^2 d|p_1| \int 2\pi |p_2|^2 d|p_2| d(\cos\theta) \quad \text{(B.2)}$$

Now, from the relativistic energy equation, and its derivative we have

$$\begin{aligned} E^2 &= m^2 + p^2 \\ EdE &= pdp \end{aligned} \quad \text{(B.3)}$$

So making this substitution, we our differential element has transformed to

$$d^3p_1 d^3p_2 = 8\pi^2 p_1 p_2 E_1 E_2 \; dE_1 dE_2 d(\cos\theta) \quad \text{(B.4)}$$

From here, the substitutions of E_+, E_-, s are straightforward and we get to the final, useful differential element

$$d^3p_1 d^3p_2 = 2\pi^2 E_1 E_2 \; dE_+ dE_- ds \quad \text{(B.5)}$$

With a transformed integration region

$$\begin{aligned} |E_-| &\le \sqrt{(1 - 4m^2/s)\,(E_+^2 - s)} \\ E_+ &\ge \sqrt{s} \\ s &\ge 4m^2 \end{aligned} \quad \text{(B.6)}$$

and the rest of the computation continues straightforwardly from here.

B.2 Derivative Interactions

In the section on photon couplings to our mediator Φ, we noted that the derivative interactions stemming from the $\partial_\mu A_\nu \partial^\mu A^\nu \partial_\alpha W^a_\beta \partial^\alpha W^{a,\beta}$ gave us something like $4[(k_1 \cdot k_2)(k_3 \cdot k_4)]$, where the $1, 2$ correspond to in state particles, and the $3, 4$ correspond to out state ones.

Consider first an interaction term in some scalar field Lagrangian that looks like

$$\mathcal{L}_{int} \sim g\phi\partial^\mu\phi\partial_\mu\phi \tag{B.7}$$

The vertex function for such a term does not stipulate which particles (in or out state) have the derivative interactions associated with them. As such, the vertex factor takes into account this discrepancy by setting

$$g\phi\partial^\mu\phi\partial_\mu\phi \to 2g(k_1k_2 + k_1k_3 + k_2k_3) \tag{B.8}$$

Similarly, a four point function with one real scalar field yields by the same logic

$$\lambda\partial_\mu\phi\partial^\mu\phi\partial_\nu\phi\partial^\nu\phi \to 4\lambda[(k_1 \cdot k_2)(k_3 \cdot k_4) + (k_1 \cdot k_3)(k_2 \cdot k_4) + (k_1 \cdot k_4)(k_2 \cdot k_3)] \tag{B.9}$$

So it stands to reason that our derivative interactions, which contain two undetermined fields, will have a vertex factor structure like

$$\partial_\mu\phi^*\partial^\mu\phi^*\partial_\nu\phi\partial^\nu\phi \to 4[(k_1 \cdot k_2)(k_3 \cdot k_4)] \tag{B.10}$$

The only difference between the complex scalar field we are considering here and the vector fields in the work, is that of the polarization states, which are considered separately.

Appendix C

Mathematica Notebook

Numerical Boltzmann Equation

Boltzmann Equation Numerical

Preliminaries

Here we compute some numerical factors, nothing too important here,

$$\texttt{N}\left[\texttt{Zeta[3]} / \left(\pi^2 * 1.67\right)\right]$$

0.0729304

$$\texttt{Integrate}\left[p^2\, \texttt{E}^{-T^{-1}\left(m+p^2/(2\,m)\right)} \Big/ \left(2\,\pi^2\right),\ \{p,\ 0,\ \infty\}\right]$$

$$\text{ConditionalExpression}\left[\frac{e^{-\frac{m}{T}}}{2\sqrt{2}\,\pi^{3/2}\left(\frac{1}{m\,T}\right)^{3/2}},\ \text{Re}\left(\frac{1}{m\,T}\right)>0\right]$$

Numerics of the s-wave

Here we will be computing numerical results for abundances of relics with only s-wave interactions. P-wave interactions may or may not be considered in a following section

Toy Model

We use the form derived in http://hitoshi.berkeley.edu/229C/HW5.nb.pdf as it is the generic solution to finding the abundance of a cold relic. Note that our parameters are all in GeV, where m is the mass of the relic to be computed, g is actually g_*, related to the effective degrees of freedom of our system (look up a bit more on this), which is about 100 at early times (T>1GeV from Kolb and Turner), σ is the thermally averaged cross section, $\langle\sigma v\rangle$, and mpl is the Planck mass. Derivation of this differential equation is found in my notebook as well as on the above mentioned website. We make a quick note that the y in the differential equation is related to the abundance Y by a change of variables, namely y = [s(m)/H(m)] Y $\langle\sigma v\rangle$

$$\texttt{genericAuto} = \texttt{NDSolve}\left[\left\{y'[x] == \frac{-1}{x^2}\left((y[x])^2 - \left(0.192\ \texttt{mpl}\ m\ \sigma\ x^{3/2}\ \texttt{E}^{-x}\right)^2\right),\ y[1] == 0.192\ \texttt{mpl}\ m\ \sigma\ 1^{3/2}\ \texttt{E}^{-1}\right\} \texttt{/.}\ \{m \to 1000,\ g \to 100,\ \sigma \to 10^{-10},\ \texttt{mpl} \to 2.44 * 10^{18}\},\ y,\ \{x,\ 1,\ 10000\},\ \texttt{Method} \to \texttt{"Automatic"},\ \texttt{AccuracyGoal} \to \infty\right]$$

{{y → InterpolatingFunction[Domain: {1., 1.00 × 10^4} Output: scalar]}}

$$\texttt{generic} = \texttt{NDSolve}\left[\left\{y'[x] == \frac{-1}{x^2}\left((y[x])^2 - \left(0.192\ \texttt{mpl}\ m\ \sigma\ x^{3/2}\ \texttt{E}^{-x}\right)^2\right),\ y[1] == 0.192\ \texttt{mpl}\ m\ \sigma\ 1^{3/2}\ \texttt{E}^{-1}\right\} \texttt{/.}\ \{m \to 1000,\ g \to 100,\ \sigma \to 10^{-10},\ \texttt{mpl} \to 2.44 * 10^{18}\},\ y,\ \{x,\ 1,\ 10\,000\,000\}\right]$$

{{y → InterpolatingFunction[Domain: {1., 1. × 10^7} Output: scalar]}}

```
y[10000000] /. generic
```

{22.8686}

$$\texttt{genericSS} = \texttt{NDSolve}\left[\left\{y'[x] == \frac{-1}{x^2}\left((y[x])^2 - \left(0.192\ \texttt{mpl}\ m\ \sigma\ x^{3/2}\ \texttt{E}^{-x}\right)^2\right),\ y[1] == 0.192\ \texttt{mpl}\ m\ \sigma\ 1^{3/2}\ \texttt{E}^{-1}\right\} \texttt{/.}\ \{m \to 1000,\ g \to 100,\ \sigma \to 10^{-10},\ \texttt{mpl} \to 2.44 * 10^{18}\},\ y,\ \{x,\ 1,\ 10000\},\ \texttt{Method} \to \texttt{"StiffnessSwitching"}\right]$$

{{y → InterpolatingFunction[Domain: {1., 1.00 × 10^4} Output: scalar]}}

```
g = LogLogPlot[Evaluate[y[x] /. generic], {x, 1, 10000}, PlotRange → {{1, 10000}, {1, 10^13}} , AxesLabel → {x, y}]
```

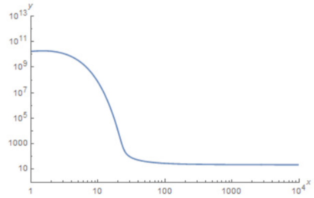


```
y[10000000] /. generic
```

{22.8686}

```
gAuto = LogLogPlot[Evaluate[y[x] /. genericAuto], {x, 1, 10000}, PlotRange → {{1, 10000}, {1, 10^13}}, PlotStyle → Green, AxesLabel → {x, y}]
```

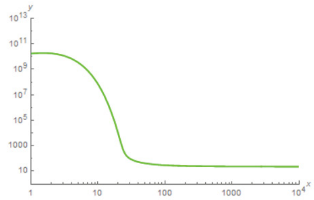


```
gSS = LogLogPlot[Evaluate[y[x] /. genericSS], {x, 1, 10000}, PlotRange → {{1, 10000}, {1, 10^13}}, PlotStyle → Red, AxesLabel → {x, y}]
```

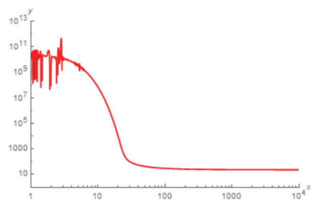


```
Show[g, gAuto, gSS]
```

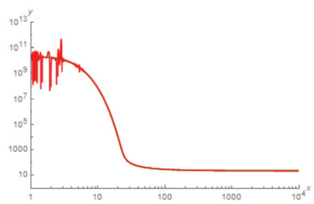

We often want to see the relative change in abundance from the early universe to now, and so lets replot with the Y (abundance) axis recast as log(Y/Y_eq), where Y_eq is just our initial Y(1) condition. A note on the different methods used in NDSolve, sometimes a differential equation cannot be solved without explicitly selecting a method due to something called 'stiffness constraints' in *Mathematica*. I have exhibited that all 3 methods I have used above (automatic, stiffnessSwitching, and the unlabelled one) yield consistent results with one another. We will be switching between methods in the next part depending on which one works.

```
LogLinearPlot[Evaluate[Log10[y[x] / (0.192 * 2.44 * 10^18 * 1000 * 10^-10 * E^-1)] /. generic ], {x, 1, 1000}, PlotRange → {{1, 1000}, {0, -10}} , AxesLabel → {x, Log[(y / y_eq)]}]
```

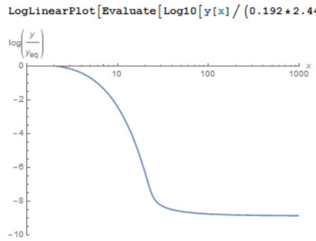

So we see that Y has been suppressed by about 10 orders of magnitude from the freeze out. Note the log is base 10 and not base e.

Baryon-Symmetric Universe (Kolb and Turner Example)

In an attempt to replicate the results of figure 5.1 in Kolb and Turner, we first insert parameters for nucleon-nucleon annihilation where σ -> c1 m_π^{-2}, m -> 1GeV, however mathematica seems to be running into some numerical errors. Note c1 is described as an order 1 constant by KT. These errors are rectified by using the method StiffnessSwitching in NDSolve, which we have showed above to yield consistent results, if somewhat choppy in the small x limit. The unlabelled and automatic methods fail here in *Mathematica*.

```
BaryonSymm = NDSolve[{y'[x] == -1/x^2 ((y[x])^2 - (0.192 mpl m σ x^3/2 E^-x)^2), y[1] == 0.192 mpl m σ 1^3/2 E^-1} /. {m → 1, g → 10, σ → (0.139)^-2, mpl → 2.44 * 10^18 }, y,
  {x, 1, 10000000}, Method → "StiffnessSwitching"]
```

{{y → InterpolatingFunction[Domain: (1. 1.×10^7) Output: scalar]}}

Testing grounds for a better solution to these differential equations

```
Needs["DifferentialEquations`NDSolveProblems`"];
Needs["DifferentialEquations`NDSolveUtilities`"];
Needs["FunctionApproximations`"];
```

```
TestBaryonSymm = NDSolve[{y'[x] == -1/x^2 ((y[x])^2 - (0.192 mpl m σ x^(3/2) E^-x)^2), y[1] == 0.192 mpl m σ 1^(3/2) E^-1} /. {m → 1, g → 10, σ → (0.139)^-2, mpl → 2.44 * 10^18},
  y, {x, 1, 10000}, SolveDelayed → True]
```

NOTE can also use Method -> {"EquationSimplification" -> "residual"} instead of SolveDelayed -> True (check syntax) since the solvedelayed method is effectively discontinued

```
{{y → InterpolatingFunction[ Domain: (1. 1.00×10^4) Output: scalar ]}}
```

```
z = LogLogPlot[Evaluate[y[x] /. TestBaryonSymm], {x, 1, 10000}, PlotRange → {{1, 10000}, {1, 10^32}} , AxesLabel → {x, y}, PlotStyle → Red]
```

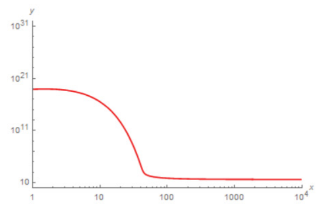


```
m = LogLogPlot[Evaluate[y[x] /. BaryonSymm], {x, 1, 10000}, PlotRange → {{1, 10000}, {1, 10^32}} , AxesLabel → {x, y}]
```

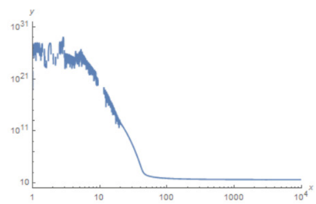


```
Show[m, z]
```

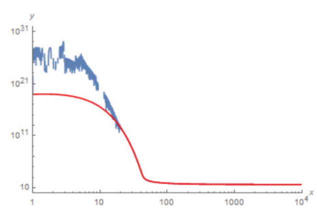

As we can see, the stiffness switching method has created a messy small x zone, and it even appears to be missing some points of interest. I'm not sure what exactly would be causing this, but I don't think it should effect the final abundance results. In the line below I have taken a good approximation to y_∞ which is related to the abundance fraction, Y_∞ by a change of variables. This noise problem has been solved by utilizing the new method above. This plot remains as a comparison, and to exhibit the jump that occurs in stiffnessswitching between the initial condition and the first step

```
y[10000000] /. BaryonSymm
```

{42.6314}

```
LogLinearPlot[Evaluate[Log10[y[x] / (0.192 * 2.44 * 10^18 * 1 * (0.139^-2) * E^-1)] /. TestBaryonSymm ], {x, 1, 10000000}, PlotRange → {{1, 10000}, {0, -20}} , AxesLabel → {x, Log[(y / y_eq)]}]
```

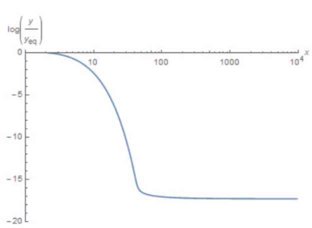

To find the remaining relic density Y_∞, we make use of our transformation y_∞=[s(m)/H(m)] Y_∞ <σv> noting from a step in our derivation, [s(m)/H(m)] = 0.368 $g_*^{1/2}$ m m_{pl} where s is the entropy and H is the hubble parameter (each represented in terms of m). Using g_*=100, and our prior values for masses and cross sections, we get that Y_∞= 9.1732* 10^{-20} (KT value is $Y_\infty = 7 * 10^{-20}$ for comparison). Note in a semi-rough approximation, $y_\infty = x_f$ by definition (look at form of diff eq we are solving for late time values of x, y), and so estimating y(10,000,000) = y_∞ yields a freeze out at x_f = 42.6314, which is right around the kolb and turner value. I think we have fairly good confidence in this algorithm now. NOTE now I think that g_* should perhaps be 10 instead of 100, so just making the substitution in here yields something not amazing, $2.9 * 10^{-19}$ so perhaps I'll look through the algorithm to find if this g_* replacement must be made elsewhere. Our assumption of g_* = 100 should still hold for the TC case though, as T = m/x = 30ish which yields g_*=100 still (pg 65 or 66 in KT for plot of these g values in SU(3) X SU(2) X U(1))

Technibaryon DM Relic Density

Here we look at the TechniColour SU(3) gauge group, behaving as a sort of new QCD group. If we assume a massive DM technibaryon particle (m-> 1000 Gev), and have the cross section going as $4\pi/m^2$ (analogous to the cross section in proton-proton scattering), we get the results below.

```
wimpDensityHeavy = NDSolve[{y'[x] == -1/x^2 ((y[x])^2 - (0.192 mpl m σ x^(3/2) E^-x)^2), y[1] == 0.192 mpl m σ 1^(3/2) E^-1} /. {m → 1000, g → 100, σ → 4 π/(1000^2), mpl → 2.44 * 10^18},
  y, {x, 1, 10000000}, Method → {"EquationSimplification" → "Residual"}]
```

{{y → InterpolatingFunction[Domain: {1., 1.×10^7} Output: scalar]}}

Note, using SolveDelayed -> True also works, but appears to have been phased out by the software some time ago. It returns a purely cosmetic error warning, but still evaluates in the way our 'Method' works now. It appears that what this method does is numerically solve the differential equation at every step instead of analytically trying to solve and simplify before plugging stuff in. Better double check this in the future, but it seems to be the 'magical' solution we have been looking for, as it doesnt change any late time behaviour but smooths out (and doesnt cause a jump) in the early time part of the Boltzmann equation. Use method->"StiffnessSwitching" to see what we had prior, though I will leave an example of this in the Baryon Symmetric case

{{y → InterpolatingFunction[Domain: {1., 1.00×10^4} Output: scalar]}}

```
LogLogPlot[Evaluate[y[x] /. wimpDensityHeavy], {x, 1, 10000}, PlotRange → {{1, 10000}, {1, 10^23}}]
```

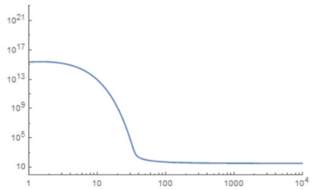


```
y[10] /. wimpDensityHeavy
```

{1.34612×10^13}

```
y[10000000] /. wimpDensityHeavy
```

{34.4125}

So our freeze out time seems to be at $y_\infty = x_f = 34.4125$
Analagous to our previous computation, we get an abundance Y_∞ of $3.05 * 10^{-16}$

Note now that if our theory actually has a low confinement scale (lets say 7.5 MeV) than the annihilation will take place by interchange of light glueballs. If we instead estimate the cross section to be $1/(0.0075^2)$ we have a very different result.

```
wimpDensityLow = NDSolve[{y'[x] == -1/x^2 ((y[x])^2 - (0.192 mpl m σ x^(3/2) E^-x)^2), y[1] == 0.192 mpl m σ 1^(3/2) E^-1} /. {m → 1000, g → 100, σ → 4 π/(0.0075^2), mpl → 2.44 * 10^18},
  y, {x, 1, 10000000}, Method → {"EquationSimplification" → "Residual"}]
```

{{y → InterpolatingFunction[Domain: {1., 1.×10^7} Output: scalar]}}

```
LogLogPlot[Evaluate[y[x] /. wimpDensityLow], {x, 1, 10000}, PlotRange → {{1, 10000}, {1, 10^43}}]
```

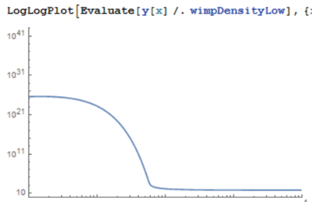


```
y[10000000] /. wimpDensityLow
```

{57.7605}

This freeze out time is now $x_f = 57.7605$
And abundance of $Y_\infty = 3.618 * 10^{-25}$

Bibliography

[1] Peskin, M., Shroeder, D., **An Introduction to Quantum Field Theory**. 1995. Westview Press

[2] Burgess, C.P., Moore, G., **The Standard Model: A Primer**. 2007. Cambridge University Press

[3] Griffiths, D., **Introduction to Elementary Particles**. 2008. Wiley-VCH

[4] Georgi, H., **Lie Algebras in Particle Physics**. 1999. Westview Press

[5] Arfken, G., Weber, H., Harris, F., **Mathematical Methods for Physicists**. Elsevier, Academic Press.

[6] Wu, S. *et al.* (**1957**) *Physical Review*, **105**, 1413.

[7] Higgs, P., *Broken Symmetries and the Masses of Gauge Bosons*, 1964, Phys. Rev. Lett. **13**, 508

[8] "The 2004 Nobel Prize in Physics - Popular Information". Nobelprize.org. Nobel Media AB 2014. Web. 23 Feb 2017. `http://www.nobelprize.org/nobel_prizes/physics/laureates/2004/popular.html`

[9] Weinberg, S., *A Model of Leptons*, 1967, Physical Review Letters, **19** (21): 1264-1266

[10] Salam, A., *Elementary Particle Physics: Relativistic Groups and Analyticity*, 1968, Eighth Nobel Symposium

[11] Glashow, S. L., *Partial-Symmetries of Weak Interactions*, 1961, Nuclear Physics, **22** (4): 579-588

[12] Mathieu, V., Kochelev, N., Vento, V., *The Physics of Glueballs*, 2009, Arxiv[hep-ph/0810.4453]

[13] Particle Data Group (revisions by Jackson, J.D., Tovey, D.R.), *Kinematics*, 2016, `http://pdg.lbl.gov/2016/reviews/rpp2016-rev-kinematics.pdf`

[14] Wudka, J., *A short course in effective Lagrangians*, 1999, Arxiv[hep-ph/0002180]

[15] Baummann, D., **Cosmology: Part III Mathematical Tripos**, Chapter 3, http://www.damtp.cam.ac.uk/user/db275/Cosmology/Lectures.pdf

[16] Kolb, E., Turner, M., **The Early Universe** 1994, Westview Press

[17] Mukhanov, V., **Physical Foundations of Cosmology**, 2005, Cambridge University Press

[18] Dodelson, S., **Modern Cosmology**, 2003, Academic Press

[19] Particle Data Group (revisions by Olive, K.A., Peacock, J.A.), *Big-Bang Cosmology*, 2016, :http://www-pdg.lbl.gov/2016/reviews/rpp2016-rev-bbang-cosmology.pdf

[20] Brandenberger, R., Vafa, C., *Superstrings in the Early Universe*, 1989, Nucl. Phys. **B316**, 421.

[21] Melnikov, V., Orlov, S., *Nonsingular Cosmology as a Quantum Vacuum Effect*, 1979, Phys. Lett. A **70**, 263

[22] NASA Science Team, http://map.gsfc.nasa.gov/media/060915/060915_CMB_Timeline600.jpg

[23] Bosma, A., *The Distribution and Kinematics of Neutral Hydrogen in Spiral Galaxies of Various Morphological Types*, 1978, PhD Thesis, Groningen University

[24] Rubin, V. C., Thonnard, N., Ford, W. K., *Extended rotation curves of high-luminosity spiral galaxies. IV - Systematic dynamical properties SA through SC*, 1978, The Astrophysical Journal Letters. **225**. L107-L111.

[25] Rubin, V., Thonnard, N., Ford, W.K., *Rotational Properties of 21 Sc Galaxies with a Large Range of Luminosities and Radii from NGC 4605 (R=4kpc) to UGC 2885 (R=122kpc)*, 1980, Astrophysical Journal. **238**. 471

[26] Copi, C., Schramm, D., Turner, M., *Big-Bang Nucleosynthesis and the Baryon Density of the Universe*, 1994, Arxiv[astro-ph:9407006]

[27] Planck Collaboration, *Planck 2015 Results. XIII. Cosmological Parameters*, 2016, Arxiv[astro-ph:1502.01589]

[28] Chapline, G. F., *Cosmological Effects of Primordial Black Holes*, 1975, Nature, **253**, 251

[29] Carr, B.J., Hawking, S.W., *Black Holes in the Early Universe*. 1974, Mon. Not. R. astr. Soc. **168**, 399-415

[30] Green, A.M., *Primordial Black Holes: sirens of the early Universe*. 2014, Arxiv[gr-qc:1403.1198]

[31] Pani, P., Loeb, A., *Exclusion of the remaining mass window for primordial black holes as the dominant constituent of dark matter*. 2014, Arxiv[astro-ph:1401.3025]

[32] Duffy, L., van Bibber, K., *Axions as Dark Matter Particles*, 2009, Arxiv[hep-ph:0904.3346]

[33] Peccei, R.D., Quinn, H.R., *CP Conservation in the Presence of Instantons*, 1977, Phys. Rev. Lett., 38:1440-1443

[34] Peccei, R.D., Quinn, H.R., *Constraints Imposed by CP Conservation in the Presence of Instantons*, 1977, Phys. Rev., D16:1791-1797

[35] Abbott, L.F., Sikivie, P., *A Cosmological Bound on the Invisible Axion*, 1983, Phys. Lett. B., 120:133-136

[36] Davis, R.L., *Cosmic Axions from Cosmic String*, 1986, Phys. Lett. B., 180:225

[37] Gondolo, P., Gelmini, G., *Cosmic Abundances of Stable Particles: Improved Analysis*, 1991, `http://adsabs.harvard.edu/abs/1991NuPhB.360..145G`

[38] Murayama, H., *Early Universe HW #5 Solutions*, 2005, `hitoshi.berkeley.edu/229C/HW5.nb.pdf`

[39] Bertone, G., Hooper, D., Silk, J., *Particle Dark Matter: Evidence, Candidates, and Constraints*, 2005, Arxiv[hep-ph:0404175]

[40] Navarro, J., Frenk, C., White, S., *A Universal Density Profile from Hierarchical Clustering*, 1996, Arxiv[astro-ph:9611107]

[41] De Blok, W.J.G., *The Core-Cusp Problem*, 2009, Arxiv[astro-ph:0910.3538]

[42] Fradette, A., Pospelov, M., Pradler, J., Ritz, A., *Cosmological Constraints on Very Dark Photons*, 2014, Arxiv[hep-ph:1407.0993]

[43] Ochs, W., *The Status of Glueballs*, 2013, Arxiv[hep-ph:1301.5183]

[44] Wilson, K. G., *Confinement of Quarks*, 1974, Phys. Rev. D **10**, 2445

[45] Morningstar, C. J., Peardon, M., *The Glueball Spectrum from an Anisotropic Lattice Study*, 1999, Arxiv[hep-lat:9901004]

[46] Ochs, W., *The status of glueballs*, 2013, Arxiv[hep-ph:1301.5183]

[47] Forestell, L., Morrissey, D., Sigurdson, K., *Non-Abelian Dark Forces and the Relic Densities of Dark Glueballs*, 2016, Arxiv[hep-ph:1605.08048]

[48] Chen, Y. *et al.*, *Glueball spectrum and matrix elements on anisotropic lattices*, 2006, ArXiv[hep-lat:0510074]

[49] Cline, J.M., Liu, Z., Moore, G., Xue, W., *Composite Strongly Interacting Dark Matter*, 2014, Phys. Rev. D **81**, 095001

[50] Craig, N., Draper, P., Kilic, C., Thomas, S., *Shedding Light on Diphoton Resonances*, 2016, Arxiv[hep-ph:1512.07733]

[51] Juknevich, J., Melnikov, D., Strassler, M., *A Pure Glue Hidden Valley I. States and Decays*, 2009, Arxiv[hep-ph:0903.0883]

[52] Juknevich, J., *Phenomenology of Pure-Gauge Hidden Valleys at Hadron Colliders*, PhD Thesis, Rutgers University

[53] Juknevich, J., *Pure-Glue Hidden Valleys through the Higgs Portal*, 2010, Arxiv[hep-ph:0911.5616]

[54] Soni, A., Zhang, Y., *Hidden $SU(N)$ Glueball Dark Matter*, 2016, Arxiv:[hep-ph:1602.00714]

[55] Spergel, D. N., Steinhardt, P. J., *Observational Evidence for Self-Interacting Cold Dark Matter*, 2000, Arxiv[astro-ph:9909386]

[56] Fermi-LAT Collaboration, *Search for Gamma-ray Spectral Lines with the Fermi Large Area Telescope and Dark Matter Implications*, 2013, Arxiv[astro-ph:1305.5597]

[57] Diamanti, R., Lopez-Honorez, L., Mena, O., Palomares-Ruiz, S., Vincent, A. C., *Constraining Dark Matter Late-time Energy Injection: Decays and p-wave Annihilations*, 2014, Arxiv[astro-ph:1308.2578]

[58] Bell, N. F., Galea, A. J., Petraki, K., *Lifetime Constraints for Late Dark Matter Decay*, 2010, Arxiv[astro-ph:1004.1008]

[59] Guagnelli, M., Sommer, R., Wittig, H., *Precision Computation of a Low-energy Reference Scale in Quenched Lattice QCD*, 1998, Arxiv[hep-lat:9806005]

[60] Teper, M., *Glueball masses and other physical properties of $SU(N)$ gauge theories in $D = 3 + 1$: a review of lattice results for theorists*, 1998, Arxiv[hep-th:9812187]

[61] Deur, A., Brodsky, S.J., de Teramond, G.F., *The QCD Running Coupling*, 2016, Arxiv[hep-ph:1604.08082]

[62] Czakon, M., *The Four-Loop QCD β-Function and Anomalous Dimensions*, 2004, Arxiv[hep-ph:0411261]

[63] Hannestad, S., *What is the lowest possible reheating temperature?*, 2004, Phys. Rev. D. **70**, 043506, DOI:10.1103/PhysRevD.70.043506

[64] Baring, M., Ghosh, T., Queiroz, F., Sinha, K., *New Limits on the Dark Matter Lifetime from Dwarf Spheroidal Galaxies using Fermi-LAT*, 2015, Arxiv[hep-ph:1510.00389]

[65] HAWC Collaboration., *Dark Matter Limits from Dwarf Spheroidal Galaxies with the HAWC Gamma-Ray Observatory*, 2017, Arxiv[astro-ph:1706.01277]

[66] Cirelli, M., Corcella, G., Hektor, A., Hutsi, G., Kadastik, M., Panci, P., Raidal, M., Sala, F., Strumia, A., *PPC 4 DM ID: A Poor Particle Physicist Cookbook for Dark Matter Indirect Detection*, 2010, Arxiv[hep-ph:1012.4515]

[67] Sjostrand, T., Mrenna, S., Skands, P., *A Brief Introduction to PYTHIA 8.1*, 2007, Arxiv[hep-ph:0710.3820]

[68] Elor, G., Rodd, N., Slatyer, T., Xue, W., *Model-Independent Indirect Detection Constraints on Hidden Sector Dark Matter*, 2016, Arxiv[hep-ph:1511.08787]

[69] Pappadopulo, D., Ruderman, J., Trevisan, G., *Cannibal Dark Matter*, 2016, Arxiv[hep-ph:1602.0421]

[70] Chacko, Z., *Quirks*, 2007, Seminar at UC Davis, `http://particle.physics.ucdavis.edu/seminars/data/media/2007/nov/chacko.pdf`

[71] Curtin, D., Verhaaren, C. B., *Quirky Explanations for the Diphoton Excess*, 2016, Arxiv[hep-ph:1512.05753]

[72] March-Russell, J., West, S. M., Cumberbatch, D., Hooper, D. *Heavy Dark Matter Through the Higgs Portal*, 2008, Arxiv[hep-ph:0801.3440]

[73] Farina, M., Low, M., *Constraining Quirky Tracks with Conventional Searches*, 2017, Arxiv[hep-ph:1703.00912]

[74] The CMS Collaboration, *Search for heavy stable charged particles with* $12.9fb^{-1}$ *of 2016 data*, 2016, Tech. Rep. CMS-PAS-EXO-16-036

[75] The ATLAS Collaboration, *Search for heavy long-lived charged R-hadrons with the ATLAS detector in* $3.2fb^{-1}$ *of proton-proton collision data at* $\sqrt{s} = 13TeV$, 2016, Arxiv[hep-ex:1606.05129]

[76] The CMS Collaboration, *Search for Dark Matter in Final States with an Energetic Jet, or a Hadronically Decaying W or Z boson using* $12.9fb^{-1}$ *of data at* $\sqrt{s} = 13TeV$, 2016, Tech. Rep. CMS-PAS-EXO-16-037

[77] The ATLAS Collaboration, *Search fornew phenomena in final states with an energetic jet and large missing transverse momentum in pp collisions at* $\sqrt{s} = 13TeV$ *using the ATLAS detector*, 2016, Arxiv[hep-ex:1604.07773]

[78] The CMS Collaboration, *Search for resonant production of high mass photon pairs in proton-proton collisons at* $\sqrt{s} = 8$ *and* $13TeV$, 2016, Arxiv[hep-ex:1606.04093]

[79] Chluba, J., *Science with CMB spectral distortions*, 2014, Arxiv[astro-ph:1405.6938]